UNIVERSITY OF CAPE TOWN

FACULTY OF ENGINEERING AND THE BUILT ENVIRONMENT

DEPARTMENT OF CIVIL ENGINEERING

MSc. Eng. RESEARCH DISSERTATION

THE INFLUENCE OF CRYSTALLINE ADMIXTURES ON THE MECHANICAL AND DURABILITY PROPERTIES OF CRACKED AND UNCRACKED CONCRETE

Student Name:
Ansifrid Joachim Lekundayo (LKNANS001)

Supervisor:
Prof. Hans Beushausen

Co-supervisor:
Dr Philemon Arito

Date: 30th November 2023

Plagiarism declaration

1. I know that plagiarism is wrong. Plagiarism is to use another's work and pretend that it is one's own.
2. I have used the UCT Harvard convention for citation and referencing. Each contribution to and quotation in this thesis from the work(s) of other people has been attributed and has been cited and referenced.
3. This research thesis is my work.
4. I have not allowed, and will not allow anyone, to copy my work to pass it off as his or her work.
5. This thesis has been submitted to the Turnitin module (or equivalent similarity and originality checking software) and I confirm that my supervisor has seen my report and any concerns revealed by such have been resolved with my supervisor.

Signed by candidate

Ansifrid Joachim Lekundayo

November 2023

Executive summary

In South Africa context, water scarcity calls for water retaining structures to perform with respect to strength and seepage. Thermal differential and shrinkage strains often cause cracking which allow seepage under the high hydraulic pressure. Continuous maintenance and repair strategies have become vital to prevent seepage and deterioration over their service lives. Self-healing of concrete promotes reduced water permeability without the need for maintenance and repair. Innovative concrete self-healing methods include the use of microencapsulation, hollow glass tubes, bacteria, and crystalline admixtures. Crystalline admixtures are directly incorporated into the concrete during mixing to react with water and cement particles to induce self-healing. This study intended to determine the influence of crystalline admixtures on mechanical and durability properties of cracked and uncracked concrete.

An experimental methodology involved casting ten concrete mixes. Concrete specimens were obtained by coring, cutting, and introducing crack using the three-point bending test. Experimental tests conducted were, microscopy tests, strength tests, and durability tests.

The XRF test results indicated that cement was a significant component of CAs, thus, the hydrations were expected to be similar to ordinary Portland cement. SEM-EDS tests results revealed that the precipitates extracted from the crack area after healing were found to be composed of polymorphs of calcium carbonate and CSH. The presence of Sr^{2+} and Mg in the concrete matrix influenced by the calcium carbonate precipitates.

The influence of the CAs on mechanical properties of concrete revealed that incorporation of crystalline admixtures generally improves the compressive strengths and splitting strength of concretes with higher water filled porosity than the concretes with lower water filled porosity. In practice, these crystalline admixtures were deduced to have little to no noticeable effect on compressive strength when used in high quality concretes.

In durability properties, the influence of CAs on OPI, WSI, and water filled porosity tests were determined on uncracked concrete. OPI test results deduced that, CA-4 concrete recorded the highest decrease in permeability of 51.02% and 43.77% for w/b of 0.4 and 0.6, respectively. This was attributed to the swelling of the concrete matrix, precipitation of calcite crystals, and the likely increased dosage of CA-4 used in the

concrete mix. WSI test results indicated that all concrete mixes showed “good” quality with sorptivity values at curing ages 4, 8, and 12 weeks except concretes with w/b of 0.4 at 12 weeks with excellent quality. The sorptivity values were deduced to decrease with an increase in curing age due to the continuing hydration which refined the microstructure of concrete and increase resistance to capillary absorption of liquid. Water filled porosity test results were found to be influenced by the w/b ratio. A decrease in w/b led to lower water filled porosity as hydration products fills the void space between cement particles. While, a higher w/b ratio resulted in higher water filled porosity as the extent to which hydration products fill up the voids is limited.

The influence of CAs on WSI, water filled porosity, and water permeability tests were determined on cracked concrete. WSI test results indicated that all the concrete mixes showed “poor” quality concrete with the incorporation of CAs having little effect in improving the sorptivity values. The inconsistency in the sorptivity values was attributed to the crack geometry variation along the depth of the concrete specimens. Water filled porosity test results indicated that the influence of the w/b ratio applies to cracked concrete despite the presence of cracks. Water permeability tests indicated that the permeability (k) of concrete decreases over curing time. This was attributed to the precipitation of calcium carbonate crystals by the crystalline admixtures suggesting that these admixtures do have a positive effect in reducing permeability.

More insight on the influence of crystalline admixtures on concrete properties can be achieved by refining the quality of the data collected. Variability in test results obtained due to crack geometry can be minimised by utilising uniform crack width specimens in conjunction with free occurring cracks width for correlation of both test results and in-service performance. Furthermore, an extended curing duration should be employed to continue monitoring the healing process to determine the duration of full self-healing if any. Other microscopic techniques such as Thermogravimetric analysis (TGA) and X-Ray Diffraction Analysis (XRD) can be used to determine the reactivity, thermal/oxidative stabilities, and analysis of the structures of the crystalline admixtures. The use of water permeability test under pressure to minimise the test duration is especially useful which allow the comparison between uncracked and cracked concrete.

Acknowledgement

First, I would like to thank the Almighty God for His continuous blessings and unconditional love throughout my journey.

I want to express sincere gratitude to my supervisor and co-supervisor, Professor Hans Beushausen and Dr Philemon Arito, for their acceptance to put me under their wing, their guidance, encouragement, and continuous support of my research and studies.

Special thanks to Professor Pilate Moyo, Professor Hans Beushausen, Professor Mark G Alexander, and the entire CoMSIRU management for funding my Master's studies and providing me with the opportunity to be a part of the University of Cape Town. It is a great privilege to be a part of a prestigious university and one of the world's leading research-based universities.

I would also like to thank the concrete laboratory personnel, especially Nooredien Hassen, Charles May, and all Civil Engineering laboratory staff; Miranda Waldron of the Electron Microscope Unit, Centre for Imaging and Analysis, UCT who assisted me in the experimental work from time to time. My fellow research students for their collaborative effort during data collection and my writing.

I would also like to thank companies which will remain anonymous for agreeing to donate their material to facilitate my research. Your direct support which helped me conduct this research successfully is highly noted and appreciated.

Lastly, special thanks go to my beautiful family; my wife Godiana and my newborn daughter Abigail. Your support and courage have helped me throughout my writing process. To my parents for their unconditional love, support, and encouragement throughout my academic journey.

Table of Contents

List of Figures

List of Tables

1. Introduction

1.1. Background

Concrete is widely used in the construction of large structures such as water retaining structures, where measures to minimize the development of heat of hydration and attendant volume changes are essential (ACI 301-10, 2010). During the early stages of concrete hydration, thermal and shrinkage stresses are created due to internal and external restraints in the structure. Thermal stresses are created due to internal restraints resulting from thermal and hygral differences in the concrete members. Additional external restraints may occur due to differential shrinkage at the interface of two concrete layers cast separately or due to general geometrical restraints of the structure. If the tensile stresses exceed the tensile strength of concrete, cracks develop on the surface of the concrete.

Cracks may damage the integrity of the concrete structure and affect its durability and serviceability in the long term. In water-retaining structures, the propagation of these cracks may affect the water-retaining capability. Externally visible cracks can impair the water tightness of the structure rendering the structure less effective. Therefore, the control of cracking is particularly essential for concrete structures (Ballim & Graham, 2009).

Minimizing concrete cracks associated with thermal and shrinkage stresses without interfering with the performance of the structure while simultaneously improving durability requires innovative techniques. Concrete self-healing provides an innovative idea in inducing healing to cracks, thereby maintaining water-retaining capability. Self-healing of concrete is divided into two categories: autogenous and autonomous self-healing. Autogenous self-healing refers to the ability of concrete to self-heal with the help of its generic materials. Self-healing relying on external healing agents not part of the cement composition is known as autonomous self-healing (Rooij et al., 2013).

Several studies (Palin, Wiktor & Jonkers, 2015; Palin, Jonkers & Wiktor, 2016; Snoeck et al., 2016) have shown that concrete cracks of the order 0.1 ~ 0.2 mm with slight leakage can autogenously self-heal provided water is available at the crack. However, if the widths are of the order of 0.2 ~ 0.3 mm or more, autogenous self-healing is rendered ineffective and external healing agents must be introduced in the concrete to assist in self-healing (Tong, 2015). Several studies on the different methods of

autonomous self-healing have been conducted (Wu, Johannesson & Geiker, 2012; Roig-Flores et al., 2015, 2016; Zhang et al., 2018). These methods include the use of hollow glass tubes, microencapsulation, bacteria, and crystalline admixtures (Coppola, Coffetti & Crotti, 2018).

Hollow glass tubes are embedded in the concrete to act as vascular tunnels connected to an external reservoir containing healing agents such as epoxy resin, methyl methacrylate, and ethyl cyanoacrylate. The glass tubes break when cracking occurs and release the healing agents, triggering the healing mechanism (Van Tittelboom et al., 2011). Another method is microencapsulation, in which a coating surrounds healing agents to produce small capsules of micrometric dimensions (Coppola, Coffetti & Crotti, 2018). The coating protects the healing agents during the mixing procedure in the concrete (Huang et al., 2016). The healing mechanism is triggered once the cracks rupture the capsules releasing the healing agents.

Incorporating bacteria in concrete during mixing also assists in concrete self-healing. When concrete cracks, the bacteria react with moisture through urea hydrolysis and organic acids oxidation processes, precipitating calcium carbonate, which heals the cracks (Huang et al., 2016). Another method is the use of crystalline admixtures, which are hydrophilic chemical compounds incorporated in concrete to precipitate insoluble compounds capable of healing the cracks and resisting water penetration (Roig-Flores et al., 2015).

Among these methods, crystalline admixtures are the easiest way to induce autonomous self-healing as the admixtures are directly incorporated into concrete during mixing. In casting large concrete volumes, hollow glass tubes present a challenge of early rupture (Van Tittelboom et al., 2011). Microencapsulation compromises the bond between the capsules and concrete and adversely affects concrete's mechanical properties if many capsules are used (Wu, Johannesson & Geiker, 2012). Thus, further research on the use of crystalline admixtures to promote concrete self-healing is required to help understand the influence of crystalline admixtures on concrete's durability and mechanical properties.

1.2. Problem statement

The occurrence of cracks in large structures like water-retaining structures accelerates leakage and deterioration by providing preferential access to aggressive agents such as chlorides and sulphates. Maintenance and repair practices have, thus, become the

focus of improving durability. However, continuous maintenance and repairs are expensive, and the continued expenditure growth in recent years has significantly exceeded the investment cost for new structures (Coppola, Coffetti & Crotti, 2018).

Furthermore, durable repair techniques are problematic to achieve. The majority of the repairs last for only ten to fifteen years. This duration is not economical compared to the usual 100-year service life of water-retaining structures (Haoliang & Ye, 2014). Autonomous self-healing is a potential maintenance-free method against leakage and deterioration and a continuing process during the structure's service life (Sisomphon, Copuroglu & Koenders, 2012). Therefore, there is a need for further research on the potential of autonomous self-healing methods.

As stated before, crystalline admixtures are a simple method, involving incorporating the admixtures in the concrete during mixing. However, the effectiveness of the self-healing mechanism has not been quantified to date. The American Concrete Institute indicated that the crystalline admixtures react with water and cement particles to form modified calcium silicate hydrates and pore-blocking precipitates in the existing cracks and capillaries (Phelan et al., 2010). In contrast, Sisomphon, Copuroglu & Koenders, (2012) reported that calcium hydroxide - a by-product of cement hydration - reacts with the crystalline admixtures to form crystalline products which fill pores and cracks in the concrete. Research has established that this unknown interaction between the crystalline admixtures and concrete can assist concrete in self-healing (Roig-Flores et al., 2016; Escoffres, Desmettre & Charron, 2018; Wang et al., 2018; Zhang et al., 2018).

In the South African construction market, many crystalline admixtures products are being marketed. Products technical and material safety datasheets have been attached to the admixtures products that supposedly induce autonomous self-healing and improve the mechanical and durability properties of concrete. Thus, further research is required to investigate the influence the crystalline admixtures on the mechanical and durability properties of cracked and uncracked concrete.

1.3. Research aims

The primary aim of this study is to investigate the influence of crystalline admixtures on the properties of uncracked and cracked concrete. The specific aims of this study are:

a) To characterize self-healing products, present in the crack-healed specimens.

b) To investigate the influence of the crystalline admixtures on the mechanical properties of uncracked and cracked concrete.

c) To investigate the durability properties of uncracked and crack-healed concrete with crystalline admixtures at different w/b ratios.

1.4. Research scope

This research is limited to the following aspects:

a) Ordinary Portland cement (OPC) (CEM 1 52.5 N).

b) Two water-binder ratios of 0.40 and 0.60, represent high and medium-strength concrete, respectively.

c) Two ranges of crack widths of (0 - 0.30) mm and (0.31 – 0.40) mm, represent small and large crack widths in concrete, respectively. The small crack width range were selected as the acceptable crack widths limit in reinforced structures as per SANS 10100-1, (2000).

1.5. Research outline

This thesis consists of five chapters:

a) Chapter One gives an introduction to the study. It includes the background information, problem statement, research aims and expected outcomes, and scope.

b) Chapter Two presents a critical and in-depth review of published literature.

c) Chapter Three contains the experimental methodology, including all the investigated parameters, a description of materials and equipment used, and test methods used for the study.

d) Chapter Four presents an analysis and discussion of the experimental data.

e) Chapter Five presents the conclusions and recommendations that have been arrived at based on the data collected from the experimental investigation.

2. Literature review

This chapter provides the literature review on crack healing of concrete structures with crystalline admixtures. It is divided into five main sections. Section 2.1 details concrete durability as a function of concrete structure design. Section 2.2 details the factors affecting concrete durability. Section 2.3 discusses cracking in concrete. Sections 2.4 and 2.5 detail crack self-healing and crystalline admixtures healing, respectively.

2.1. Concrete durability

Traditionally, the procedures for designing concrete mixes and concrete structures focused on the strength of concrete, while other mechanical properties like shrinkage, coefficient of thermal expansion, and creep relating to durability received secondary consideration. However, the modern concrete practice has moved away from prescriptive approaches and towards performance approaches for durability reasons, at least for large structures like water-retaining structures (Alexander, Bentur & Mindess, 2017). The change has come about for two reasons. Firstly, it is relatively easy to achieve high-strength of concrete with modern concrete technologies. Secondly, the increasing awareness of concrete sustainability has become apparent that designing for durability effectively reduces carbon footprint than increasing the strength of concrete. Furthermore, common structural failures are rarely due to strength deficiency but rather inadequate durability.

Durability relates to material performance over the intended service life of the structure in a given environment. Therefore, designers consider what acceptable performances are likely to be in a given environment and then design according to a set of performance criteria. The constructor's responsibilities will ensure that the structure is consistent with the designer's specifications and show proof that the as-built structure meets the durability design criteria (Alexander, Ballim & Beushausen, 2009).

2.2. Factors affecting concrete durability

Deterioration is the failure of the designed structures to perform according to the designed specifications. Deterioration results from the interactions between the concrete system and its environment. Factors associated with the concrete system influence the ability of the concrete to resist deterioration, while environmental factors influence the degree of aggressiveness the concrete has to withstand (Alexander, Bentur & Mindess, 2017b).

Figure 2-1 shows the factors that affect concrete durability. Critical factors in the concrete system category are the water-binder ratio and binder type for intrinsic factors and curing and early age temperature history for extrinsic factors. In contrast, a critical factor for the degree of aggressiveness is the effect of cracking due to shrinkage and temperature effects (Alexander, Ballim & Beushausen, 2009).

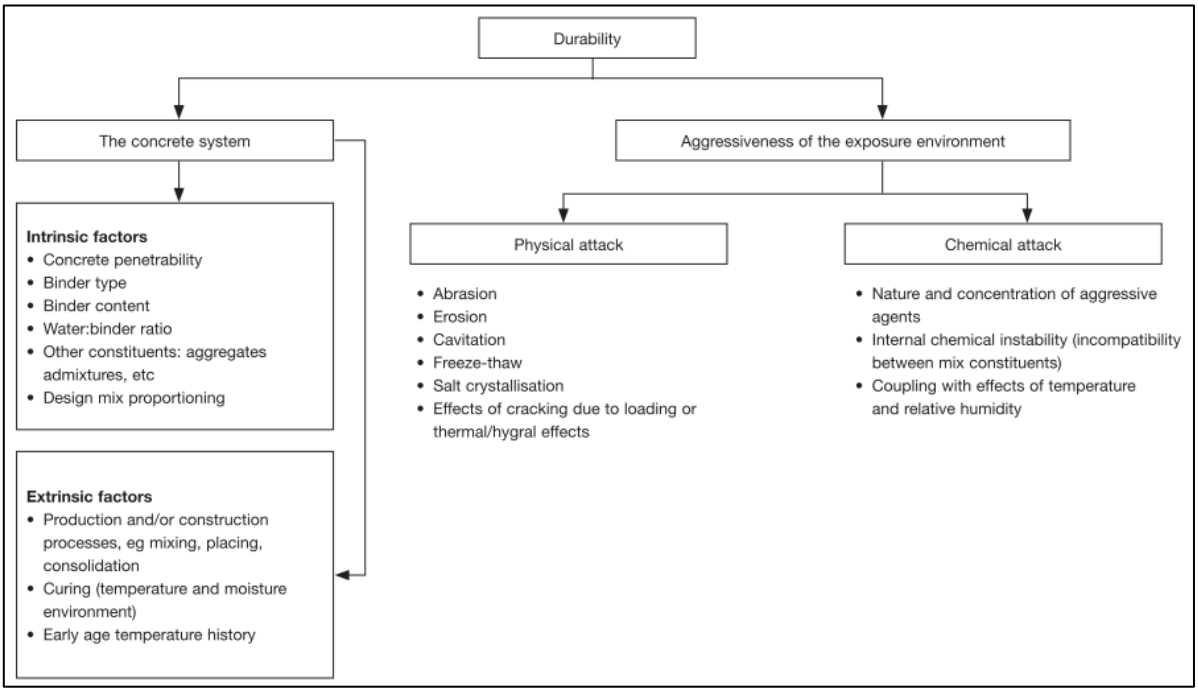

Figure 2-1: Factors affecting concrete durability (Alexander, Ballim & Beushausen, 2009)

In water retaining structures, durability is measured in terms of permeability and seepage of water out of the structures. Critical factors in the concrete system category are the early joint failures and water proofing systems for extrinsic factors. In contrast, critical factors for the degree of aggressiveness are the physical attack and chemical attack, respectively. Physical attack is the effect of cracking due to loading and temperature, while, chemical attack is the nature and concentration of aggressive agents such as alkali silica reaction (ASR), softwater attack, reinforcement corrosion due to carbonation and chloride ions ingress (Alexander, Ballim & Beushausen, 2009).

2.2.1. Water-binder ratio

Concrete strength and general permeability properties are directly dependent on the w/b ratio. It is possible to modify the strength and general permeability of concrete by manipulating the w/b ratio. The strength and general permeability of hardened concrete are determined by the properties of the hardened cement paste (Mindess, Young & Darwin, 2003).

The capillarity water filled porosity is controlled by the variation in the w/b ratio. As the w/b ratio decreases, capillarity water filled porosity decreases and vice versa (Figure 2-2). A lower w/b ratio translates to higher strength which increases resistance to cracking from internal and external stresses. Furthermore, a lower w/b ratio decreases the permeability of concrete, which controls the ingress of moisture in the concrete i.e., concrete wick action. The rate of ingress of moisture governs the movement of water during heating or freezing cycles, and the ingress of water-soluble aggressive ions in concrete which is responsible for inducing deterioration (Mindess, Young & Darwin, 2003).

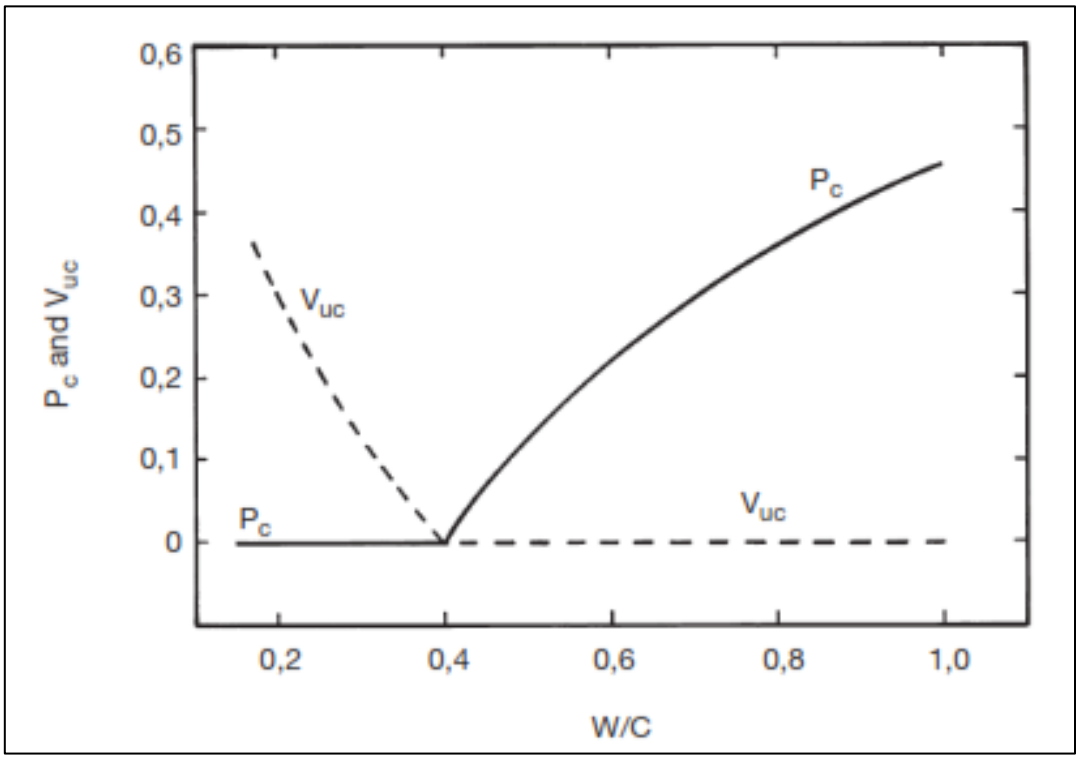

Figure 2-2: Capillarity water filled porosity (P_c) and volume fraction of unhydrated cement (V_{uc}) vs w/c (Grieve, 2009)

The permeability of concrete is governed by the paste water filled porosity and is affected by internal cracking at the paste-aggregate interface. The permeability can be measured using D'Arcy's law of flow through a porous medium. It should also be noted that D'Arcy's equation holds for an uncracked concrete specimen. However, this is not the case in practical situations, as the cracking at the paste-aggregate interface increases moisture flow through concrete. However, the equation can give approximate engineering values necessary for design estimations (Alexander, Ballim & Beushausen, 2009).

2.2.2. Binder type

The selection of binder type is critical in concrete design, especially for large structures. Cement blends containing supplementary cementitious materials (SCMs) such as fly ash (FA), ground granulated blast furnace slag (GGBFS), and silica fume (SF) react more slowly than ordinary Portland cement (OPC). The incorporation of SCMs in cement reduces capillary water filled porosity as hydration time increases, leading to a denser concrete microstructure as it ages. Furthermore, the thermal effects (associated with the hydration of cement) can be delayed due to slower hydration reactions on the incorporation of cement extenders (Batog & Giergiczny, 2017).

2.2.3. Curing

Proper curing of concrete fills the capillaries with water ensuring sufficient hydration to reduce water filled porosity and achieve the desired strength and durability of concrete (Alexander & Beushausen, 2009).

It is crucial to begin curing as soon as the concrete surface is exposed to the atmosphere, as delayed curing results in calcium hydroxide being deposited in the entrances of the capillaries by the evaporating pore water. Carbon dioxide from the air can penetrate concrete through pores and reacts with calcium hydroxide through the carbonation process to form calcium carbonates. The carbonation process will render the capillaries impermeable to water for continued hydration and reduce the degree to which the cementitious materials hydrate (Kellerman & Crosswell, 2009).

Cement blends containing supplementary cementitious materials (SCMs) react slower than Portland cement (PC), thus require additional curing time for sufficient for hydration to reduce the water filled porosity.

2.2.4. Early temperature history

The development of heat of hydration is vital for water-retaining structures which must remain free of water-permeable cracks. Lower heat of hydration translates to lower thermal stresses induced within concrete. The early tensile strength of concrete should exceed the value of thermal stresses induced to prevent the formation of cracks (Ballim & Graham, 2009).

Determining stresses and strains due to thermal changes has improved the optimization of mix designs, temperature, and curing conditions to counteract their

effects. Concrete designers prefer cement blends with a decreased amount of Portland cement clinker, which reduces the rate of development of heat of hydration. Fly ash and ground granulated blast furnace slag (GGBS) are some of the SCMs used in large concrete applications (Batog & Giergiczny, 2017).

Table 2-1: Total heat of hydration of South African Portland cements blends (Ballim & Graham, 2009)

Cementitious material	Approximate heat of reaction, kJ/kg, under adiabatic conditions after:		
	3 days	5 days	7 days
CEM I	315	350	375
High early strength PC	370	380	390
50% PC + 50% GGBS	240	300	325
30% PC + 70% GGBS	190	240	265
70% PC + 30% FA	250	275	300

2.2.5. Cracking

The presence of cracks substantially modifies the transport properties of concrete. The kinetics of different transport processes vary due to the presence of cracks. In uncracked concrete, transport processes are related to concrete water filled porosity, while in cracked concrete, it is related to the crack properties. Parameters such as crack width and shape, crack density, and degree of connectivity, as well as the crack origin, govern the transport mechanism in cracked concrete (Alexander, Ballim & Beushausen, 2009).

In water retaining structures, thermal and shrinkage cracks vary from small internal micro-cracks occurring due to thermal and shrinkage differences to large cracks caused by poor construction practices, errors in design and detailing, and undesirable interaction with the environment. Cracks do affect durability by allowing the ingress of aggressive agents for concrete deterioration.

2.3. Cracking in concrete

Cracks affect the service life of concrete structures by allowing ingress of aggressive agents (carbon dioxide, chlorides, softwater, or sulphates, amongst others) that shorten the initiation time to reinforcement corrosion. The water scarcity in South Africa calls for water retaining structures to perform with respect to strength and

seepage, thus, crack control is essential to maintain water-tightness for durability and corrosion protection of reinforcements.

Cracking in water-retaining structures occurs due to the restraint of thermal differences and differential shrinkage resulting from cement hydration and cast layers of concrete cast differently. The extent and distribution of the cracks significantly affect the service lives of structures like water-retaining structures whose sole purpose is to store and retain water (Ballim & Graham, 2009).

2.3.1. Thermal cracking mechanism

Cement hydration can cause high-temperature changes as high as 85°C under adiabatic conditions in mass concrete structures (ACI Committee 201, 2001). These high-temperature changes create thermal stresses within the concrete. The development of thermal stresses is dependent on the degree to which free thermal expansion and contraction of the structure are restrained. The forms of restraints are classified as either external or internal (Klemczak et al., 2017).

Internal restraint results from a non-uniform distribution of temperature in the hardening concrete (Figure 2-3). As cement hydrates, it initially generates heat at a rate greater than the heat loss to the environment, thus causing an increase in the temperature of the concrete. As the rate of heat generation progressively reduces, the heat loss to the environment becomes dominant thus, the concrete cools and contracts. If the concrete is unrestrained and fully insulated (i.e., preventing temperature differentials and internal restraint) the concrete would expand and contract without creating any stresses. However, in practice partial restraint is always present leading to the development of stresses. If the concrete properties were constant, a restrained element would generate compressive stresses during heating and relieve these stresses during cooling. The elastic modulus of concrete changes considerably during the first few days after casting, being relatively low during the heating period compared with the value during cooling. For a given magnitude of restrained thermal strain, the compressive stresses generated during heating are lower than the tensile stress generated during cooling, resulting in a residual tensile stress at the end of the heat cycle. This restrained movement induces stresses in the concrete, which can cause cracking (Bamforth, 2018).

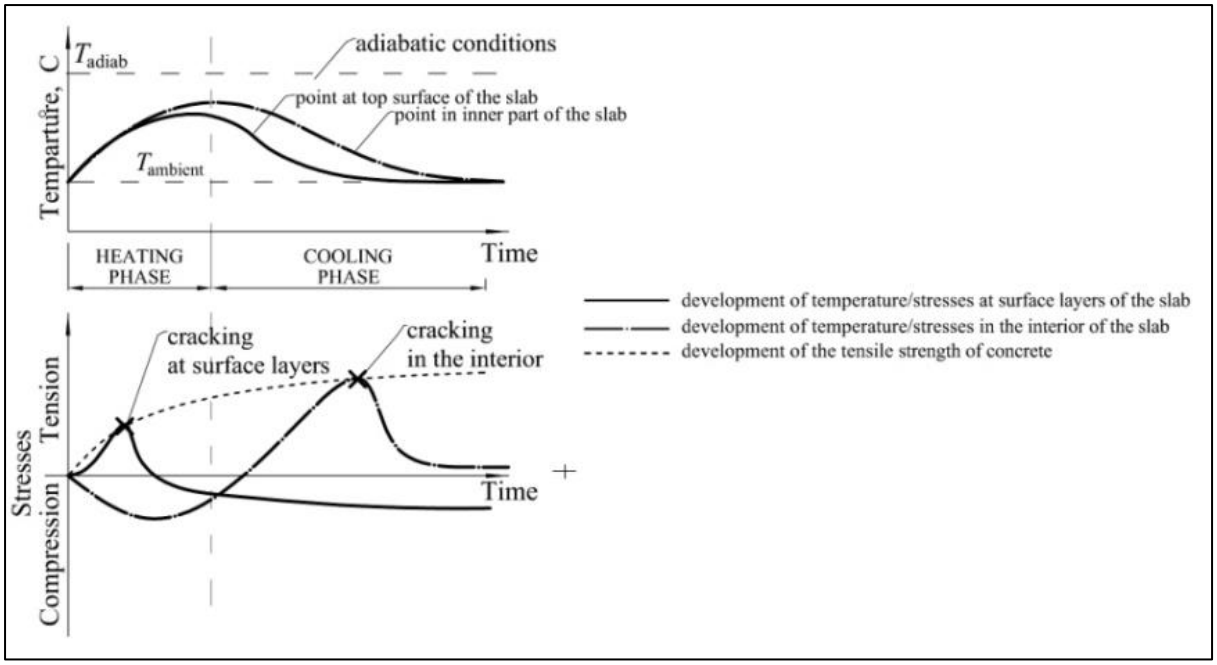

Figure 2-3: Development of crack in mass concrete as a function of temperature (Klemczak et al., 2017)

External restraint occurs when new concrete is cast against a rigid structure. Tensile stresses are induced during the cooling phase of the new concrete as a result of restrained contraction by the mature concrete layer (Figure 2-5). If these stresses exceed the tensile strength of the concrete, cracks will form on the new concrete layer starting from the bottom and progressing upward throughout the concrete section (Ballim & Graham, 2009).

It is worth noting that in some cases the restrained tensile strain developed may be insufficient to cause early-age thermal cracking, but may contribute to strains that cause cracking in the longer term. Thus, it is important to recognise the significance of these residual strains during the design process. It is also important to recognise other deformations that may be occurring during the early heat cycle, in particular autogenous shrinkage that occurs to some degree in all structural concrete (Bamforth, 2018).

2.3.2. Shrinkage cracking mechanism

Shrinkage is the change in the volume of concrete over time due to the effect of the hydration of cement and the loss of water to the environment. The moisture loss, if not controlled in large surface applications, can cause cracking. In concrete, free shrinkage strain of concrete usually exceeds the tensile strain capacity and restrained concrete will crack. Cracking due to shrinkage result in cracks which are unexpected

and at random locations. Such cracking may be aesthetically unacceptable and is undesirable from the point of view of durability. Thus, in liquid-retaining structures, cracks allowing leakage are unacceptable, and special design and construction precautions should be taken to control cracking in these structures. Design codes provide guidance on acceptable crack-widths for different exposure conditions and on control of cracking (Figure 2-4).

Restraints in shrinkage cracking mechanism of concrete are internal and external. Internal restraint is offered by aggregate and reinforcement, resulting in micro-cracking at the aggregate paste interfaces and tension being induced in the concrete with corresponding compression stresses in the steel. Furthermore, internal type of restraints is created by uneven drying of the concrete. The inner core dries more slowly than the outer zones and thus restrains the surface shrinkage, and this may lead to surface cracking (Alexander & Beushausen, 2009).

External restraint is caused when new concrete is bonded to an older substrate, or when friction operates between a member and its base, for example in concrete pavement slabs. Such external restraint frequently leads to cracking. Particular attention should be paid to the problem of controlling shrinkage cracking in thin reservoir walls which are cast onto existing large bases. The function of shrinkage steel in such cases should be to distribute the cracks and limit their widths. Tensile stresses due to restrained shrinkage are relieved to some extent by creep. This might result in less cracking, or alternatively cracking might occur later (Alexander & Beushausen, 2009).

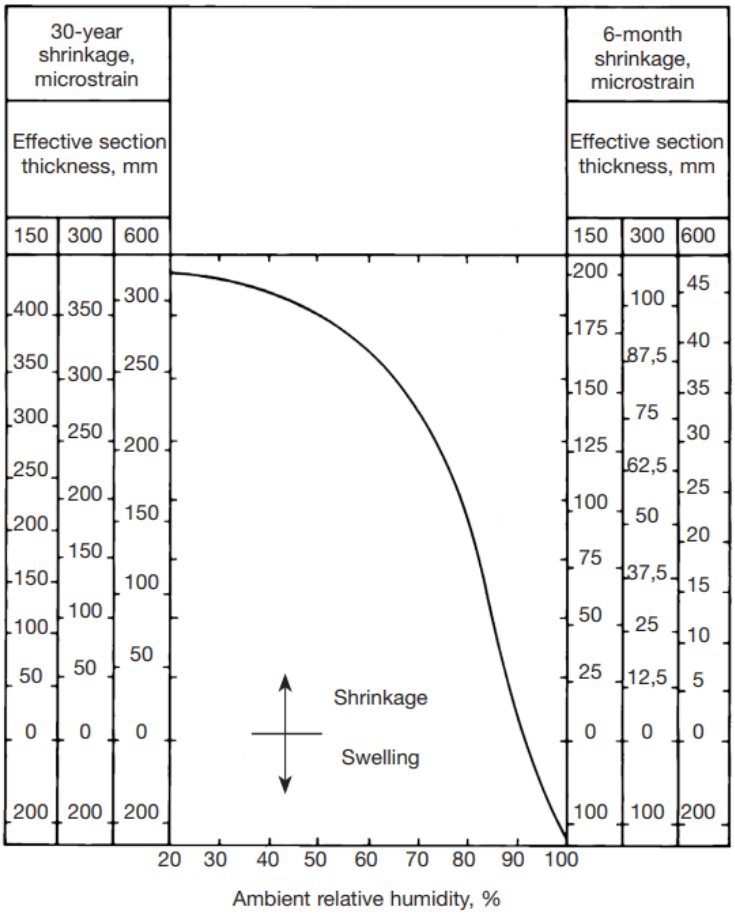

Figure 2-4: Typical drying shrinkage of normal-density concrete

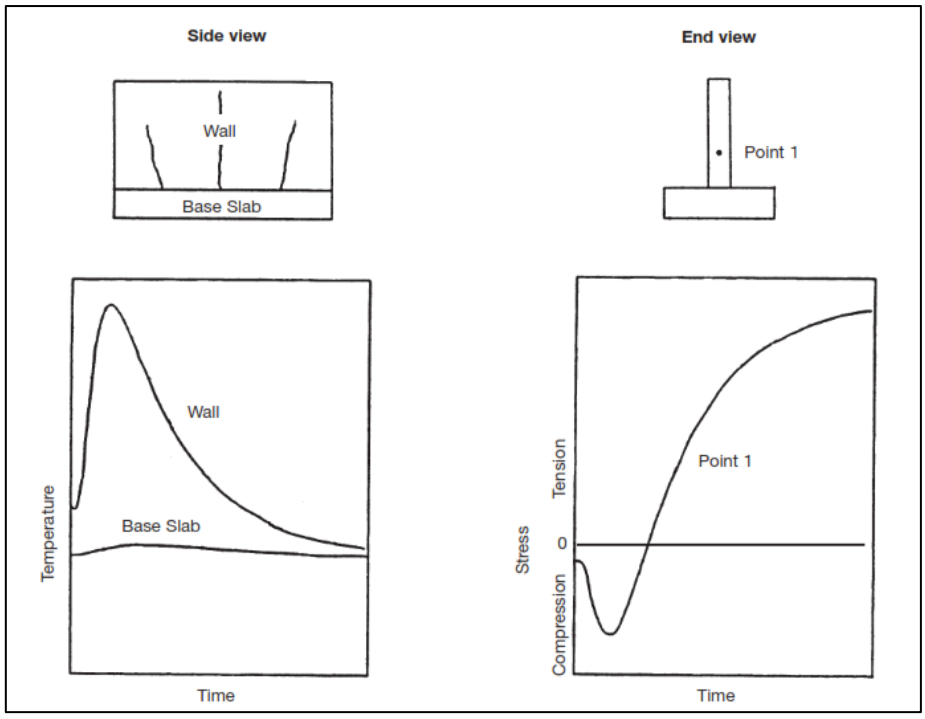

Figure 2-5: Development of stresses in a concrete wall as a result of external restraint by the previously cast base slab (Ballim & Graham, 2009)

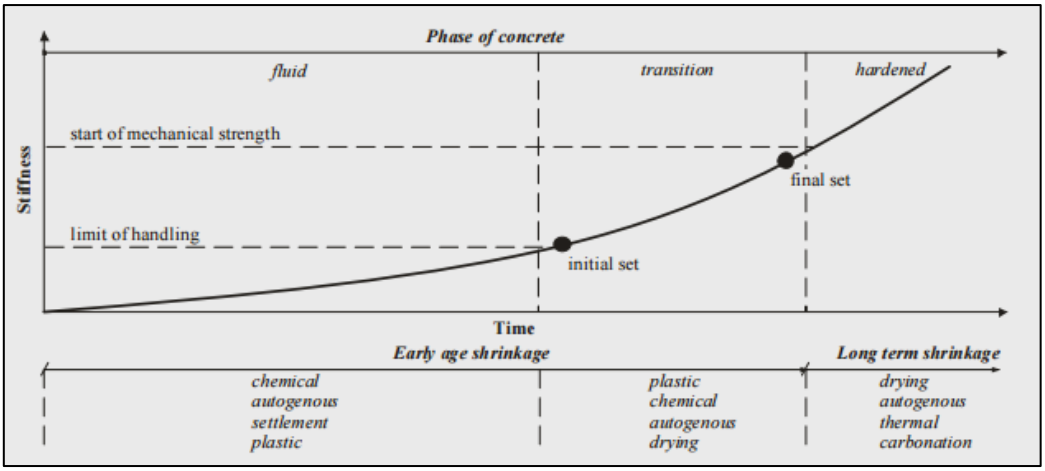

Figure 2-6: Types of shrinkage (Mircea & Faur, 2012)

Shrinkage occurs in different forms as autogenous, carbonation, plastic, and drying shrinkage. Autogenous shrinkage is the volume reduction caused by the internal consumption of water due to the cement hydration process. Carbonation shrinkage is the volume reduction occurring over an extended period caused by carbon dioxide and hardened cement paste reaction. Carbonation shrinkage is severe in intermediate humidity, where moisture content is available for chemical reactions. Drying shrinkage is the more pronounced shrinkage occurring due to moisture loss to the environment (Alexander & Beushausen, 2009).

Important to note, adequate moist-curing of concrete delays the onset of shrinkage and increases the tensile strength of the concrete. Furthermore, the elastic modulus of the concrete also increases with the period of curing, thus stresses resulting from restrained shrinkage strains are likely to be higher. The likelihood of cracking will depend mainly on potential shrinkage, relaxation properties, elastic modulus, and tensile strength of the material, as well as the degree of restraint.

Measures to reduce shrinkage-induced cracking include the following:

a) Low water content and binder content consistent with strength and durability requirements should be used in mix design.
b) Use of strategically placed joints to accommodate shrinkage movement and control cracking.
c) Correct construction practice such as minimising differential shrinkage between adjacent members.
d) Application of proper curing methods.

e) During mass concreting, or constructing during hot weather, precautions should be taken to limit the heat build-up in the concrete.

2.4. Crack self-healing

Cracks affect the serviceability of the water-retaining structures when leakage under high hydraulic heads become more pronounced (Zhang et al., 2018). Permeability has then become a vital durability indicator for cracked concrete. The concept of self-healing promotes reduced permeability of concrete over time which translates to improved durability (Coppola, Coffetti & Crotti, 2018).

The self-healing of cementitious materials can be defined as “any process by the material itself involving the recovery and hence an improvement of a performance after an earlier action that had reduced the material's performance” (Rooij et al., 2013). Self-healing was first evidenced in fractured hydraulic structures by the French Academy of Sciences in 1836 (Palin, Wiktor & Jonkers, 2015).

Cementitious materials were found to have the innate ability to self-heal under the required conditions (Rooij et al., 2013). Continuing hydration reaction and the swelling of existing hydrated products in the crack area blocked the crack pathways inhibiting the ingress of aggressive ions. The healing of the concrete cracks achieved a water-tightness matrix. The abrasion between crack surfaces contributed to the cracked concrete's compressive strength restoration and stiffness restoration (Huang et al., 2016).

Self-healing concept is one of the maintenance-free methods which promotes performance recovery (Figure 2-7) and directly saves maintenance and repair costs whose operations are usually laborious and expensive (Figure 2-8 and Figure 2-9). The service life of concrete structures can be prolonged since minimal external interactions are required. The reduction of maintenance operations over the service life of buildings is essential in realizing any concrete structures.

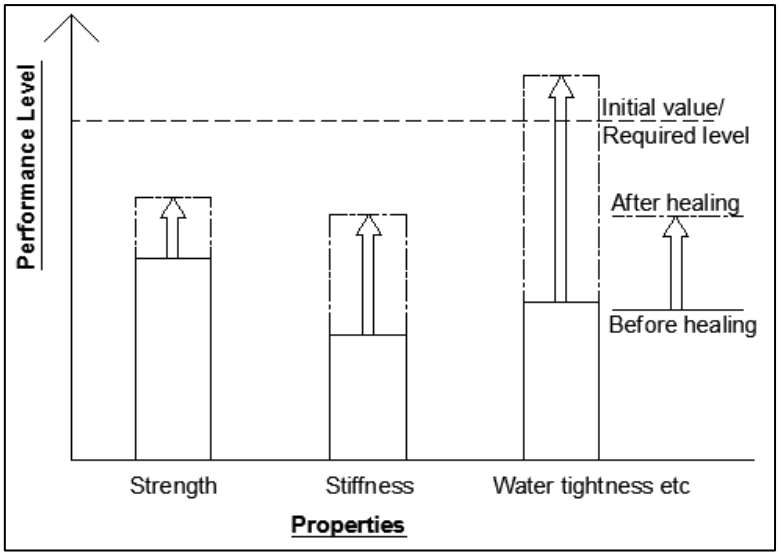

Figure 2-7: Performance recovery by a healing function (Rooij et al., 2013)

The self-healing of cementitious materials can be divided into two categories: autogenic and autonomic self-healing. Autogenic self-healing describes the self-healing process of a cementitious material whose recovery utilizes its generic materials. Autonomic self-healing describes the self-healing process whose recovery uses engineered additions (Rooij et al., 2013).

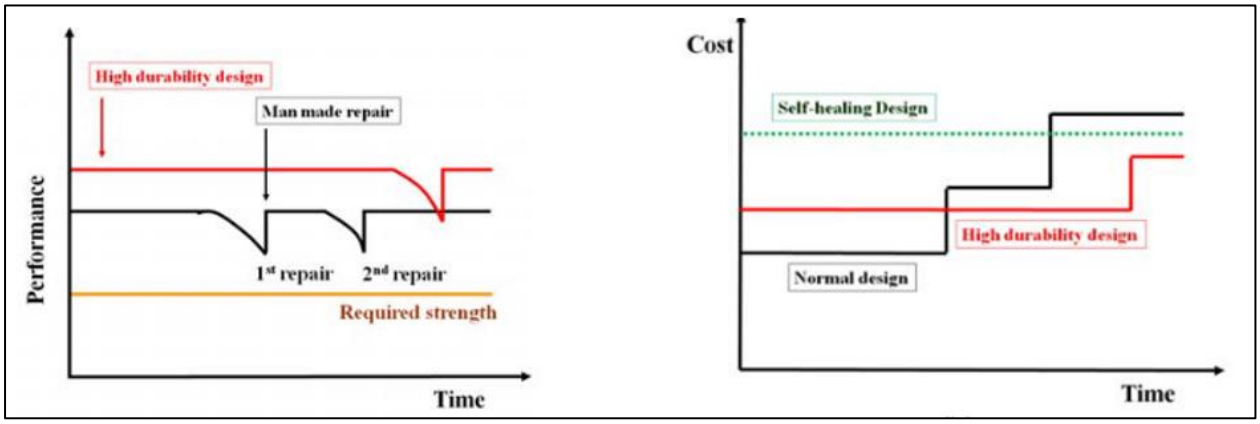

Figure 2-8 A graph of performance and cost over time for normal structures (black line) against self-healing concrete structures (Ahn & Kishi, 2010)

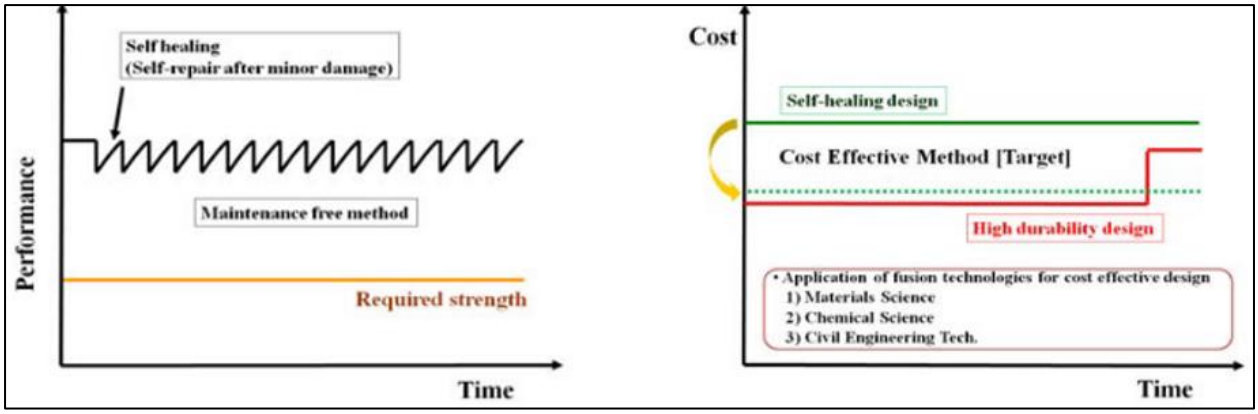

Figure 2-9: A graph of performance and cost over time for high-durability design structures (red line) against structures made with self-healing concrete (Ahn & Kishi, 2010)

2.4.1. Autogenic self-healing

The autogenic self-healing mechanism can be of chemical, mechanical, and physical phenomenon (Figure 2-10). The chemical phenomenon appears in two aspects. Firstly, by carbonation process on the crack area. Calcium carbonate, a by-product of calcium hydroxide and dissolved carbon dioxide is deposited on the crack area, healing the crack. Secondly, the additional formation of hydration products in the crack area is due to residual clinker and moisture in the environment. The mechanical phenomenon is promoted by water impurities or concrete particles resulting from crack spalling blocking the cracks' pathways. The physical phenomenon results from the swelling of hydration products in water within the crack area (Coppola, Coffetti & Crotti, 2018).

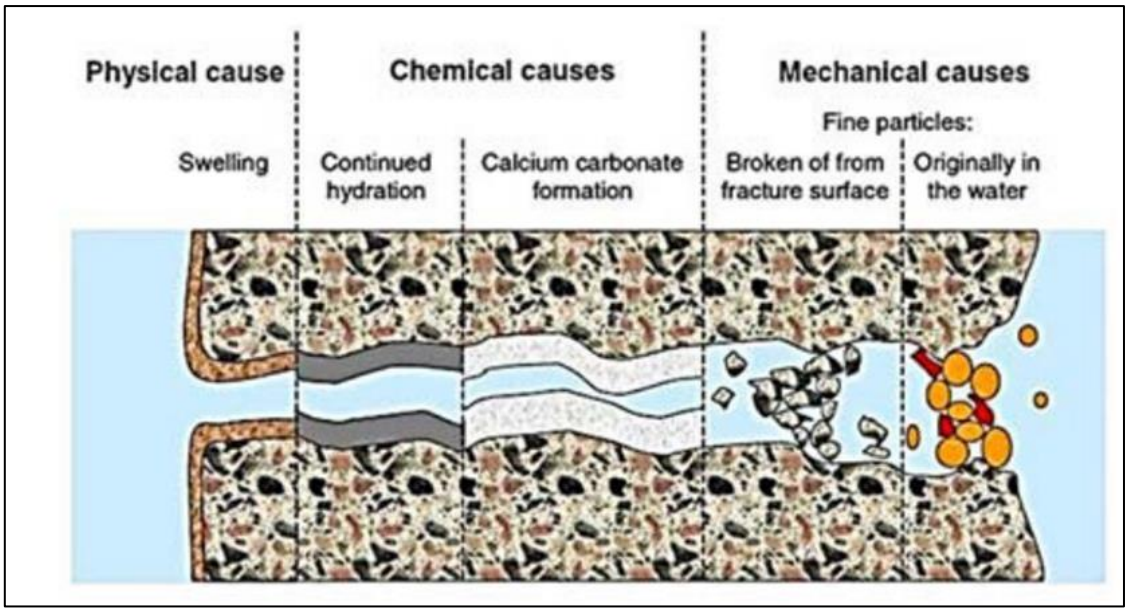

Figure 2-10: Mechanisms of autogenic self-healing (Rooij et al., 2013)

The effectiveness of autogenic self-healing is restricted to small crack widths of up to 0.2 mm (Palin, Jonkers & Wiktor, 2016), moisture availability in the crack area, crack closure induced by stress due to loads, and mix composition. Concrete with higher cement content promotes self-healing through continued hydration (Yang, Yang & Li, 2011; Qiu, Tan & Yang, 2016; Sangadji, 2017; Suleiman & Nehdi, 2018).

Autogenic self-healing suffers several setbacks. Self-healing becomes unreliable as the mix compositions of concrete are highly variable. High cement content concrete promotes healing but blended cement limits the availability of unhydrated cement and calcium hydroxide necessary for self-healing. Extenders such as blast furnace slag, silica fume, and fly ash utilize the calcium hydroxide from hydration reactions to form other hydration products (Sangadji, 2017).

The presence of moisture is necessary for autogenic self-healing. The efficiency of autogenic self-healing is rendered ineffective on concrete with limited contact with moisture. The quantification of the autogenic self-healing mechanism over a specified period proves difficult as different forms of self-healing co-exist (Sangadji, 2017). To overcome the challenge and have better control of the healing mechanisms, engineered healing agents are utilized.

2.4.2. Autonomic self-healing

Autonomic self-healing utilizes healing agents to induce self-healing of cracks. The mechanism is modelled after repairing damaged skins and tissues on animals, trees, and humans. Minor wounds are easily treated by the body, which translates to autogenic healing, but more significant wounds require outside assistance for complete recovery (Rooij et al., 2013).

2.4.2.1. Approaches to autonomic self-healing

Joshi et al., (2017) proposed three different approaches to supply the healing agents within the concrete to promote self-healing properties. The approaches are described based on the delivery mechanisms, which are vascular-based, capsule-based, and intrinsic-based. Vascular-based healing agents are filled in hollow channels with an internal diameter ranging from 0.8 mm to 4 mm. The channels are embedded within the concrete matrix and release the healing agents when the crack ruptures the hollow channels releasing the healing agents (Figure 2-11a). Self-healing using hollow

channels is similar to the capillaries in an animal circulatory system, with blood flowing out of platelets on a wound to induce healing (Wu, Johannesson & Geiker, 2012).

Capsule-based healing agents (Figure 2-11b) are stored in glass capsules which are either spherical (with diameters ranging from 5 μm up to 5 mm) or cylindrical capsules (with diameters ranging from 0.8 mm up to 5 mm). The capsules are embedded in a concrete matrix and are ruptured on the crack formation releasing the healing agents initiating self-healing (Restuccia et al., 2017).

In the intrinsic approach, the healing agents are directly embedded within the concrete matrix during mixing. The healing materials such as crystalline admixtures, calcium sulfo-aluminate-based expansive additives (CSA), calcium hydrogen phosphates, carboxylic acid-based admixtures, and crystalline admixtures (CA) possess a latent self-healing functionality triggered by the crack formation and induce self-healing (Figure 2-11c). This study will focus on the self-healing of crystalline admixtures.

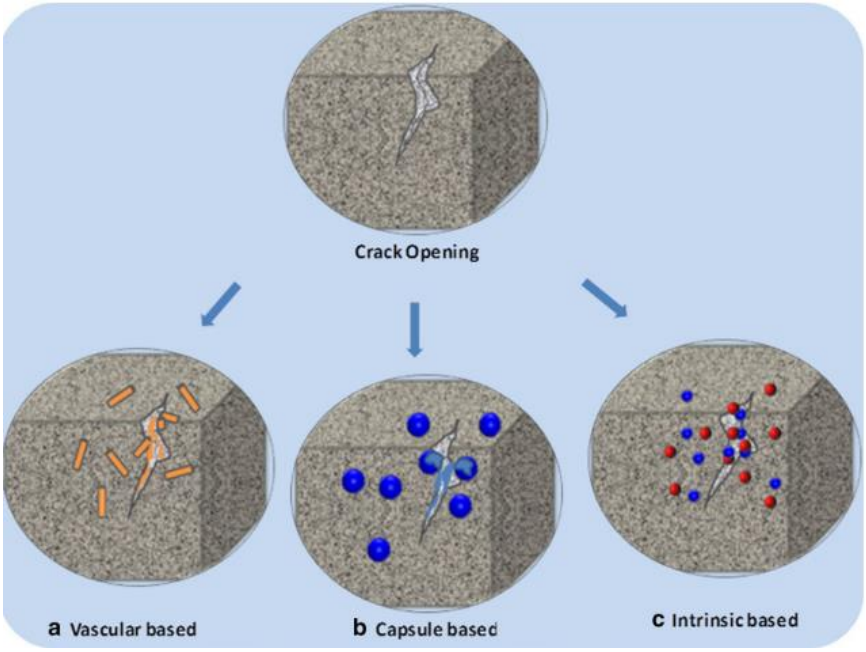

Figure 2-11: Approaches to autonomic self-healing (Joshi et al., 2017)

2.5. Self-healing based on crystalline admixtures

2.5.1. Crack healing mechanism

Crystalline admixtures are hydrophilic compounds that react with water and cement particles to form calcium silicate hydrates and pore-blocking precipitates in the existing microcracks and pores (Phelan et al., 2010). The resulting crystalline deposits become integrally bound, with the hydrated cement paste becoming a permanent part of the

concrete structure. Furthermore, the crystalline deposits can lie dormant in the concrete and activate once cracks develop over the service life of the concrete inducing autonomic healing in the presence of moisture (Phelan et al., 2010).

$$3\mathrm{CaO}.\mathrm{SiO_2} + \mathrm{M_XR_X} + \mathrm{H_2O} \rightarrow \mathrm{Ca_XSi_XO_XR}.(\mathrm{H_2O})_\mathrm{X} + \mathrm{M_XCaR_X}.(\mathrm{H_2O})_\mathrm{X} \qquad \text{Equation 2-1}$$

The self-healing mechanism is under debate by different researchers. Other studies have concluded that the crystalline admixtures react with calcium hydroxide, a by-product of cement hydration, to precipitate calcium carbonate as the primary healing product (Sisomphon, Copuroglu & Koenders, 2012; Roig-Flores et al., 2016). Material characterization techniques can be used to understand the crystallographic information of the different healing products before and after incorporation into concrete.

2.5.2. Factors affecting crystalline admixtures crack healing

2.5.2.1. Crack width

Crack width significantly affects the effectiveness of crack self-healing. Narrow cracks are likely to be healed entirely due to the small space of cracks to be filled. As a result, fewer reaction products of self-healing are needed to fill a crack with a small width. Wider cracks need a longer time to be effectively healed (Meharie, Kaluli & Abiero-Gariy, 2017).

Coppola, Coffetti & Crotti, (2018) achieved 50% of healing with crack healing measuring up to 0.3 mm after adding 1% by cement mass of carboxylic-acid-based admixture. Roig-Flores et al., (2015) achieved 90% healing in cracks measuring 0.3 mm after 42 days of curing. However, inducing healing to a crack width greater than 0.4 mm proved ineffective as the increase in water flow through a crack caused random crystals migration in concrete.

2.5.2.2. Age at pre-cracking

The age of pre-cracking plays a vital role in the self-healing of cracks. The presence of unhydrated cement present in concrete with a low water-to-cement ratio becomes the dominating mechanism for young concrete. Also, blended cements containing latent hydraulic binders have slower hydration than Ordinary Portland cement, which guarantees the presence of unreacted binder material in concrete.

Qian et al., (2015) results for the self-healing potential of early-age cracks indicated excellent repairing ability for small cracks formed at an early age of 7 days. The repair effect reduced significantly with the increasing cracking ages of 14, 28, and 60 days. This was attributed to continuous hydration over time (Qian et al., 2015). Furthermore, Luo, Qian & Li, (2015) results indicated that the crack healing ratio of specimens dropped significantly along with the extension of cracking age. The hydration degree and internal structure of concrete in different cracking age affect the self-healing ability as the cement hydration degree increases thus decreasing the cement paste water filled porosity.

2.5.2.3. Healing conditions and duration

Exposure conditions have the most determinant factor in self-healing efficiency. Different healing schemes have established the response of crystalline admixtures on crack self-healing, simulating practical applications (Figure 2-12). Exposure of cracks in the presence of moisture in most self-healing techniques produces a significant amount of healing (Van Mullem, et al., 2018). Self-healing is most effective in narrow cracks of up to 0.30 mm wide when permanently immersed in water, while specimens under the wet and dry cycle exposure conditions have lower healing and closing capabilities, even for crystalline specimens.

Roig-Flores et al., (2015) investigated self-healing incorporating crystalline admixtures on four healing exposure schemes. The resulting self-healing efficiency in order of decreasing permeability rate obtained was water immersion (around 90%), water contact (around 80%), humidity chamber (around 15%), and air exposure (0%).

Roig-Flores et al., (2016) investigated crack self-healing of concrete with crack widths below 0.3 mm in three healing exposure conditions: water immersion, air exposure, and wet/dry cycles to identify healing efficiency. After six months, complete healing was observed for specimens permanently or periodically immersed in water (Figure 2-13). Complete self-healing was achieved for water-immersed specimens even under repeated cracking and healing cycles up to one year after the first cracking.

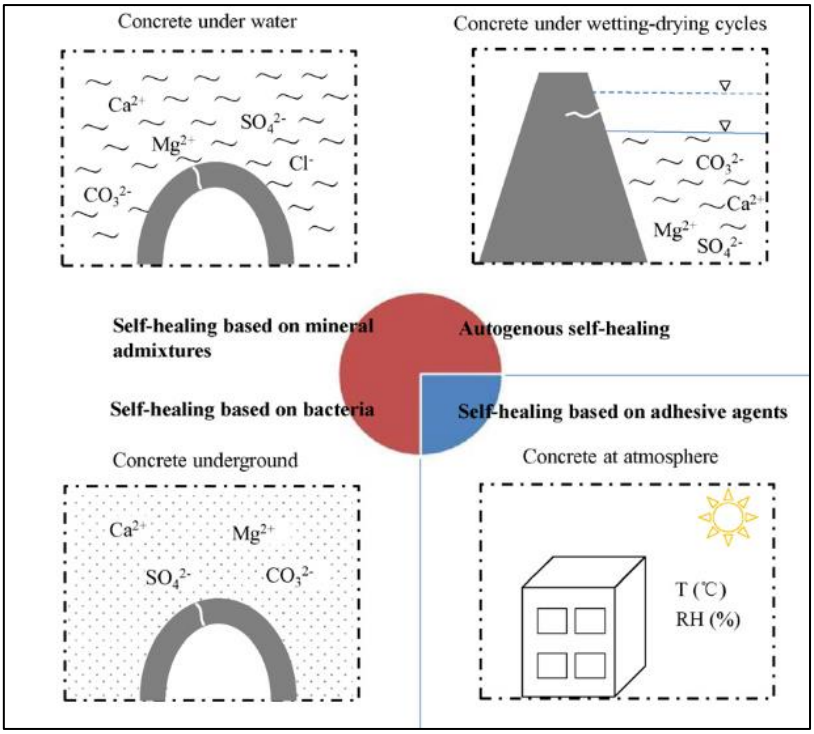

Figure 2-12: Different exposure conditions for crack self-healing (Huang et al., 2016)

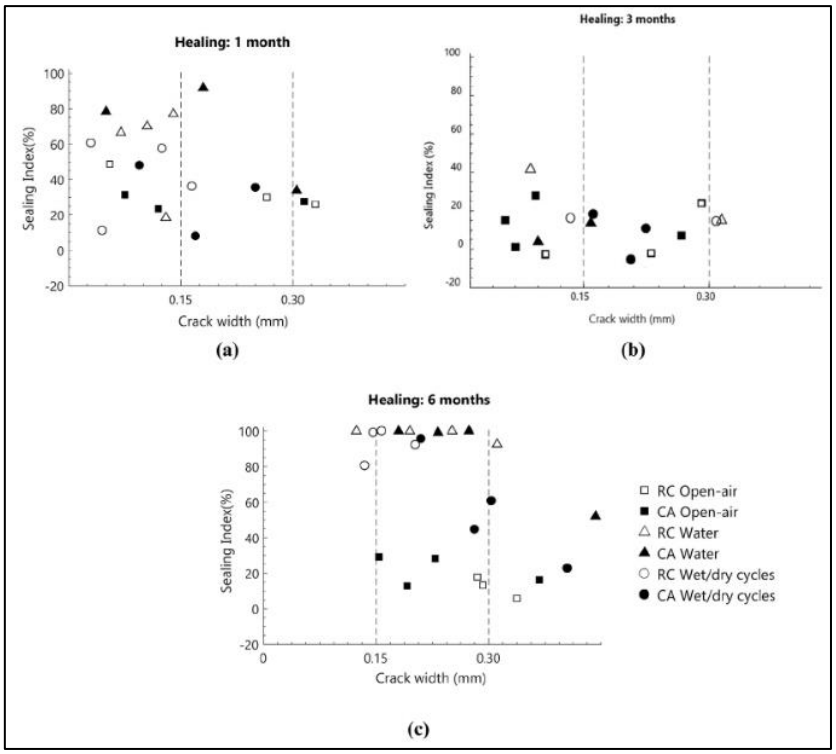

Figure 2-13: Self-healing Index (%) on different curing exposures as a function of crack width, exposure conditions, and mix design (Cuenca, Tejedor & Ferrara, 2018)

2.5.3. Tests used to examine and quantify crack self-healing

Evaluation of crack self-healing of cementitious materials requires understanding different initial and boundary conditions that can affect the obtained results. Two stages are involved in the assessment of crack self-healing. Firstly, the induction of a controlled crack on a specimen is to be investigated. The crack is induced in the form of either a localized crack or multiple cracking patterns. Secondly, the evaluation of crack closure and the recovery of durability and mechanical properties with respect to the undamaged specimens undergoing the same curing conditions. The comparison is vital to differentiate between self-healing and natural time-gain and ageing of mechanical properties (Van Mullem, et al., 2018).

Induction of cracks is done mechanically to control the opening of the crack using three or four-point bending tests for specimens used to investigate recovery of mechanical properties (SANS 6253, 2006). In controlling a position in which crack has to originate, a notch has to be introduced in a sample (Van Mullem, et al., 2018). The tests are commonly employed for plain or reinforced concrete. Compression tests have been employed in studies on the recovery of compression strength after severe loading (Van Mullem, et al., 2018). Tensile splitting tests are used to pre-crack specimens used to investigate the recovery of durability properties. The tests are used to comply with the standards related to durability properties (SANS 3001-CO3-1, 2015; SANS 3001-CO3-2, 2015). Park & Choi, (2018) employed tensile splitting tests to quantitative evaluate crack self-healing in cement-based materials by absorption tests.

Tests used to evaluate the self-healing of cementitious materials can be grouped into two categories (Figure 2-15). Firstly, are the tests are used to observe the self-healing mechanism. Scanning Electron Microscopy (SEM) and X-ray Fluorescence (XRF) tests conducted as per ASTM E1621-13, (2013) have been successfully utilized to examine the self-healing products. Secondly, are the tests used to quantify the crack self-healing. These are sub-divided into tests evaluating crack closing, recovery of durability properties, and recovery of mechanical properties. The use of a digital photographic camera and crack meter is suitable for assessing the crack closing progress. Permeability measurements and durability index tests are used to quantify the recovery of durability properties. Compression and flexural strength tests are some of the tests used to quantify the recovery of mechanical properties (Rooij et al., 2013). The recovery of mechanical properties has to be evaluated through the same test

employed for pre-cracking (Ferrara, Krelani & Carsana, 2014; Muhammad et al., 2016; Van Tittelboom et al., 2016; Van Mullem, et al., 2018).

2.5.3.1. Evaluating crack closing

Crack closure is the most direct manifestation of self-healing, and thus it is a necessary step for verifying crack self-healing (Van Mullem, et al., 2018). Standard tests employed to verify and quantify crack closure are the photographic camera and crack meter, respectively.

a) Photograph camera

   Photography cameras can take pictures periodically to monitor the crack characteristics in specimens during testing and after healing. The photogrammetry evidence can be used to verify crack closure as healing is progressing.

b) Crack meter

   The crack meter measures the closing of a crack to an accuracy of 0.1 mm.

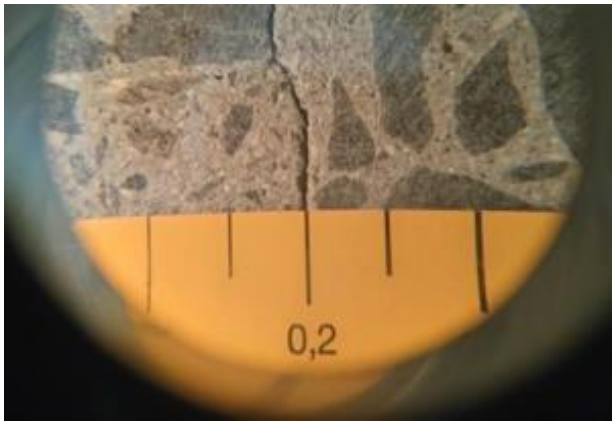

Figure 2-14: Crack width measurement using crack meter (Sohawon, 2018)

2.5.3.2. Scanning electron microscopy (SEM)

SEM tests are used to reveal topography, morphology, composition, and crystallographic information of the precipitates inside a healed crack. Characterization of the healing products helps to understand the nature of the healing mechanism. Analysis of the self-healing products precipitated on a cracked surface requires the healed products to be separated from the original cement matrix (Park & Choi, 2018). However, cracks in concrete are irregular, and the self-healing products on the cracked surfaces cannot be obtained in their original states. SEM test allows the analysis of fractured specimens without extracting the healed products, making it

suitable for repeated observations over the healing duration (Cuenca, Tejedor & Ferrara, 2018).

2.5.3.3. Recovery of durability properties

Crack self-healing is evaluated by comparing the uncracked reference specimens, pre-cracked specimens, and healed specimens.

a) Water permeability test

This test involves subjecting specimens to water pressure and evaluate the flow of water going through the cracks. Roig-Flores et al., (2015) successfully used the water permeability test to study the effect of crystalline admixture on different environments. The testing is based on the British standard test to measure water depth penetration through concrete specimens (BS EN 12390-8, 2009). However, instead of measuring the depth penetration, water flow readings are taken. The self-healing efficiency was evaluated by comparing water flow during a 5 min testing time before and after healing. The same specimen was used to compensate for the uncertainties due to the variability of crack width. Asensio, et al., (2018) proposed the following equation to evaluate self-healing efficiency which uses the same specimen and compares the water flow through it before and after healing.

$$\mathrm{SH} = \frac{\mathrm{W_{initial}} - \mathrm{W_{final}}}{\mathrm{W_{initial}}} \qquad \text{Equation 2-2}$$

Where;

SH = Self-Healing index,

$W_{initial}$ = amount of water passing through the target specimen before healing, and

W_{final} = amount of water passing through the target specimen after healing.

b) Oxygen permeability index test (OPI)

Oxygen permeability test has been employed in assessing the overall microstructure and macrostructure of the concrete. It is particularly sensitive to macro-voids and cracks, which act as short-circuits for the permeating gas. Morimoto et al., (2009) performed air permeability tests on cementitious specimens, before cracking, immediately after cracking and after crack healing.

Comparing permeability coefficients between uncracked reference specimens to the cracked and healed specimens provided a basis for evaluating self-healing efficiency.

c) Water sorptivity index test

Sorptivity is an indicator of the ability of concrete to absorb and transmit liquid by capillary suction. Measurement of the capillary water absorption for cracked concrete specimens with and without healing can evaluate self-healing efficiency. Rooij et al., (2013) proposed the following equation to evaluate self-healing efficiency from sorptivity test results.

$$SH = \frac{S_{unhealed} - S_{healed}}{S_{unhealed} - S_{uncracked}} \quad \text{Equation 2-3}$$

Where;

SH = Self-Healing index,

$S_{unhealed}$ = sorptivity index for the cracked and unhealed specimen,

S_{healed} = sorptivity index for the cracked and healed specimen, and

$S_{uncracked}$ = sorptivity index for the uncracked reference specimen.

However, the reliability of this technique is in question. If the capillary rise in the partially healed crack is higher than the initially wider crack, the desirable effect of partial healing may not be noticed from weight measurements (Van Mullem, et al., 2018).

2.5.3.4. Recovery of mechanical properties

Recovery of mechanical properties is measured through the structural behaviour of a healed cracked cross-sections specimen. The test performed for pre-cracking is repeated after the scheduled healing period to evaluate self-healing efficiency. Comparing the mechanical property at the moment of pre-cracking and after the planned healing period is used to indicate self-healing efficiency (Van Mullem, et al., 2018).

a) Flexural strength test

Ferrara, Krelani & Carsana, (2014) evaluated the self-healing efficiency by comparing the bending stress exhibited by the same specimen during the pre-cracking stage and at the end of the prescribed curing period in the cracked

state using a three-point bending test. The recovery of bending stiffness and load-bearing capacity was instrumental in quantifying suitable self-healing indices for the analysed mechanical properties.

b) Compressive strength test

Compression tests are employed to assess the self-healing performance of cement-based materials. The test induces a diffused state of damage, compared to an attained fraction of the compressive strength after healing (Van Mullem, et al., 2018).

Mechanical properties of concrete evolve with time, even without healing, especially for specimens subjected to conducive healing conditions (e.g., water immersion, high relative humidity). Differentiating between self-healing and continuing hydration is vital; thus, the availability of uncracked specimens subjected to the same curing conditions as the cracked specimens can provide a base of reference during test results analysis.

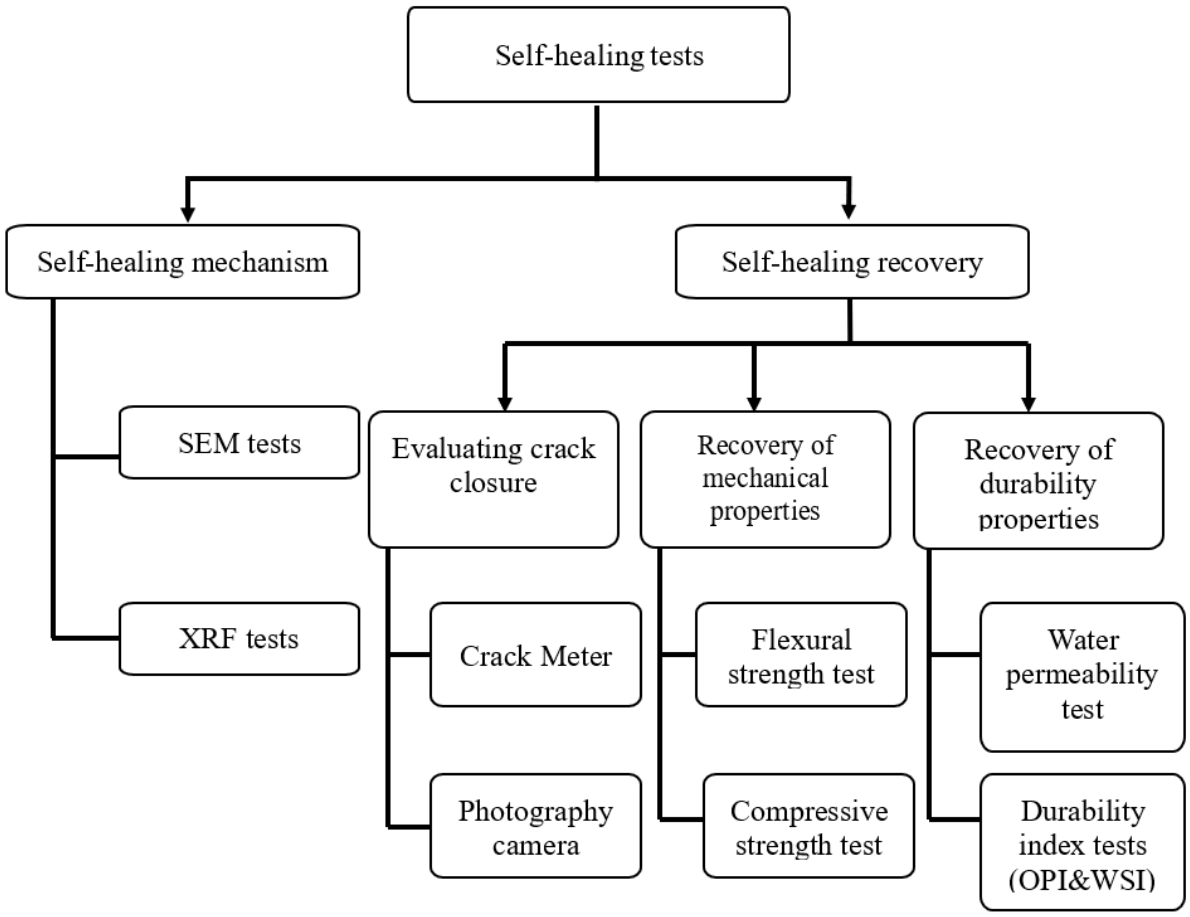

Figure 2-15: Categories of self-healing tests based on Rooij et al., (2013)

2.6. Summary

This chapter presented the overview of self-healing of concrete using crystalline admixtures which are directly incorporated in the concrete during mixing. Their underlying mechanism has been a subject of debate. Crystalline admixtures react with calcium hydroxide, a by-product of cement hydration, to precipitate calcium carbonate as the primary healing product (Sisomphon, Copuroglu & Koenders, 2012; Roig-Flores et al., 2016). Other studies have concluded that crystalline admixtures are hydrophilic supplementary cementitious materials that react with water and cement particles to form calcium silicate hydrates and pore-blocking precipitates in the existing microcracks and pores (Phelan et al., 2010; Wang et al., 2018). Further study is necessary to contribute to the body of knowledge on the mechanism of self-healing.

The evaluation of crack self-healing by crystalline admixtures is done by induction of crack on a specimen to determine crack closure and determine the durability and mechanical properties of concrete specimens after healing (Van Mullem, et al., 2018). The effectiveness of the crystalline admixtures in promote self-healing is affected by crack width induced, the age of pre-cracking, and the exposure conditions.

Roig-Flores et al., (2015) achieved 90% healing in induced cracks measuring 0.3 mm after 42 days of water curing. However, inducing cracks of width greater than 0.3 mm proved ineffective as the water flow through a crack caused random crystals migration in concrete. Qian et al., (2015) results for self-healing potential of early age cracks indicated excellent repairing ability to cracks formed at 7 days. However, effectiveness decreases significantly with the increasing of cracking ages of 14, 28, and 60 days. This was attributed to continuous hydration over time. Exposure conditions have the most determinant factor in self-healing efficiency. Roig-Flores et al., (2016) investigated crack self-healing of concrete with crack widths below 0.3 mm in three healing exposure conditions: water immersion, air exposure, and wet/dry cycles to identify healing efficiency. After six months, complete healing was observed for specimens permanently or periodically immersed in water. Complete self-healing was achieved for water-immersed specimens even under repeated cracking and healing cycles up to one year after the first cracking. The effectiveness of the crystalline admixtures available in the South African market have to be evaluated. Thus, the above aspects provided the basis for further investigation, the details of which are presented in Chapter three (3).

3. Experimental methodology

3.1. Introduction

This chapter presents the scope of the experimental investigation, including materials used, test variables, and a description of the tests conducted. The tests conducted were divided into three categories: characterization tests, durability tests, and strength tests. A summary of the experimental investigation is presented in Figure 3-1.

3.2. Experimental overview

The experimental investigation considered two variables, being two (2) water/binder ratios (w/b of 0.4 and 0.6) and four (4) types of crystalline admixtures. The variables were used to cast ten concrete mixes. The concrete specimens were demoulded after 24 hours and subsequently cured initially in a water bath at 23 ± 2°C for 21 days to simulate good construction practices like retaining formwork. After initial curing, the specimens were cored and cut according to SANS 3001-CO3-1, (2015). The specimens were subjected to load using the three-point loading test to obtain cracked specimens (Figure 3-5). Steel clamps were put along the circumference of the specimens and tightened. Desired crack-width ranges were obtained by monitoring the cracks with a crack meter, and the specimens were cured in a water bath for 28, 56, and 84 days to promote self-healing.

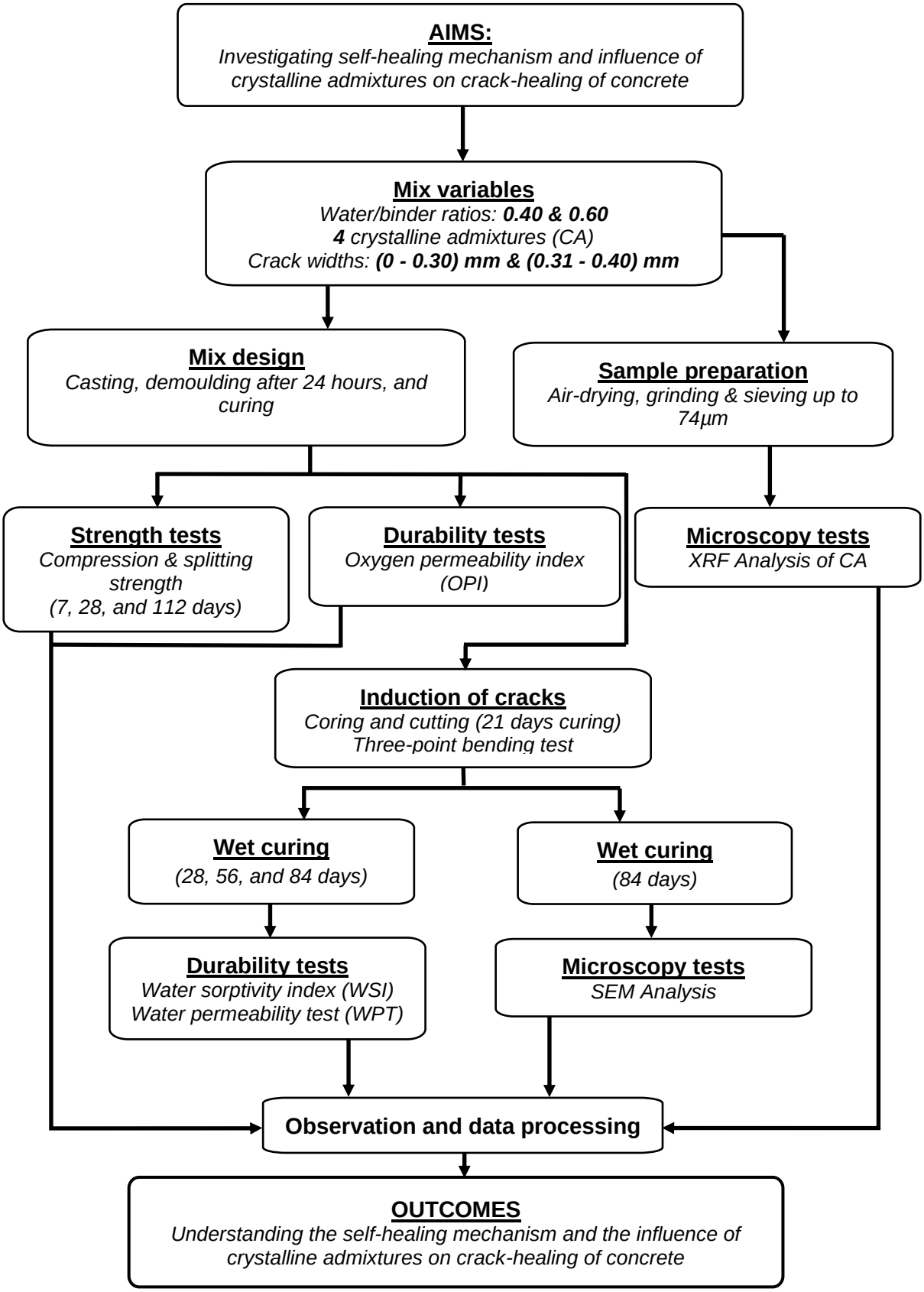

Figure 3-1: Flow chart of the experimental methodology

3.3. Experimental variables

The following variables were used in this study:

a) Two w/b ratios of 0.4 and 0.6. A w/b ratio of 0.4 was selected to represent high-quality concrete, and a w/b ratio of 0.6 was selected to represent low-quality concrete.

b) Four crystalline admixtures were used to represent the some of the most common crystalline admixtures used in construction. The crystalline admixtures were given pseudo names CA-1, CA-2, CA-3, and CA-4 to avoid conflict of interest.

c) Two ranges of crack widths were used. Small crack widths range of 0 – 0.30 mm and larger than 0.30 mm.

3.4. Materials

The following materials were used:

a) Ordinary Portland cement (OPC CEM I 52.5N), supplied by PPC. The OPC was selected to ascertain the influence of the crystalline admixtures on concrete properties.

b) 19 mm greywacke stone was used as coarse aggregate [Crushing density (CBD) = 1490 kg/m^3, particle relative density = 2.72]. The sieve analysis was performed according to SANS 201, (2008), and the grading curves are presented in Figure 3-2. Detailed sieve analysis results are provided in Appendix H.

c) A 60/40 blend of Philippi dune sand and greywacke crusher sand was used as fine aggregates. A portion of the dune sand was replaced with greywacke crusher sand to compensate for the lack of particle size, passing the 150 and 75 µm sieve sizes. Sieve analysis of the fine aggregates was carried out according to SANS 201, and the grading curves are presented in Figure 3-3. Detailed sieve analysis results are provided in Appendix H.

d) Four crystalline admixtures (C.A.) were used in this study. The physical and chemical properties are provided in Appendix I.

e) Chryso® Plast Omega 103 from Chryso Southern Africa was used as a Superplasticiser (SP).

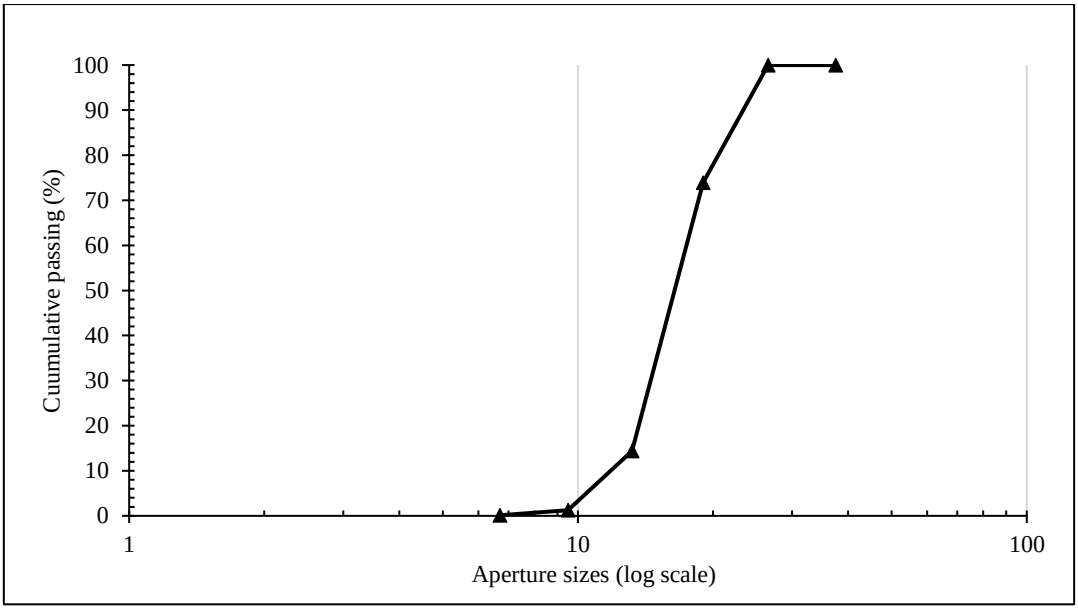

Figure 3-2: Grading curve of 19 mm greywacke stone

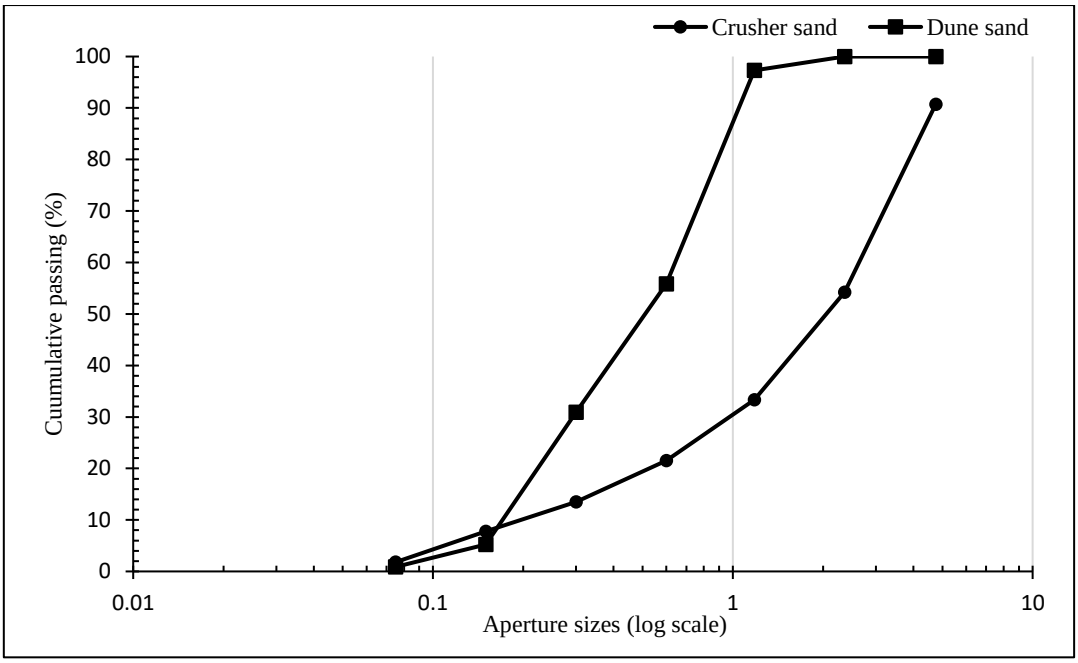

Figure 3-3: Grading curves of fine aggregates

3.5. Experimental procedure

The following testing regime was followed:

a) Mix design, casting, and curing

b) Specimen preparation: coring and cutting

c) Induction of cracks on cut specimens

d) Hardened properties tests: after 7, 28, and 112 days of wet curing

e) Durability properties tests: after 28, 56, and 84 days of wet curing

3.5.1. Mix design

The mix design was based on the volumetric mix design method used by the Cement and Concrete Institute (Addis & Goodman, 2009). Table 3-1 summarises the mix design used in this study.

Table 3-1: Mix design

Constituents (kg/m^3)	Control		CA-1		CA-2		CA-3		CA-4	
	Mix 1	Mix 2	Mix 3	Mix 4	Mix 5	Mix 6	Mix 7	Mix 8	Mix 9	Mix 10
w/b ratio	0.4	0.6	0.4	0.6	0.4	0.6	0.4	0.6	0.4	0.6
Cement (CEM I 52.5N)	463	308	463	308	463	308	463	308	463	308
CA dosage (Addition by mass of cement)	0	0	4.63	3.08	4.63	3.08	4.63	3.08	9.26	6.16
Crusher sand	331	387	331	387	331	387	331	387	331	387
Dune sand	497	580	497	580	497	580	497	580	497	580
Greywacke stone	1020	1020	1020	1020	1020	1020	1020	1020	1020	1020
Water	185	185	185	185	185	185	185	185	185	185
SP	1.39	0.93	1.39	0.93	1.39	0.93	1.39	0.93	1.39	0.93

Note: The dosages of the crystalline admixtures were used as per the technical data sheet of individual suppliers.

3.5.2. Casting and Curing

The concrete mixes were batched and cast in appropriate moulds according to SANS 5861-1, (2006); SANS 5861-2, (2006); SANS 5861-3, (2006). Superplasticiser was used to regulate the workability of concrete. A slump range of 75 - 100 mm was chosen, which corresponds to the workability of general concrete construction.

Curing for uncracked specimens was done by covering with a polythene sheet to prevent moisture loss for 24 hours. The specimens were demoulded and cured in a water bath at (23 ± 2) ^{o}C. Specimens for strength properties testing were cured for 7,

28, and 112 days. Specimens for durability properties testing were cured for 28, 56, and 84 days.

Curing for cracked specimens was done by covering with a polythene sheet to prevent moisture loss for 24 hours. The specimens were demoulded and initially cured in a water bath for 21 days, before extraction of core specimens. Thereafter cracked and stored in water for ages of 28, 56, and 84 days to induce healing (Figure 3-4).

Figure 3-4: Curing of the cracked specimens

3.5.3. Induction of cracks (Three-point bending test)

Prior to induction of cracks, crack widths of up to 0.30 mm were selected to be small crack widths as per the structural use of concrete (SANS 10100-1, 2000). Cracks of widths larger than 0.30 mm were selected to be medium to large crack widths (Roig-Flores et al., 2015).

The proposed methodology for the induction of cracks is based on the flexural strength test of concrete (SANS 5864, 2006). Flexible ties were attached at the top of the specimens to prevent the rupture of the specimens during the crack inducement (Figure 3-5).

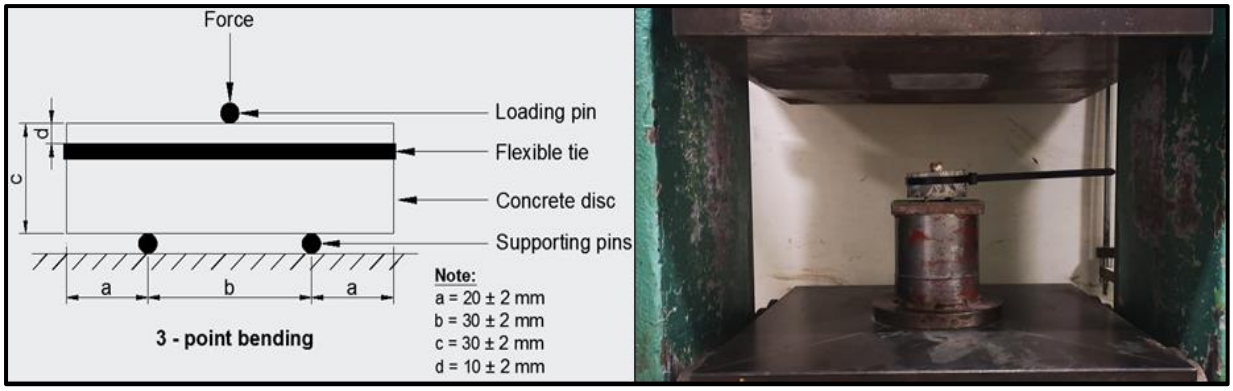

Figure 3-5: Arrangement for three-point bending test based on SANS 5864, (2006).

After inducing the cracks, the specimens were fastened by 75 mm steel clamps along their circumference (Figure 3-6). The steel clamps cause a state of constraint to promote autonomous healing by stabilising the cracked specimens.

Figure 3-6: Steel clamp to introduce the state of constraint in the specimens after induction of cracks

3.6. Test methods

The experimental tests conducted in this study were divided into three categories. Microscopy tests were used to characterize the elements and compounds present in the crack-healed specimens. Strength tests were used to investigate the influence of the crystalline admixtures on the strength properties of concrete, and durability tests were used to investigate the durability properties of the crack-healed specimens.

3.6.1. Microscopy tests

Two microscopy tests were conducted, namely the X-Ray Fluorescence test (XRF) and the Scanning Electron Microscopy-Energy-Dispersive Spectroscopy test (SEM-EDS). XRF was done on powdered specimens of the crystalline admixtures according

to ASTM E1621-13, (2013), while the SEM-EDS tests were conducted on crystalline healing products deposited on the crack area according to ASTM C1723-16, (2016).

3.6.1.1. X-Ray Fluorescence test (XRF)

The XRF test involved analysing the composition of major and trace elements in the specimens by exposing X- rays from an XRF spectrometer. The interaction between the X-ray photons of a spectrometer and atoms of the elements of interest found in the specimen resulted in the emission of X-rays which are characteristic of the element. The X-rays were detected with a semiconductor material producing a pulse of electrical current. The electrical pulses detected displayed the X-ray energy spectrum. The intensity of the X-rays produced provided a measure of the element present by comparison with standards (Bran-Anleu et al., 2018).

Four 100 g powder specimens of the crystalline admixtures were prepared and submitted for XRF analysis testing. The XRF testing procedure included specimen preparation, excitation and radiation measurements. Specimen preparation involved air-drying the specimens and grinding to reduce the particle size distribution of up to 74 µm. 100 g of the test specimen was selected, mixed with a binder (ratio of 10 ±1 g to 20 ± 1 g), and grounded in a Seibtechnik swing mill for 2 to 4 minutes. The blend was pressed into a briquette using fixed pressure of 140 MPa to 550 MPa, maintaining the pressure for 10 s allowing air to escape (ASTM E1621-13, 2013).

Figure 3-7: XRF spectrometer

The briquettes were loaded in the spectrometer and exposed to X- rays (Figure 3-7). The duration and intensity of the spectrometer X-rays were operated according to the manufacturer's instructions. The counting rate measurements were recorded for each element. The concentration of various elements in the test specimens was determined using the counting rate measurements according to ASTM E1621-13, (2013).

3.6.1.2. Scanning Electron Microscopy – Energy Dispersive Spectroscopy (SEM-EDS)

SEM analysis involved focusing a high-energy electron beam on the surface of test specimens to produce a magnified image for analysis. These images provide information indicating topographical variations, chemical composition, and crystalline structure in the observed specimens (ASTM C1723-16, 2016). Furthermore, the elemental composition of the observed surface of the specimens was determined with the combination of energy-dispersive X-ray spectroscopy (EDS) that measured the energy of each X-ray pulse absorbed by the detector.

One 100x100x100 mm concrete cube was cast for each mix to produce specimens for SEM-EDS test. The specimens were covered by a polythene sheet to prevent moisture loss for 24 hours. The specimens were then demoulded and cured in a water bath at (23 ± 2) ^{o}C for 21 days, before extraction of core specimens according to SANS 3001-CO3-1, (2015). The specimens were induced with cracks based on the flexural strength test of concrete (SANS 5864, 2006). Thereafter, the specimens were cured for 84 days to induce autonomous healing for SEM analysis testing.

SEM analysis test procedure included specimen preparation, image analysis, and X-ray microanalysis. After curing, the specimens were oven dried and split to expose the self-healing products within the crack area. The self-healing products were identified by visual inspection and then carefully scraped to analyse the products precipitated on a cracked surface. The self-healing products were carefully scraped from the crack area using a spatula. The extracted specimens were mounted to a high vacuum SEM, and testing was done according to ASTM C1723-16, (2016).

3.6.2. Strength tests (compressive and tensile splitting)

Compressive and splitting strength tests were conducted on uncracked specimens according to SANS 5863, (2006), and splitting strength tests were conducted according to SANS 6253, (2006). One hundred and eighty cubes for strength tests were cast using 100 x 100 x 100 mm moulds. Eighteen cubes for compressive strength and splitting strength tests were tested for each mix after 7, 28, and 112 days of casting.

3.6.3. Durability Index tests on cracked and uncracked Specimens

Three durability tests were conducted, namely the oxygen permeability index test (OPI), water sorptivity index test (WSI), and water permeability test. OPI testing was conducted according to SANS 3001-CO3-2, (2015), WSI testing was conducted according to the durability index testing manual (Alexander, 2017), and, the water permeability test was adapted from a permeability test setup proposed by Wang et al., (1997).

Six 100x100x100 mm concrete cubes were cast from each concrete mix to produce uncracked reference specimens. The cubes were cured in a water bath for 28, 56, and 84 days. After each curing duration, the cubes were cored and cut into concrete disc specimens with 70 ± 2 mm diameter and thickness of 30 ± 2 mm according to (SANS 3001-CO3-1, 2015). The specimens were marked and preconditioned at 50 ± 2 ºC in the oven for seven days in preparation for the durability tests.

Seven 100x100x100 mm concrete cubes were cast for each mix to produce cracked specimens. The cubes were initially cured in a water bath for 21 days. After initial curing, the cubes were cored and cut into concrete disc specimens with 70 ± 2 mm diameter and thickness of 30 ± 2 mm according to SANS 3001-CO3-1, (2015). The specimens were pre-cracked according to SANS 5864, (2006) and subsequently cured in a water bath for 28, 56, and 84 days (Figure 3-4).

3.6.3.1. Oxygen permeability index (OPI)

The OPI test involved measuring the pressure decay of oxygen through the concrete discs. The discs were placed in a permeability cell, as shown in Figure 3-8. Pressure readings were taken for six hours or up to 50 kPa (whichever came first), after which the test was stopped. The OPI was defined as the negative logarithm of the coefficient of oxygen permeability k, (m/s) and the test was conducted on uncracked specimens according to SANS 3001-CO3-2, (2015).

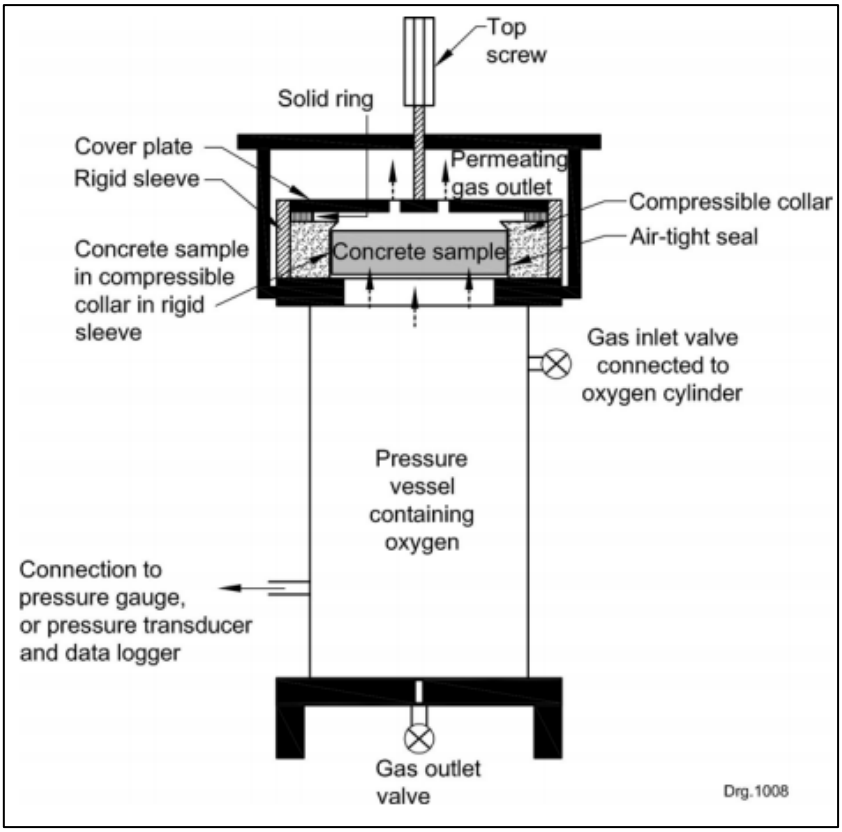

Figure 3-8: Schematic representation of a permeability cell according to SANS 3001-CO3-2, (2015)

Furthermore, the OPI values were expressed in the coefficient of permeability in order to quantify the influence of crystalline admixtures in decreasing permeability. The decrease in permeability was calculated using Equation 3-1.

$$\%\ \text{decrease in permeability} = \left(\frac{k_{\text{control concrete}} - k_{\text{CA concrete}}}{k_{\text{control concrete}}} x\ 100\right)\% \qquad \text{Equation 3-1}$$

3.6.3.2. Water sorptivity index (WSI)

The WSI testing involved measuring the absorption rate of calcium hydroxide solution through dry concrete discs under capillary action. The outer edges of the discs were sealed with tape to promote the one-directional movement of the liquid. The specimens were placed in a few millimetres of calcium hydroxide solution with the testing side facing the solution (Alexander, 2017). The testing was conducted on both cracked and uncracked specimens.

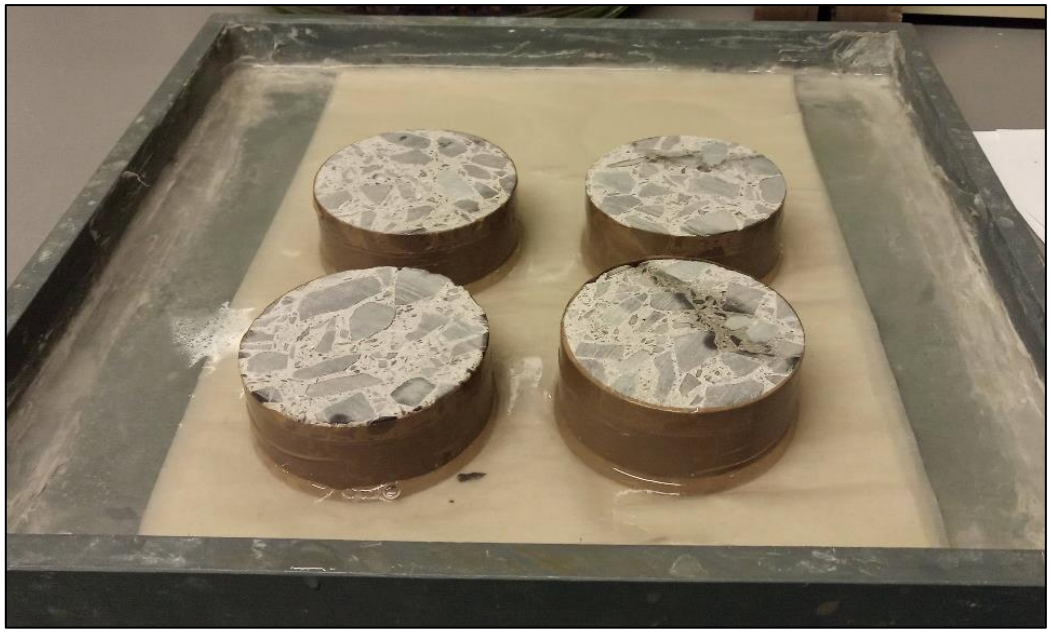

Figure 3-9: Water sorptivity test setup on cracked specimens

In uncracked concrete, sorptivity test is influenced by the capillaries and their degree of interconnection, thus, concrete permeability is related to water filled porosity. Presence of cracks in cracked concrete substantially modifies transport properties of concrete, thus permeability is dependent on the crack properties. Properties such as crack width and shape, crack density and degree of connectivity, and crack origin govern transport in cracked concrete (Alexander, Ballim & Beushausen, 2009).

3.6.3.3. Water permeability test

The water permeability test involved measuring the capacity of the specimens to transfer fluid through their pore structure under a pressure gradient while the pores are saturated with that fluid. The concrete discs were placed in a falling head permeameter (Figure 3-11). Water head readings were taken at regular intervals depending on the flow rate until constant head readings were observed, after which the test was stopped. The coefficient of permeability (k, in mm/s) was calculated based on Darcy's law for steady-state flow.

The water permeability testing procedure comprised of specimen vacuuming and saturation, test setup, and permeability measurement. Specimens were prepared by coring and cutting concrete cubes into concrete disc specimens with 70 ± 2 mm diameter and thickness of 30 ± 2 mm according to SANS 3001-CO3-1, (2015). The concrete discs were first vacuumed at a pressure between -75 kPa and -80 kPa for 3 h ± 15 min. Deaired water was added, and the specimens were vacuumed underwater

for 1 h ± 15 min. The deaired water was obtained by boiling water and cooling it to room temperature. After vacuum saturation, the specimens were left to soak for 18 ± 1hr (Alexander, 2017).

After removal from the vacuum saturation tank, the specimens were placed in a water permeability cap, and covered with a wet cloth on top to prevent moisture loss (Figure 3-10). Silicone was applied on the circumferential surface of the specimens to prevent water leakage on the sides during testing (Wang et al., 1997).

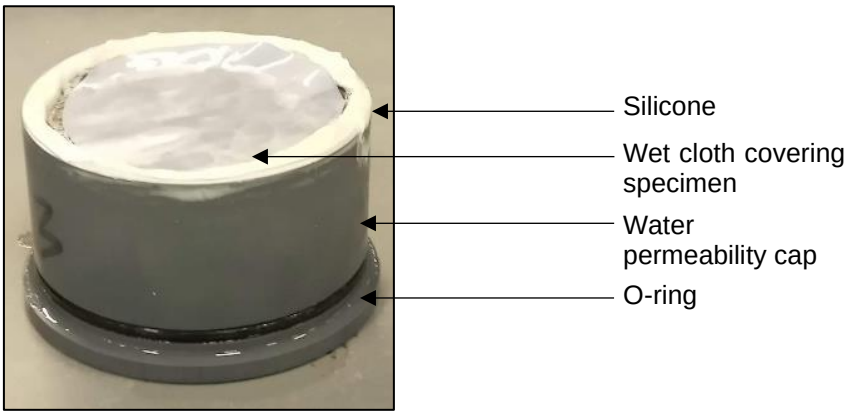

Figure 3-10: Water permeability cap: specimen conditioning before testing

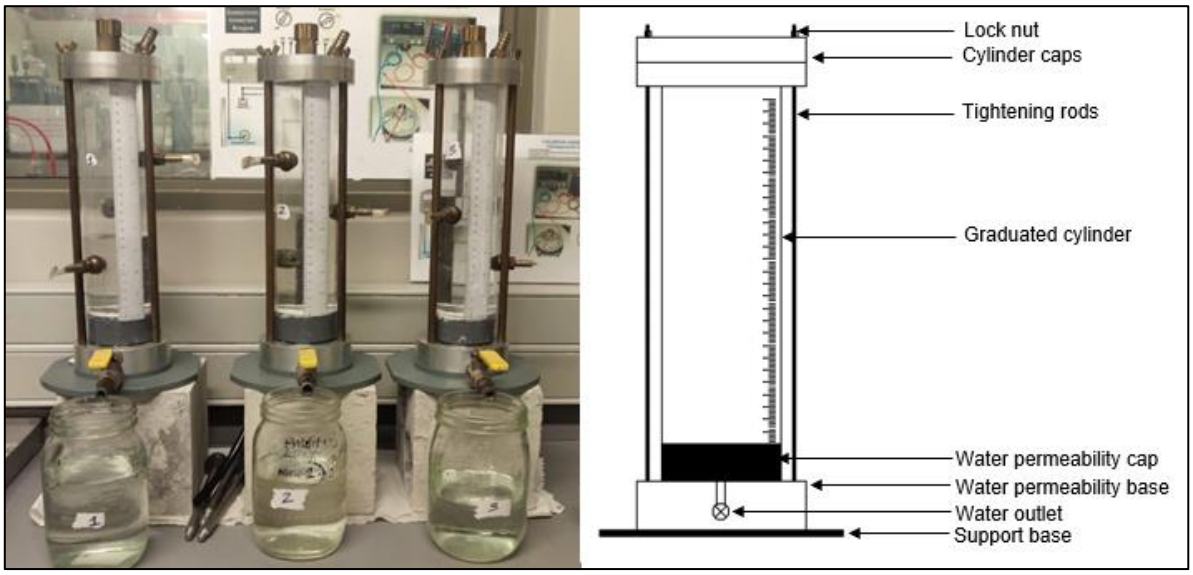

Figure 3-11: Water permeability test setup

After the silicone had been set typically after 1 hour, the specimens were mounted and clamped in the permeameter. A container was placed at the bottom of the permeameter to collect leakage water through the specimen (Figure 3-11). The permeameter was filled with a water head of 300 mm. The water permeated from top to bottom due to the pressure head. Water levels were measured at regular time intervals, depending on the water flow rate of the specimen, and, after each

measurement, the water was refilled to the original level. The testing was repeated until constant flow was reached. The coefficient of permeability (k, in mm/s) based on Darcy's law for a falling water head was calculated by plotting a graph of cumulative flow results against time (Wang et al., 1997).

4. Results and discussion

4.1. Introduction

This chapter presents the results, analysis and discussion of the laboratory investigations described in Chapter 3. The tests comprised X-ray fluorescence (XRF), scanning electron microscopy with energy-dispersive X-Ray spectroscopy (SEM-EDS), compressive and splitting strength, oxygen permeability index, water sorptivity index, and water permeability tests. The test results are presented in the following sub-sections.

4.2. Microscopy results

4.2.1. XRF results

The XRF test was used to identify and quantify the oxides of major and trace elements of crystalline admixtures and cement. The oxides in crystalline admixtures (CA) and ordinary Portland cement were analysed and compared. Figure 4-1 presents the results of the XRF test conducted on cement and CA powders. Detailed results are presented in Appendix A.

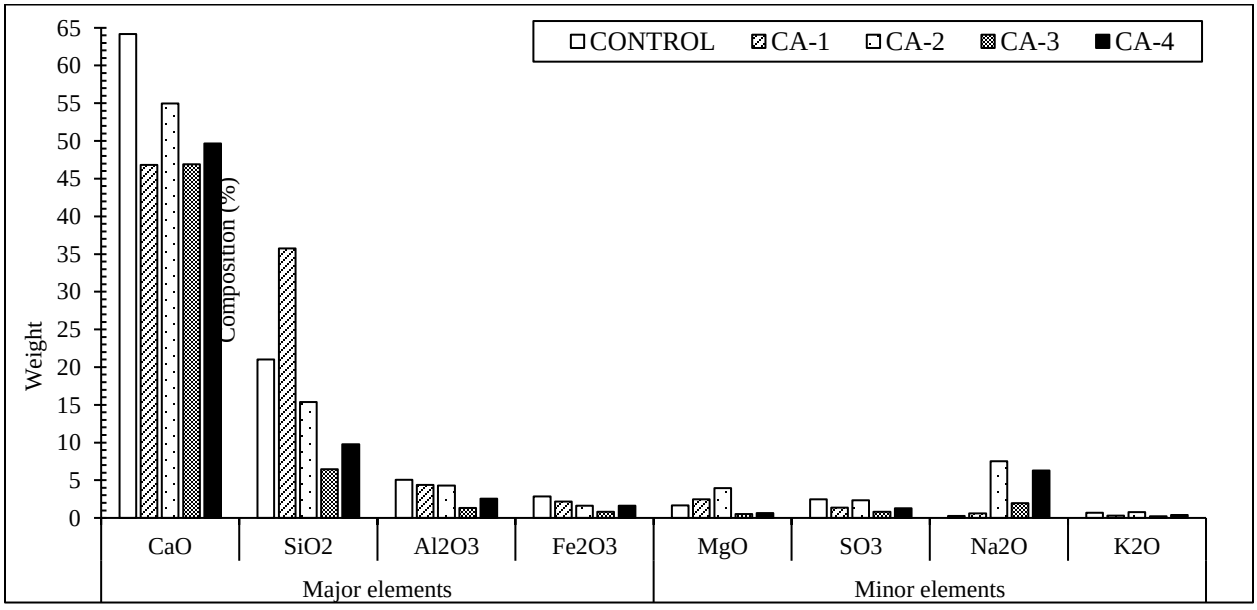

Figure 4-1: Chemical composition of cement and crystalline admixture obtained by XRF test

Oxides are essential components of strength development in hydration reactions. Reactivity in hydration reactions is a function of lime content (Grieve, 2009). From Figure 4-1, the oxides of major and trace elements in all crystalline admixtures are similar. Thus,

the hydration reactions of the crystalline admixtures are expected to be similar to each other (Grieve, 2009).

The concentration of the oxides for different crystalline admixtures was also analysed. Few notable differences were observed in crystalline admixtures CA-1, CA-2, and CA-3. CA-1 had the highest silica content of 35% and CA-2 had the highest lime content of 55%. CA-3 had the lowest concentration of lime, silica, alumina, and iron with 47%, 7%, 2%, 1%, and 1%, respectively as it has some reliance on amino alcohols.

The oxides concentrations in comparison to ordinary cement were analysed. Cement was observed to have the highest lime content with 65%. The oxides composition was found to be similar to that of ordinary cement. These findings coincide with results from Elsalamawy, Mohamed & Abosen, (2019) and Wang et al., (2018), where, XRF analysis revealed that the CA are mainly composed of cement, silica, and carbonated materials. Therefore, the crystalline admixtures are expected to hydrate like cement.

4.2.2. SEM-EDS results

Self-healing precipitates extracted from cracked surfaces were analysed with scanning electron microscopy with energy-dispersive X-Ray spectroscopy (SEM-EDS) to understand their morphology, elemental composition, and differences. SEM observed the morphologies of self-healing crystals, and EDS analysed the elemental composition. The morphologies of the healed precipitates helped to understand the microstructure and the crystals precipitated at the crack area (Elsalamawy, Mohamed & Abosen, 2019). The microstructures helped to determine the chemical composition of the crystals. The scales used were 100 µm, 50 µm, and 20 µm, depending on the magnification and clarity of the images of the crystals. The results of SEM-EDS analysis are presented from Figure 4-2 to Figure 4-21. Detailed results are presented in Appendix B.

Figure 4-2 shows the morphology of the healed precipitates in control mix 1 with w/b = 0.40 and no CA content. In the absence of crystalline admixtures, SEM images results indicated orthorhombic aragonite crystals, which are among the three polymorphs of calcium carbonate. EDS results indicated the main elements to be Calcium (Ca), Carbon (C), and Oxygen (O), with an average molar ratio (C/O) of about 3 (Figure 4-3). The

development of calcium carbonate crystals in the crack area was influenced by Sr^{2+} (Zhou et al., 2004).

Figure 4-4 shows the SEM results for control mix 2 with w/b = 0.6 and no CA content. The image revealed small and dense round crystals characteristic of calcium silicate hydrate (CSH). EDS results indicated the presence of Ca, Silica (Si), C, Aluminium (Al), and O. The average molar ratio of (Ca/Si) is above 3 indicated the presence of rounded C-S-H precipitate. The results coincided with Elsalamawy, Mohamed & Abosen, (2019) findings which concluded that with increasing Ca/Si ratio, the calcium silicate hydrate gel morphed into a dense granular-like shape.

Furthermore, the average molar ratio of (C/O) was about 3, indicated the presence of calcium carbonate. However, the morphology of the carbonates was not observed in the SEM images as the area of interest may not have the carbonate precipitates.

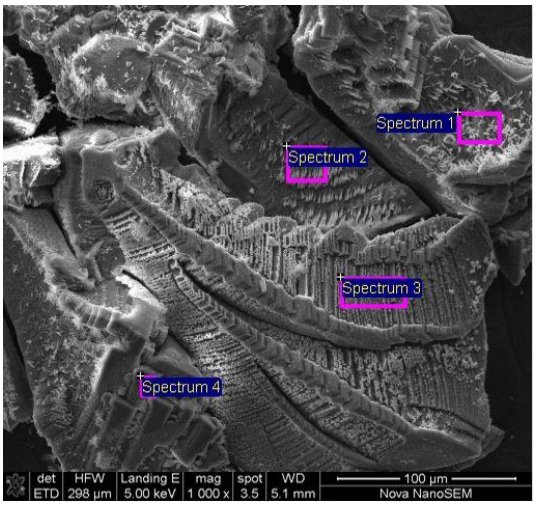

Figure 4-2: Control mix (w/b - 0.4)

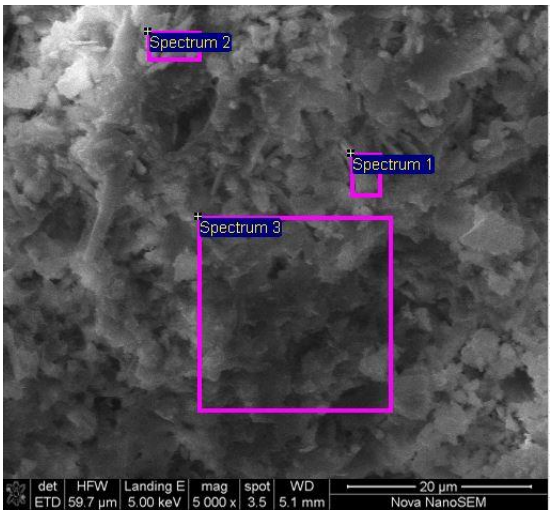

Figure 4-4: Control mix (w/b - 0.6)

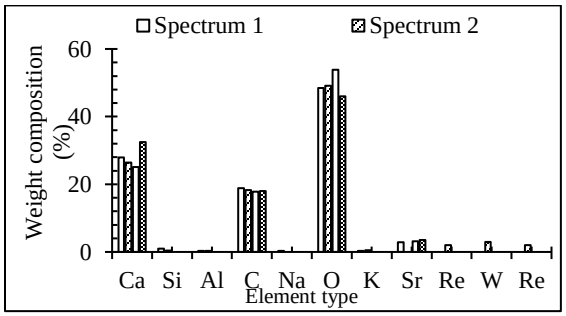

Figure 4-3: Elemental analysis of control mix (w/b – 0.4)

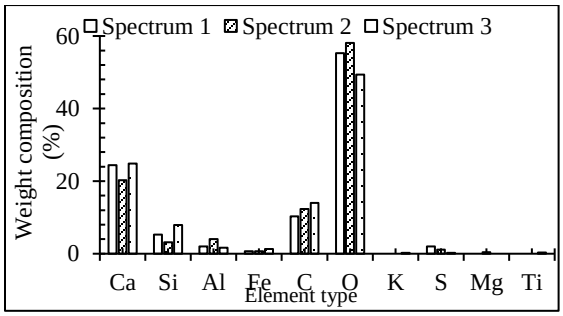

Figure 4-5: Elemental analysis of control mix (w/b – 0.6

SEM results for mix 3 with w/b = 0.4 and CA-1 content indicated the precipitates as orthorhombic aragonite crystals which, are calcium carbonate polymorphs (Figure 4-6). EDS results (Figure 4-7) confirmed the presence of Sr^{2+} in the precipitates, favouring the crystallization of aragonite crystals (Zhou et al., 2004). The aragonite precipitation as the self-healing product is coherent with the observations of Stuckrath et al., (2014) and Park & Cheol, (2019).

SEM results for mix 4 with w/b = 0.6 and CA-1 content indicated the presence of needle-like crystals (Figure 4-8). EDS analysis revealed the presence of Ca, O, Al, and S. Precipitates were identified as the morphology of C-S-H crystals (Figure 4-9). Elsalamawy, Mohamed & Abosen, (2019) findings revealed needle-like and round precipitates with calcium and silica as the main elements with average molar ratio (Ca/Si) of about 3.6. No difference was detected on the compositions of need-like and rounded crystals despite the difference in structure and morphology. Both were revealed to be C-S-H crystals. Furthermore, the average molar ratio of (C/O) was about 3, indicating the presence of calcium carbonate. Similar to mix 1, the SEM images did not reveal the carbonates precipitates on the crack area.

SEM observations of Figure 4-10 and Figure 4-12 revealed the presence of aragonite crystals in precipitates of mix 5 with w/b = 0.4 and CA-2 content and mix 6 with w/b = 0.6 and CA-2 content. EDS analysis revealed Ca, O, and C, which are the elements found in aragonites. Similar to mixes 1 and 3, the crystallization of the aragonite crystals was influenced by Sr^{2+}.

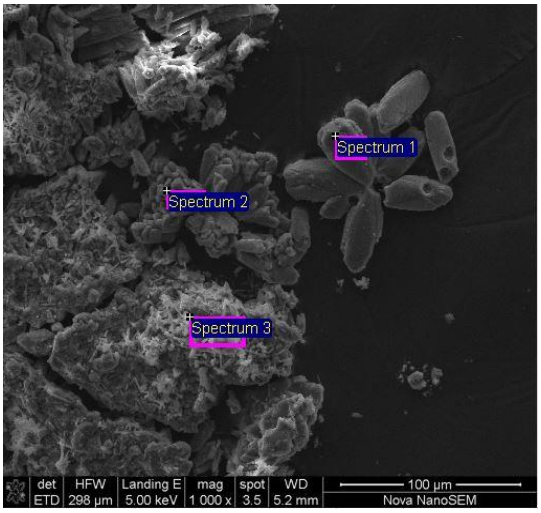

Figure 4-6: CA-1 mix (w/b - 0.4)

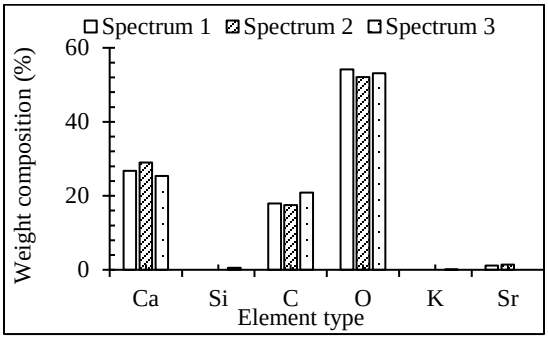

Figure 4-7: Elemental analysis of CA-1 mix (w/b – 0.4)

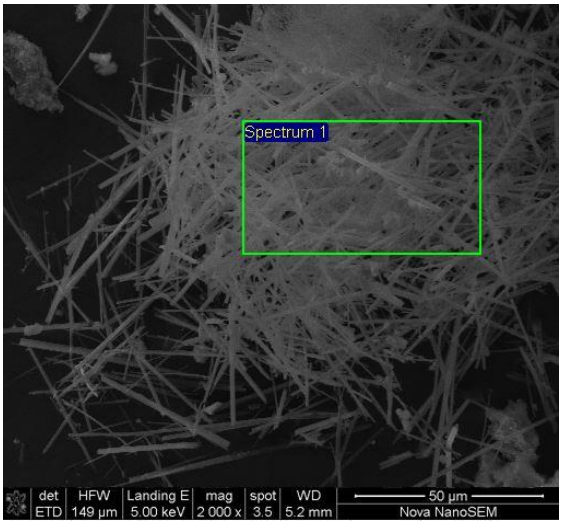

Figure 4-8: CA-1 mix (w/b - 0.6)

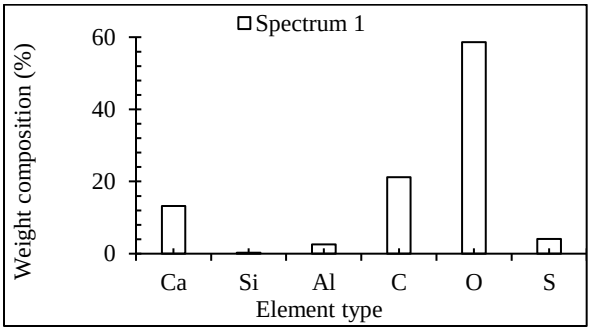

Figure 4-9: Elemental analysis of CA-1 mix (w/b – 0.6)

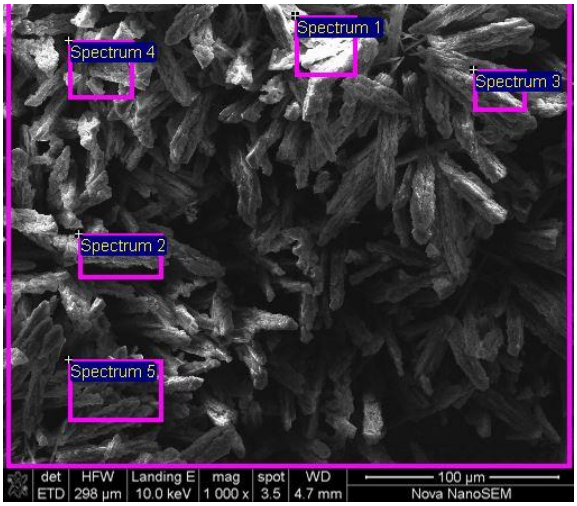

Figure 4-10: CA-2 mix (w/b - 0.4)

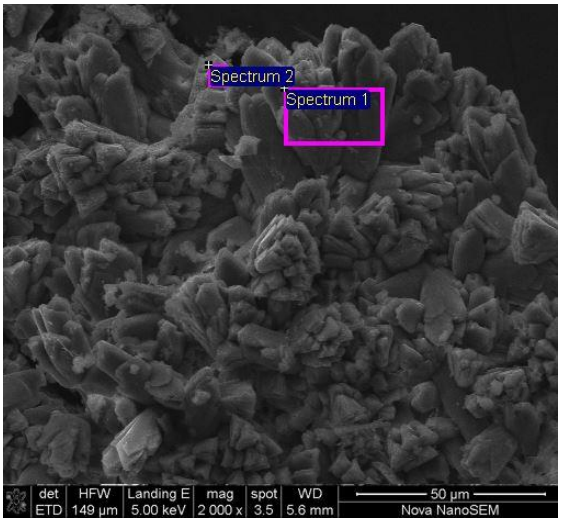

Figure 4-12: CA-2 mix (w/b - 0.6)

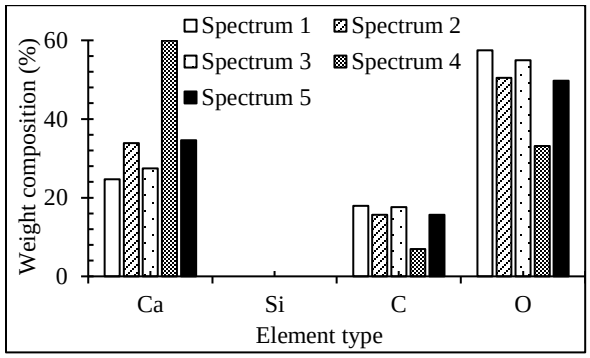

Figure 4-11: Elemental analysis of CA-2 mix (w/b – 0.4)

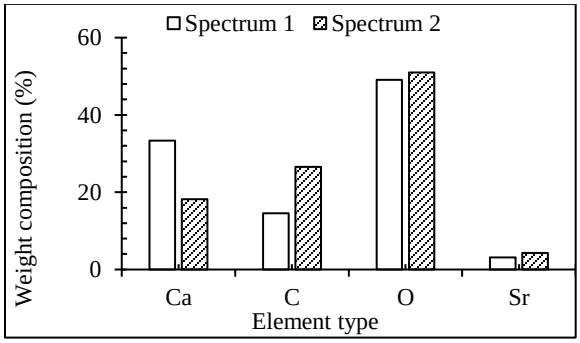

Figure 4-13: Elemental analysis of CA-2 mix (w/b – 0.6)

SEM results in mix 7 with w/b = 0.4 and CA-3 content revealed the presence of needle-like crystals of ettringite (Figure 4-14). EDS analysis revealed the presence of abundant ettringite acicular crystals mainly containing Ca, C, O, Al, and S. The results coincide with the findings of Park & Cheol, (2019) and Sisomphon, Copuroglu & Koenders, (2012), where ettringite was formed due to the addition of calcium sulfo-aluminate based expansive additive in concrete.

SEM results for mix 8 with w/b = 0.6 and CA-3 content indicated rhombohedra calcite crystals, which are the most stable polymorph of calcium carbonate (Figure 4-16). EDS analysis confirmed the presence of Sr^{2+}, which favour the formation of calcite. Similar crystals were observed in the literature on healed cracks when crystalline admixtures were utilized (Jiang et al., 2014; Elsalamawy, Mohamed & Abosen, 2019).

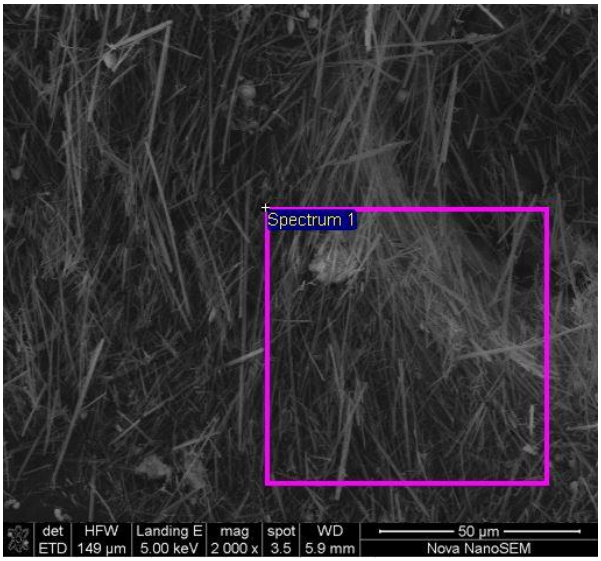

Figure 4-14: CA-3 mix (w/b - 0.4)

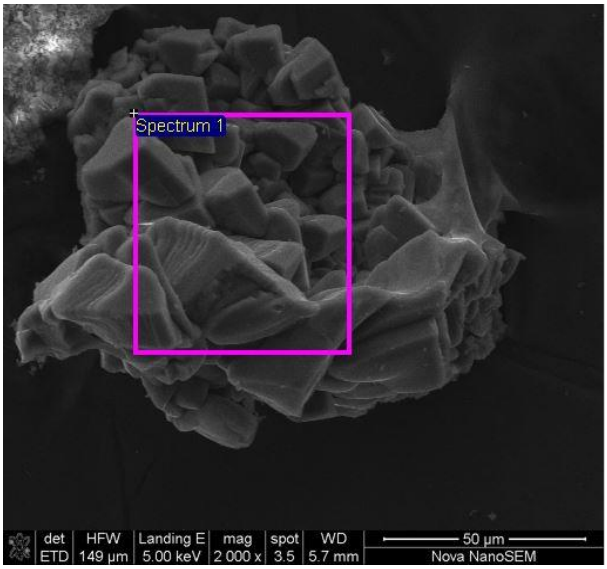

Figure 4-16: CA-3 mix (w/b - 0.6)

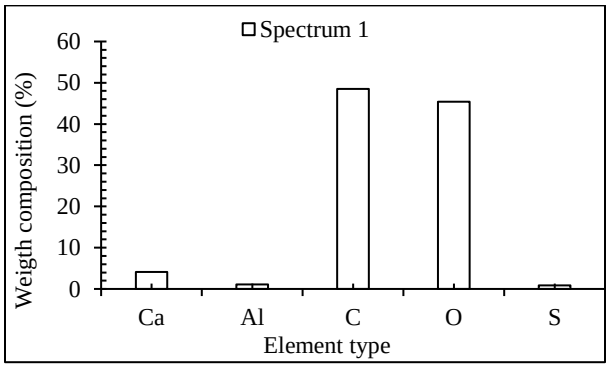

Figure 4-15: Elemental analysis of CA-3 mix (w/b – 0.4)

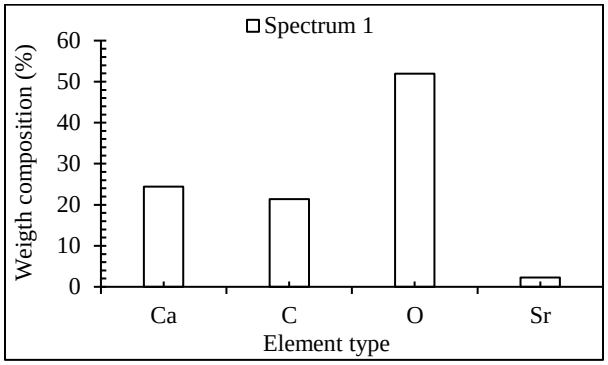

Figure 4-17: Elemental analysis of CA-3 mix (w/b – 0.6)

SEM analysis conducted on precipitates of mix 9 with w/b ratio = 0.4 and CA-4 content and mix 10 with w/b = 0.6 and CA-4 content revealed rhombohedra shaped crystals of calcite. Similar observations were observed in mix 8 precipitates (Figure 4-18) and (Figure 4-20). EDS analysis confirmed the presence of Ca, C, O, and Sr^{2+}, the ions necessary for the crystallization of calcite crystals.

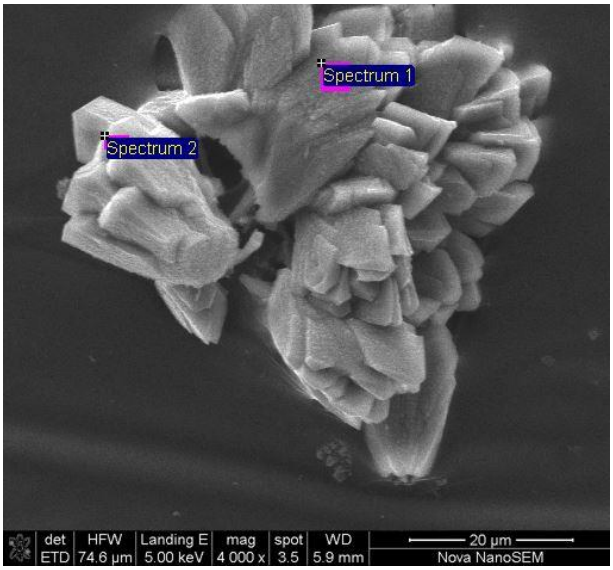

Figure 4-18: CA-4 mix (w/b - 0.4)

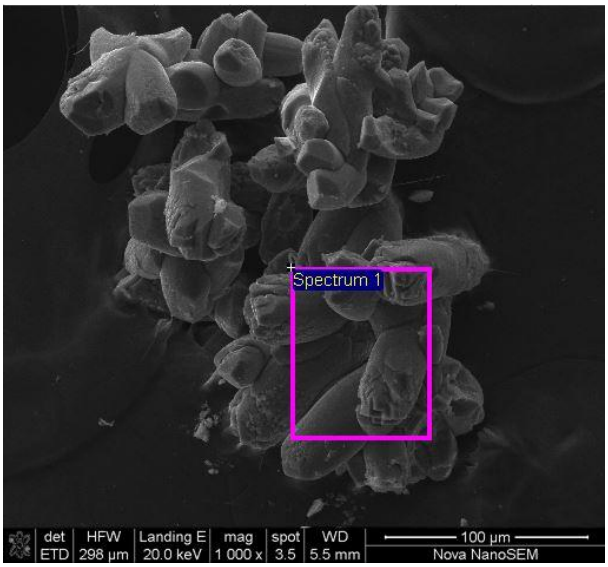

Figure 4-20: CA-4 mix (w/b - 0.6)

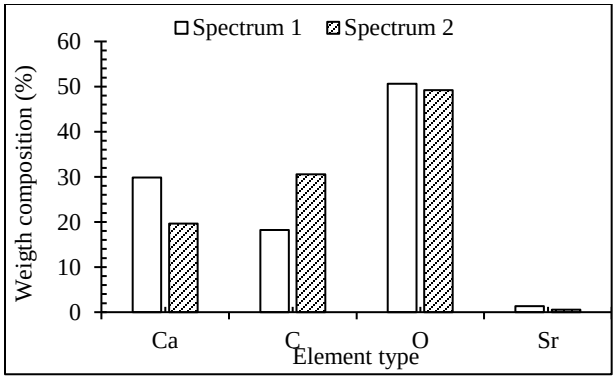

Figure 4-19: Elemental analysis of CA-4 mix (w/b – 0.4)

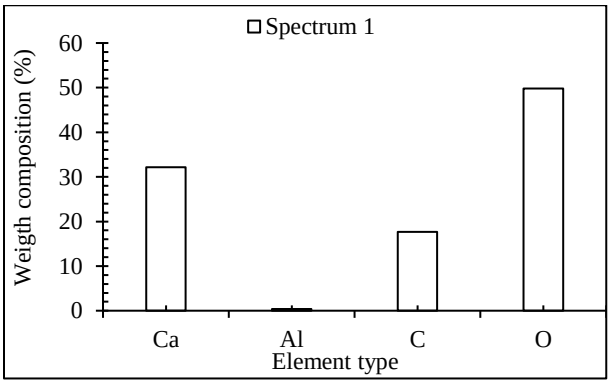

Figure 4-21: Elemental analysis of CA-4 mix (w/b – 0.6)

4.2.3. Summary

XRF and SEM-EDS tests were employed to explore the related healing mechanism. XRF testing was conducted on the powder specimens of the crystalline admixtures and cement. SEM-EDS test was carried by splitting the cracked specimens and examining the surfaces on both specimens with and without crystalline admixtures. The morphologies of self-healing materials were observed by SEM, while the corresponding elemental compositions were characterized by EDS.

XRF results concluded that the oxides composition of major and trace elements in all of the crystalline admixtures are similar. Also, the oxides compositions of all crystalline admixtures are similar to Portland Ordinary cement. Thus, hydration reactions of the crystalline admixtures were expected to be similar to each other and similar to those of cement.

SEM-EDS analysis confirmed that the self-healing products of all specimens corresponded to different morphologies of calcium carbonate with the exception of Mix 7. Orthorhombic aragonite and rhombohedra calcite crystals were dominant in the precipitates. Specimens of mixes 1, 3, 5, and 6 contained aragonite crystals and specimens from mixes 8, 9, and 10 crystals contained calcite crystals. The C/O molar ratio from mixes 2 and 4 revealed the presence of calcium carbonate crystals in the precipitates. Mix 7 revealed the presence of ettringite crystals. Ettringite was formed as a result of addition of calcium sulfo-aluminate based expansive additive in concrete. Thus, the crystalline additive incorporated has traces of alumina in its composition (Table B-4).

All of the self-healing agents studied herein behave similar autogenous healing capacity of concrete without crystalline admixtures. SEM observations and EDS analyses confirmed the presence of reaction products similar to those yielded by cement hydration on the cracked (and partially healed) surfaces. The precipitates were mainly due to the reaction between calcium ions that arise from the hydration by-product and carbonate ions from the presence of Sr^{2+} ions available in the crystalline concrete matrix.

4.3. Strength results

4.3.1. Compressive strength results

Results of compressive strength of concrete containing different types of crystalline admixtures are presented in Figure 4-22. The detailed compressive strength results are presented in Appendix C. The compressive strength of all the concrete mixes increased as the w/b ratio decreased. This was attributed to the more refined microstructure and reduced capillary water filled porosity due to continuing cement hydration. Also, the development of compressive strength increased as the curing time increased, attributed by continuing hydration of cement. Similar results were obtained by Ahn & Kishi, (2010) where, a self-healing concrete behaves similar to plain concrete.

The results were used to relate the compressive strength of concrete with crystalline admixture to the control concrete. Figure 4-23 shows that the relative strength increased with curing age of 7 days to 28 days and decreased from 28 days to 112 days. The initial increase of strength was associated with the acceleration of the hydration reaction, and the decrease was due to the deceleration of the hydration as concrete matures. This effect may favour the use of CA in construction practice where interrupted curing is likely.

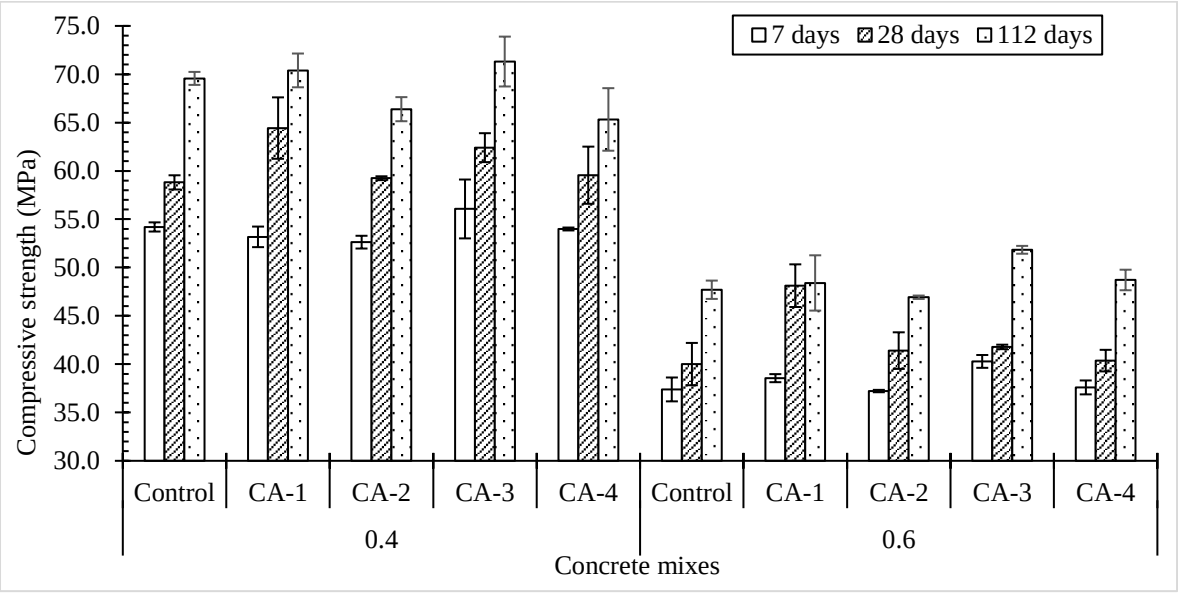

Figure 4-22: Compressive strength of concrete containing crystalline admixture at two w/b ratios

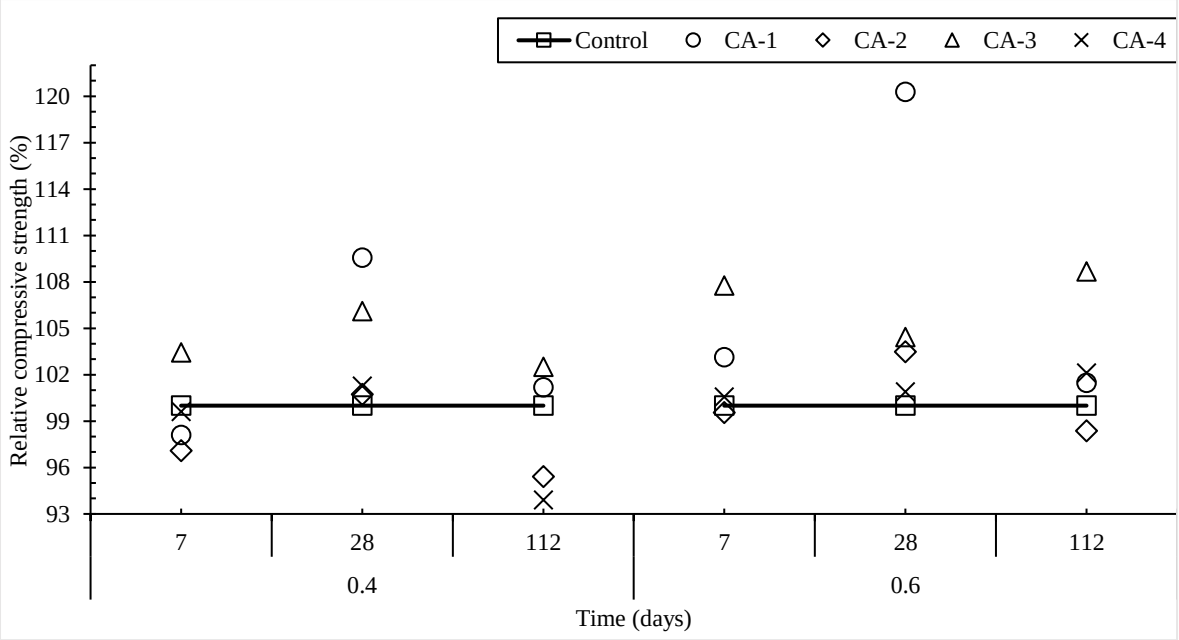

Figure 4-23: Relative compressive strength of concrete containing crystalline admixtures

Concrete with CA-1 crystalline admixture indicated significant higher compressive strength at 28 days for both w/b ratios of 0.4 and 0.6 than at 7 and 112 days. This might be attributed to the formation C-S-H crystals as witnessed in the SEM results (Figure 4-8). The increased amount of reactive silica in the admixture may have contributed to the increase in densification of CSH gel. In addition, from Figure 4-23, concretes with higher water filled porosity (i.e., w/b ratio of 0.6) indicated higher strength development than the concrete with lower water filled porosity (i.e., w/b ratio of 0.4). This is an important observation, as these admixtures are typically used in "high quality" concretes, i.e., with lower w/b ratios but not in concretes with water/binder ratios of 0.6 and higher. This shows that in practice, these admixtures probably have little to no noticeable effect when used in concrete if cured equivalently to full water immersion.

Similar results were obtained by Azarsa, Gupta & Biparva, (2019), where the improved compressive strength on concrete with crystalline admixtures was associated with a filler effect that can contribute to closing of the voids and also work as a cement hydration activator by improving the paste cement microstructure. Furthermore, the laboratory mixes with CA had higher paste volume which would have this effect too.

4.3.2. Splitting strength results

Results for splitting strength of concrete containing different types of crystalline admixtures are presented in Figure 4-24. Detailed splitting strength test results are

presented in Appendix D. The splitting strength of concrete increased as the w/b ratio decreased as curing age increased. This was attributed to the more refined microstructure of concrete forming as concrete matures.

The results were also used to relate the splitting strength of concrete with crystalline admixtures to the control concrete. Figure 4-25 shows the relative strength development with concrete with crystalline admixtures. CA-1 concrete indicated the highest splitting strength at 28 days than at 7 and 112 days for w/b ratio of 0.6. C-S-H crystals found in SEM results for CA-1 concrete may have contributed to the increased splitting strength at 28-day. Most crystalline concrete have shown an initial increase of strength associated with the acceleration of the hydration reaction, and decrease of strength was due to the deceleration of the hydration as the concrete matures.

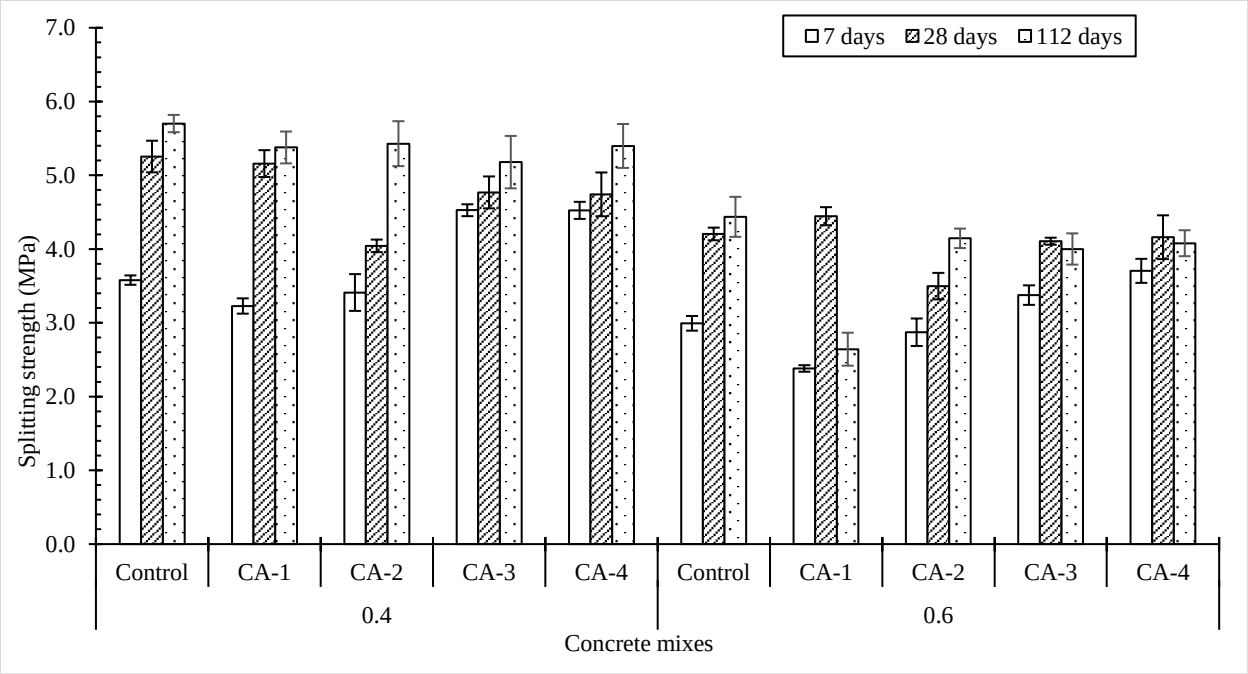

Figure 4-24: Splitting strength of concrete containing crystalline admixtures at different w/b ratios

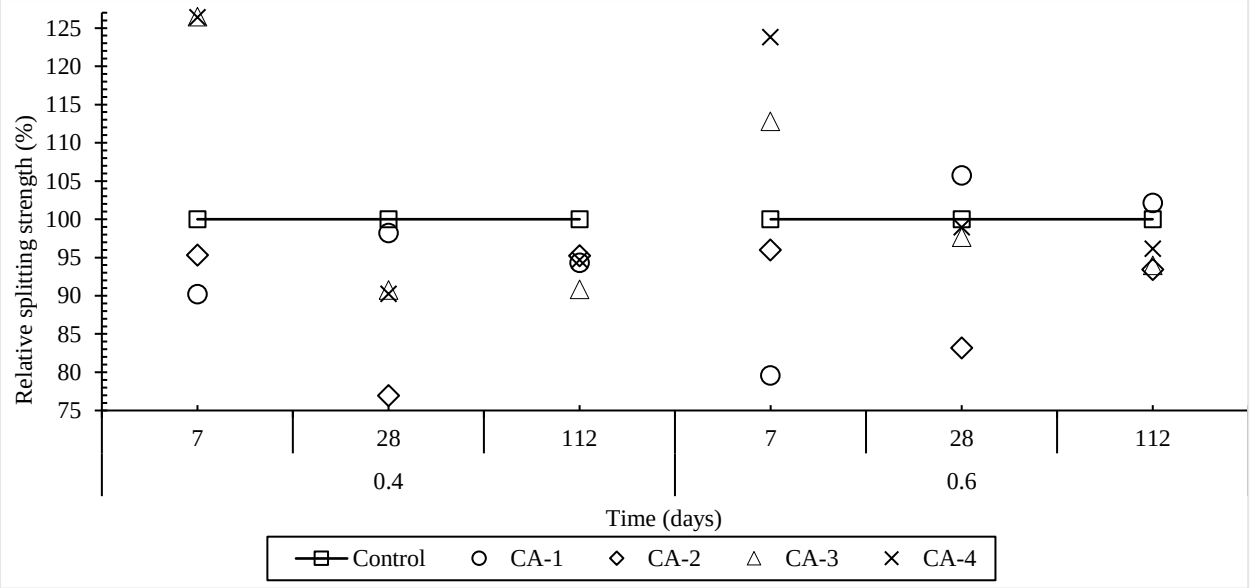

Figure 4-25: Relative splitting strength of concrete containing crystalline admixtures

From Figure 4-25, the CA-1 crystalline admixture indicated slightly higher splitting strength at 28 days for w/b ratios of 0.6. This might be attributed to the formation C-S-H crystals as a result of hydration of crystalline admixtures as witnessed in the SEM results. The increased amount of reactive silica in the admixture may have contributed to the increase in densification of CSH gel. Similar results were obtained by Zhang et al., (2018), where the mixing crystalline additive to concrete mixtures resulted in increases at 28-day ultimate tensile strains compared to plain concrete. In addition, from Figure 4-25, the development of splitting strengths from 28 day to 112-day was not observed for both w/b ratios of 0.4 and 0.6 which indicates no apparent improvement after the introduction of crystalline admixtures.

4.4. Durability results

4.4.1. Introduction

Optical microscope analysis was carried out on healed specimens from concrete with and without crystalline admixtures to observe the precipitated crystals along the cracks. The cracks were filled with white crystal products which were not able to completely restore the continuity of the matrix (Figure 4-26 to Figure 4-30). The whitish products were located not only at the mouth of the crack but also inside the crack when the specimens were split to collect the precipitates.

Furthermore, the white crystals were mostly found on the cement paste along the crack than on areas where the crack broke through an aggregate and in the paste-aggregate

interface. This is because the crystalline admixture and unhealed cement particles dispersed in concrete matrix were powerful enough to transport the healing precipitates on the surface of the cracked aggregates.

Figure 4-26: Control concrete self-healing crystals observed with an optical microscope

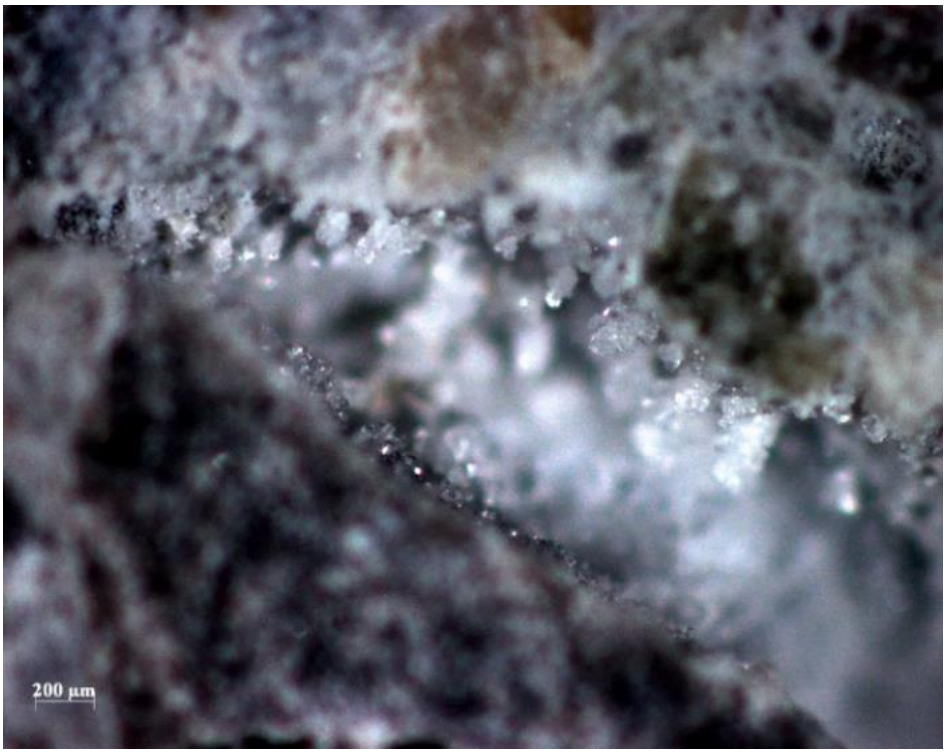

Figure 4-27: CA-1 self-healing crystals observed with an optical microscope

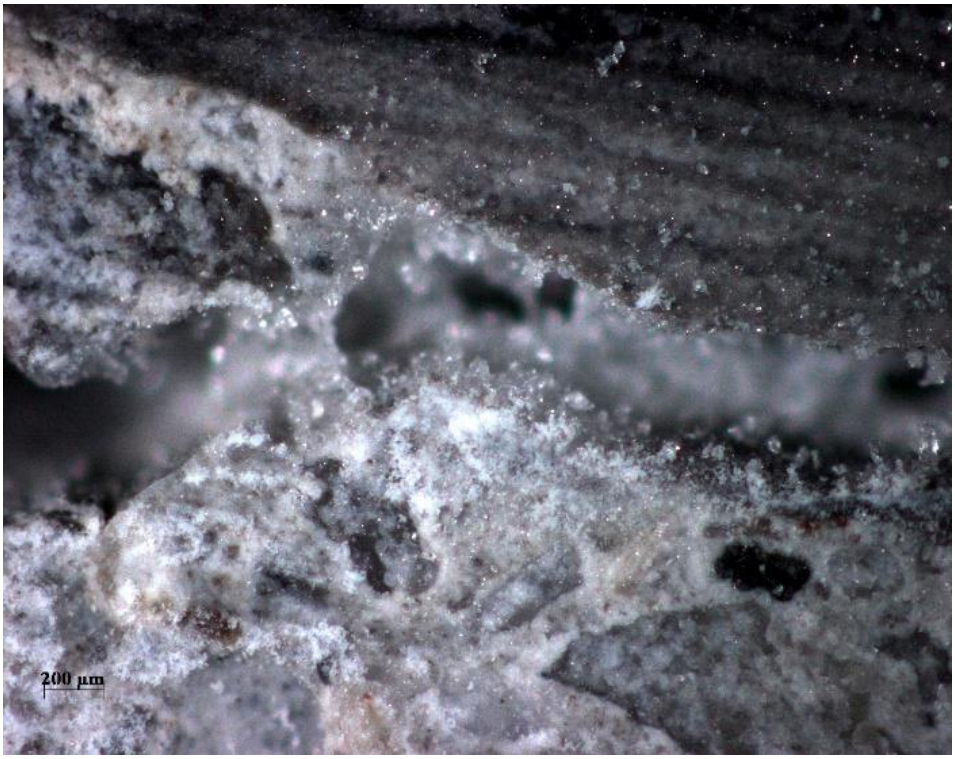

Figure 4-28: CA-2 self-healing crystals observed through an optical microscope

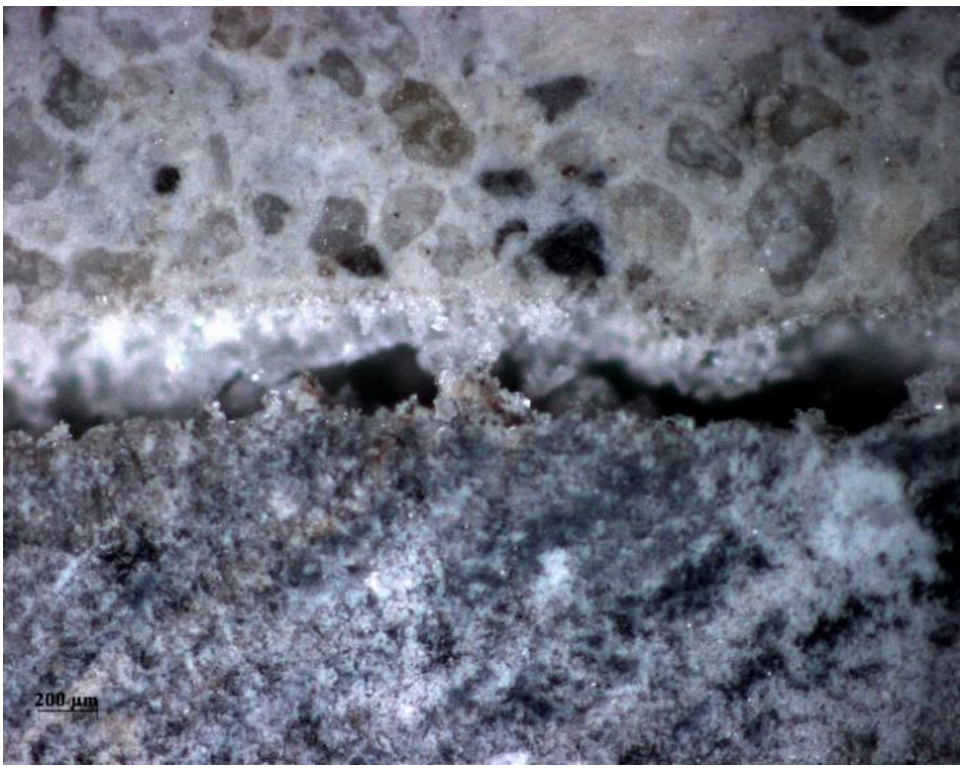

Figure 4-29: CA-3 self-healing crystals observed through an optical microscope

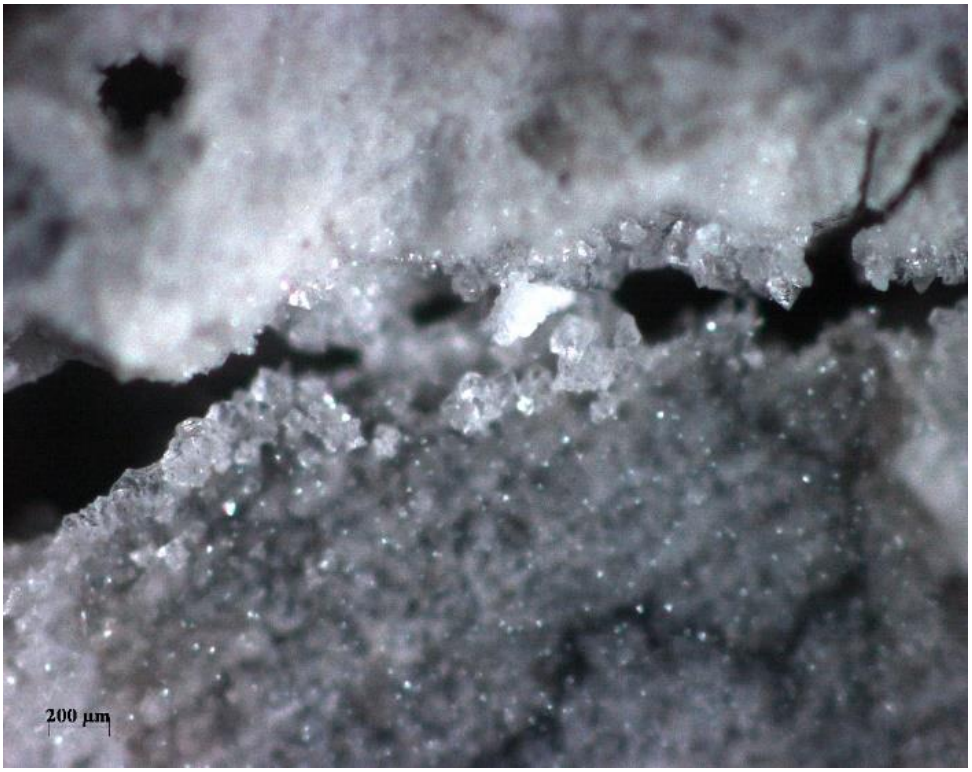

Figure 4-30: CA-4 self-healing crystals observed with an optical microscope

The self-healing crystals were carefully scraped and then scanned by SEM to obtain a further understanding of the healing mechanism. Section 4.2.2 provides an in-depth analysis of the self-healing mechanism.

Durability tests were performed on uncracked and cracked concrete specimens. Tests on the uncracked specimens were conducted to determine the influence of the crystalline admixtures on the transport properties of concrete.

Cracks modify the transport properties of concrete; thus, properties of the cracks become more important in cracked concrete. Transport properties of cracked concrete are essential for predicting the durability of concrete as the flow of aggressive agents pass through the cracks (Alexander, Ballim & Beushausen, 2009). Therefore, the durability tests on cracked specimens were used to quantify the self-healing efficiency of the crystalline admixtures by observing the durability properties at the crack area.

Table 4-1: Durability classification of concrete (Alexander, M.G., Ballim & Mackechnie, 1999)

Durability class	**OPI (log scale)**	**Sorptivity (mm/√hr)**
Excellent	> 10	< 6
Good	9.5 – 10	6 -10

Durability class	OPI (log scale)	Sorptivity (mm/√hr)
Poor	9.0 – 9.5	10 -15
Very poor	< 9.0	> 15

4.4.2. Oxygen Permeability Index results (uncracked concrete)

The Oxygen Permeability Index (OPI) represents the negative log of the coefficient of oxygen permeability, k, (m/s) through a concrete specimen. Concrete with a low OPI value allows ingress of fluid due to high connectivity of its pores. Concretes with very low coefficients of permeability (high OPI value) indicate less permeable (higher quality) concrete with regards to the ingress of fluids. The corresponding values of OPIs at curing ages of 4, 8, and 12 weeks are given in Figure 4-31. Figure 4-32 and Figure 4-33 shows the relative OPI results of uncracked concrete with different crystalline admixtures at two w/b ratios, and, the corresponding permeabilities of concrete with crystalline admixtures after 12 weeks curing, respectively. Detailed OPI results are presented in Appendix E.

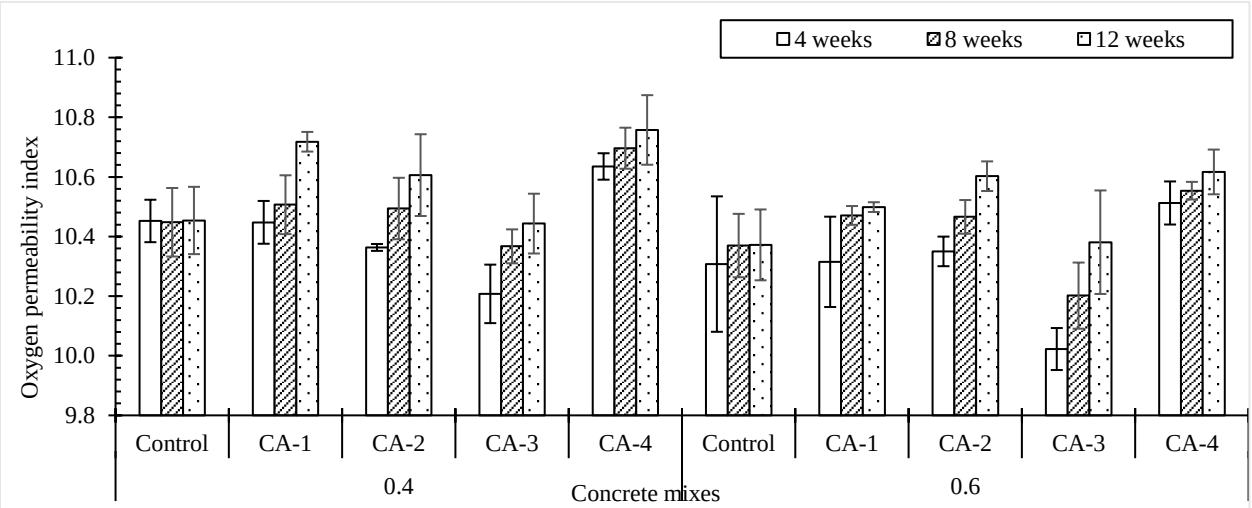

Figure 4-31: OPI results of uncracked concrete with different crystalline admixtures at two w/b ratios

From Figure 4-31, all OPI values were observed to decrease with an increase in the w/b ratio and increase with an increase in curing time indicating excellent quality with exception to CA-3 concrete at w/b of 0.6 which indicated good quality. The increase was attributed to a more refined microstructure as concrete matures (Figure 4-1) evidently by the reduced water filled porosity (Figure 4-35).

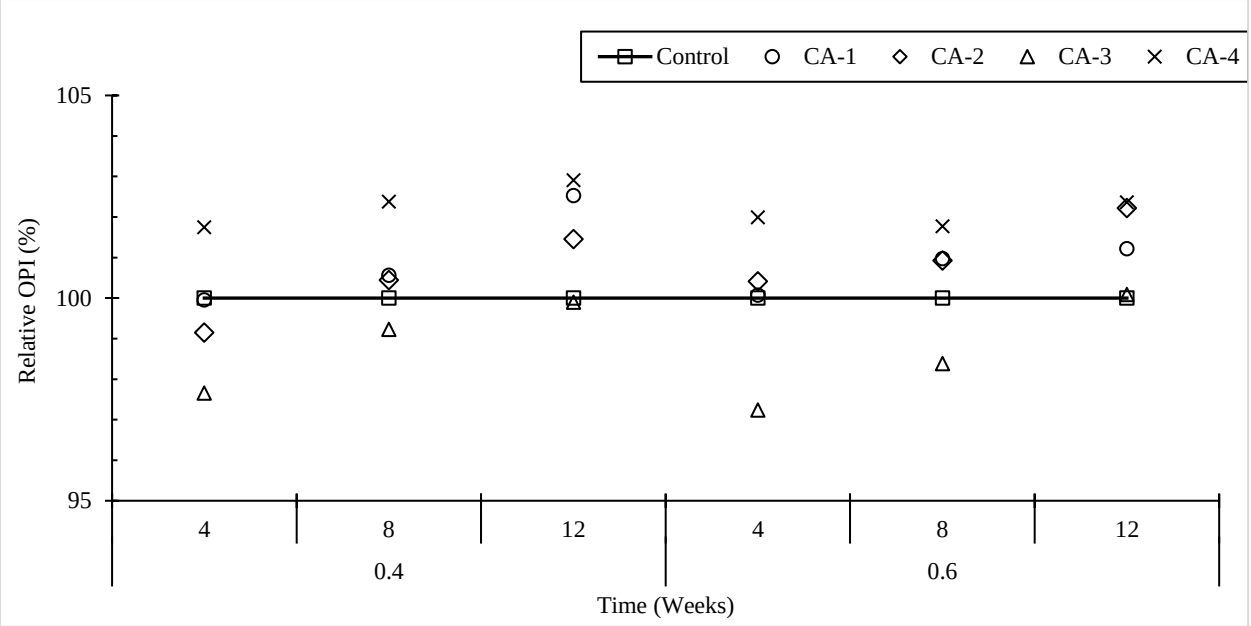

Figure 4-32: Relative OPI results of uncracked concrete with different crystalline admixtures at two w/b ratios

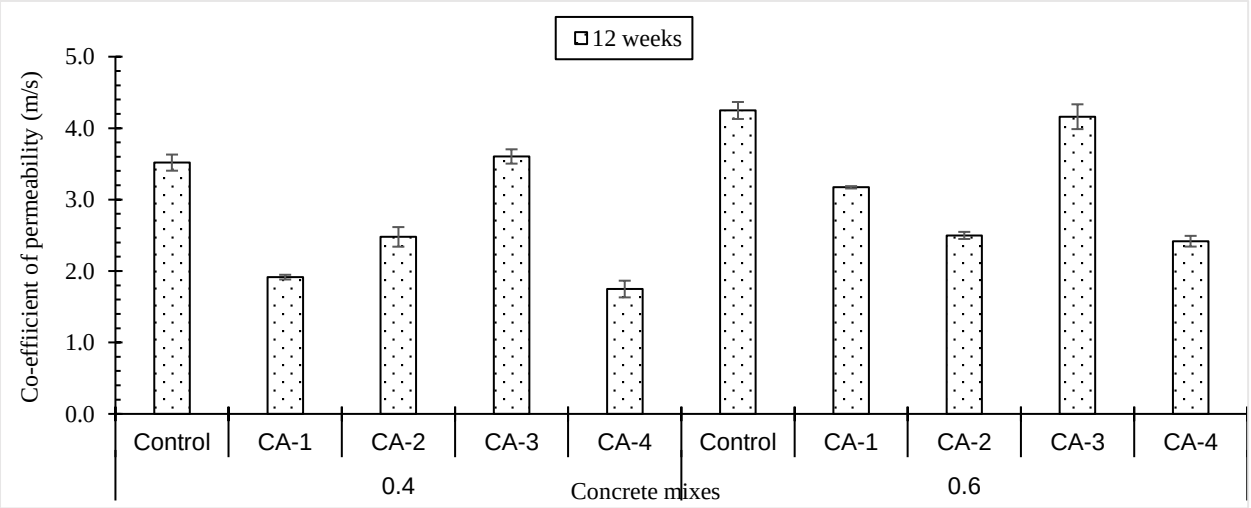

Figure 4-33: Co-efficient of permeability (k) results of uncracked concrete with different crystalline admixtures at two w/b ratios for 12 weeks

Table 4-2: Comparison of co-efficient of permeability reduction between control concrete and concrete with crystalline admixtures at two w/b ratios for 12 weeks

w/b ratio	**0.4**					**0.6**				
Concrete mix	**Control**	**CA-1**	**CA-2**	**CA-3**	**CA-4**	**Control**	**CA-1**	**CA-2**	**CA-3**	**CA-4**
Permeability reduction (%)	0	46	31	0	51	0	26	41	2	44

The OPI were expressed in relative OPI relating to control concrete to determine the percentage increase in OPI on the concrete with crystalline admixtures. Furthermore,

the OPI were also expressed in co-efficient of oxygen permeabilities (k) to determine the percentage decrease in permeability of concrete with different crystalline admixtures at two w/b ratios for 12 weeks. From Table 4-2, the oxygen permeability of all concretes exhibited a similar trend with exception of CA-3 concrete which showed an increase in permeability in relation to control concrete. The quantum of decreasing permeability was different for specimens with different crystalline admixtures. CA-4 concrete had the highest decrease in permeability of 51% for w/b of 0.4 and 44% for w/b of 0.6. Furthermore, CA-3 concrete showed no change for w/b of 0.4 and the lowest decrease of permeability 2% for w/b 0.6.

The decrease in permeability was attributed to the swelling of the matrix and precipitation of calcite crystals as presented in SEM results of CA-4 concrete (Figure 4-18 and Figure 4-20). In addition, the decrease in permeability can be attributed to the increase in dosage in the concrete mix. The results coincide with Azarsa, Gupta & Biparva, (2019) findings where they achieved 50% reduction permeability on concrete with crystalline admixtures than control mixes. The reason for the reduction in permeability with CA can be associated with a filler effect that can contribute to close the voids but can also work as a cement hydration activator by improving the paste cement microstructure. In addition, Wang et al., (2018) deduced that the reduction of permeability is attributed to the improvement in density that is caused by the hydration of CA and swelling of concrete matrix.

4.4.3. Water sorptivity index results (uncracked concrete)

The WSI test measures the rate of movement of a waterfront through concrete under capillary suction. The test is sensitive to the near-surface properties of concrete and therefore reflects the nature and effectiveness of curing. The lower the sorptivity value translates to concrete being resistant to moisture penetration. The corresponding water sorptivity values for the concrete at curing ages 4, 8, and 12 weeks are presented in Figure 4-34. Detailed water sorptivity results are presented in Appendix F.

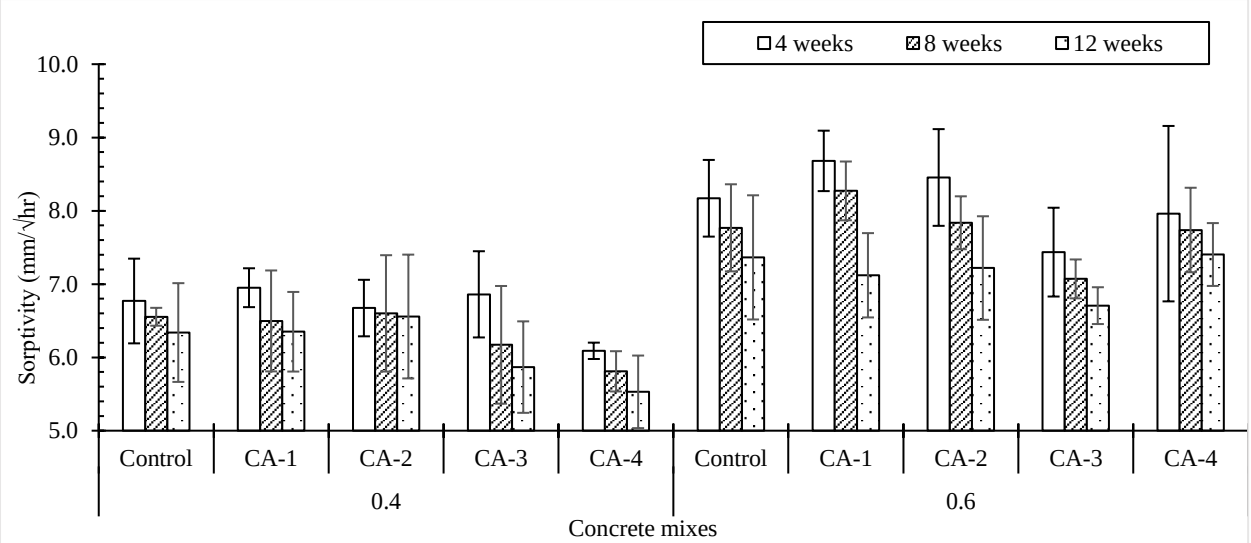

Figure 4-34: Sorptivity results of uncracked concrete with different crystalline admixtures at two w/b ratios

From Figure 4-34, all the concrete mixes showed “good” quality with sorptivity values at curing ages 4, 8, and 12 weeks except concretes with w/b of 0.4 at 12 weeks with excellent quality. A trend was observed where the sorptivity values decreased with an increase in curing age. This was attributed to the continuing hydration, which refines the microstructure of concrete by reduced pore size, or introducing additional tortuosity to pores, increasing the resistance to capillary absorption of liquid. However, few exceptions were observed in control concrete with a w/b ratio of 0.4 and CA-2 concrete at a w/b ratio of 0.4. Considering the error bars, the sorptivity values of the mixes increased as curing time increased. Sorptivity results of control with a w/b ratio of 0.4 increased from 8 weeks to 12 weeks. In addition, sorptivity results of CA-2 concrete with a w/b ratio of 0.4 increased from 4 weeks to 12 weeks. The reason was attributed to the anomaly of the specimens’ results obtained during the testing where outliers values were identified (i.e., Appendix F). All the concrete had their sorptivity values increase with an increase in w/b ratio. A higher w/b ratio increases the water filled porosity within the paste microstructure, increasing the sorptivity results (Alexander, Ballim & Beushausen, 2009).

The influence of crystalline admixtures on the sorptivity values was not observed as there was no trend observed. All the concrete mixes had sorptivity values ranging from 5 to 10. This was expected as the sorptivity test measures the rate of movement of a wetting front through concrete under capillary suction. The test method does not account for the possibility of contamination of the surface of concrete, thus, affecting

the results. For this reason, a measure of water filled porosity, representing the volume of accessible pores in the cover zone of concrete was required (Moore, Bakera & Alexander, 2021).

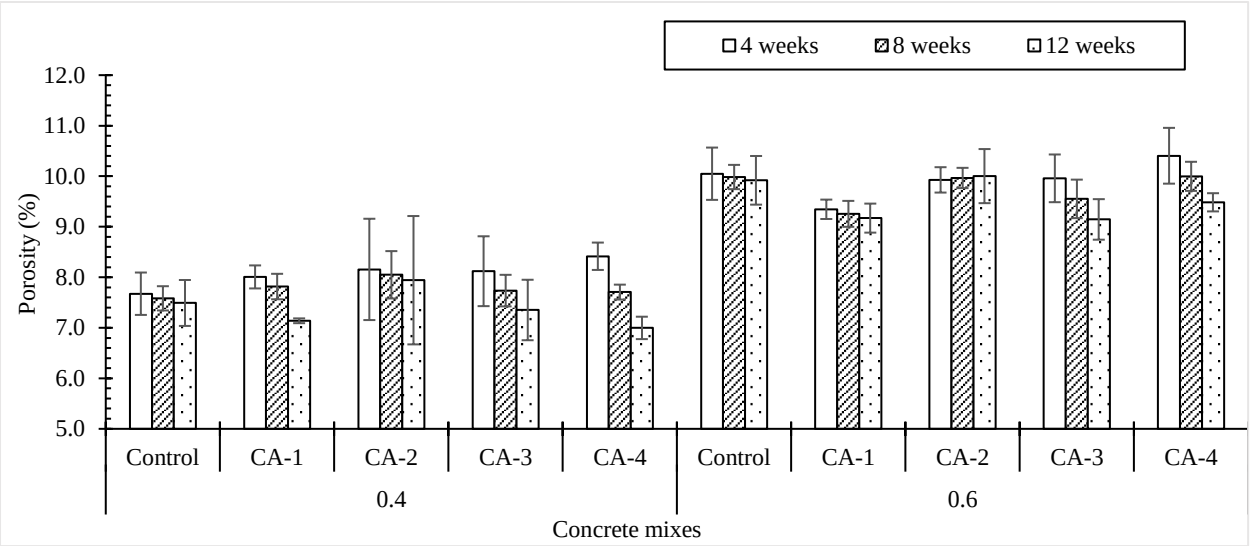

Figure 4-35: Water filled porosity results of uncracked concrete with different crystalline admixtures at two w/b ratios

From Figure 4-35, the water filled porosity results are influenced by the change in the w/b ratio of concrete. A decrease in w/b led to lower water filled porosity as the hydration process fills the void space between cement particles with hydration products. However, in a higher w/b ratio, the extent to which hydration products fill up the voids is limited, resulting in higher water filled porosity after hydration (Grieve, 2009).

4.4.4. Water sorptivity index results (Cracked concrete)

The presence of cracks modifies the transport properties of concrete. The parameters of cracks limit the prediction transport properties of cracked concrete. In the sorptivity test, cracks allow uptake of liquids by capillarity caused by the surface tension force between the crack surface and water. Narrower cracks have more capillarity force than wider cracks. The capillarity force increases as cracks continue to heal (Alexander, Ballim & Beushausen, 2009).

A water sorptivity test was conducted for the cracked concrete with crack widths more than and less than 0.3 mm at curing ages 4, 8, and 12 weeks. Sorptivity and water filled porosity results are presented in Figure 4-36 to Figure 4-39. Detailed water sorptivity and water filled porosity results are presented in Appendix F. Error bars show the standard deviation of the sorptivity values obtained from testing four concrete

discs. The variability of data was expected and was attributed to the variability of the induced cracks in the specimens.

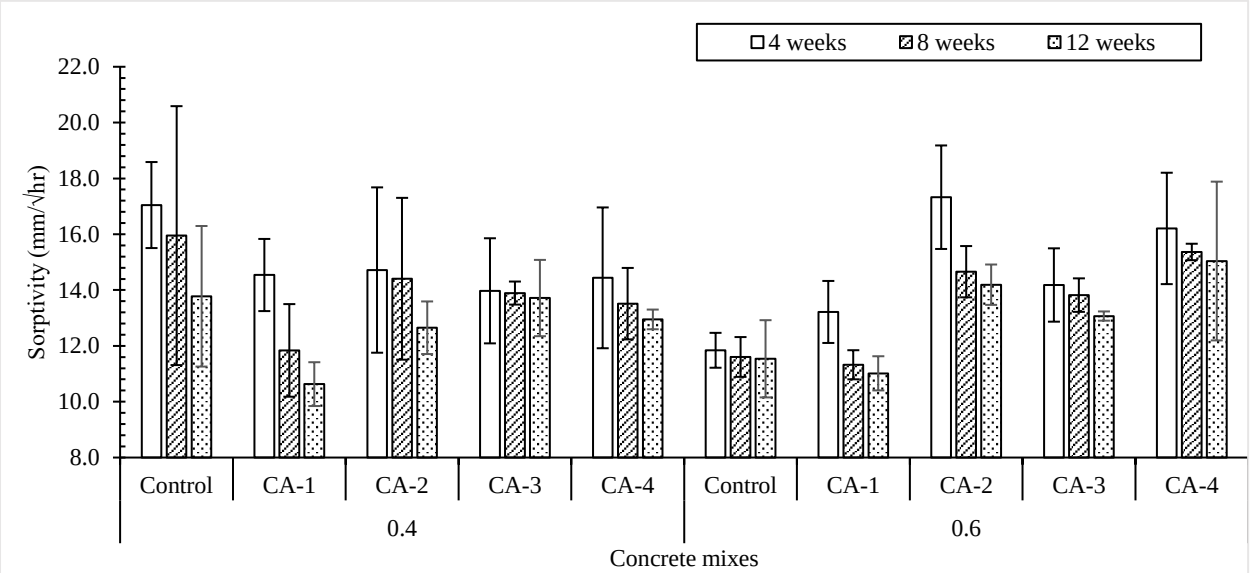

Figure 4-36: Sorptivity results of cracked concrete with different crystalline admixtures at two w/b ratios (crack width more than 0.3 mm)

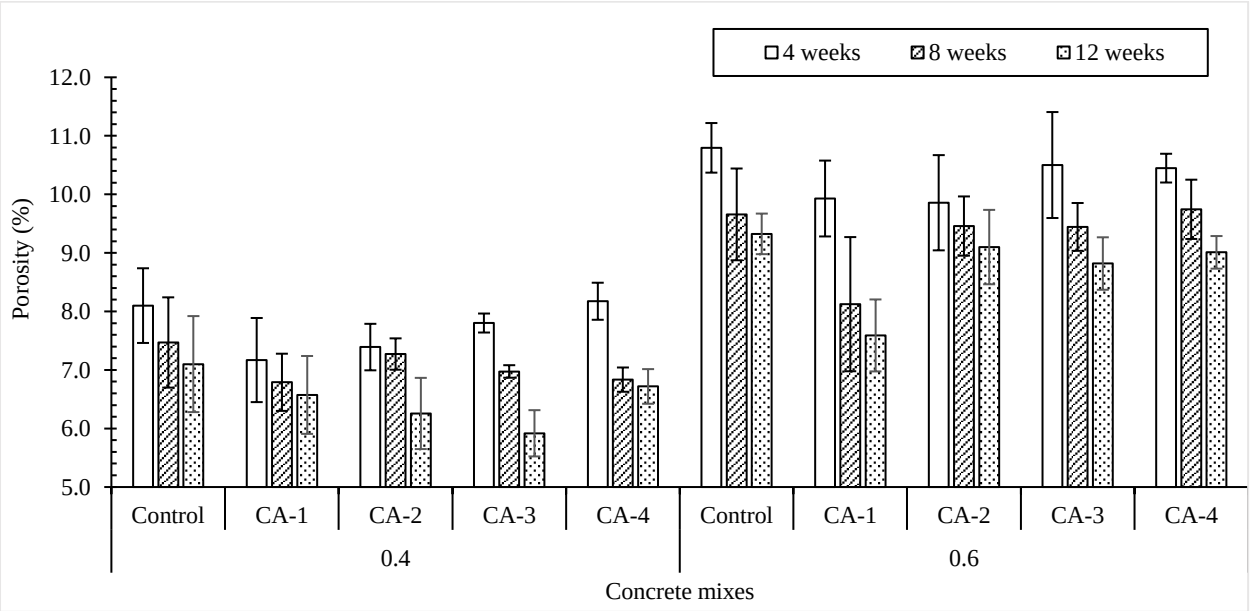

Figure 4-37: Water filled porosity results of cracked concrete with different crystalline admixtures at two w/b ratios (crack width more than 0.3 mm)

All concrete mixes had sorptivity values between 11.84 and 17.35 mm/√hr, 11.32 and 15.95 mm/√hr, and 10.63 and 15.04 mm/√hr, after 4, 8, and 12 weeks of curing, respectively. All the concrete mixes indicated “poor” quality concrete according to Table 4-1. The inconsistency in the sorptivity values was attributed to the crack geometry. The presence of crack results in a higher sorptivity value due to capillary

force due to surface tension between the crack surface and the liquid. Narrower cracks allow more uptake of liquids than wider cracks. The variability in results can be expected as the crack width varies along with the depth of the concrete specimen.

From Figure 4-36, the incorporation of crystalline admixtures had little effect in improving the sorptivity values of cracked concrete. (Wang et al., 2018) deduced that the precipitation of $CaCO_3$ does not contribute much to the decrease in permeability, but rather the swelling of the concrete matrix.

From Figure 4-37, water filled porosity results indicate the influence of the w/b ratio on concrete water filled porosity applies to cracked concrete. Despite the presence of cracks, an increase in w/b led to higher water filled porosity as the extent to which hydration products fill up the voids and the crack area is limited.

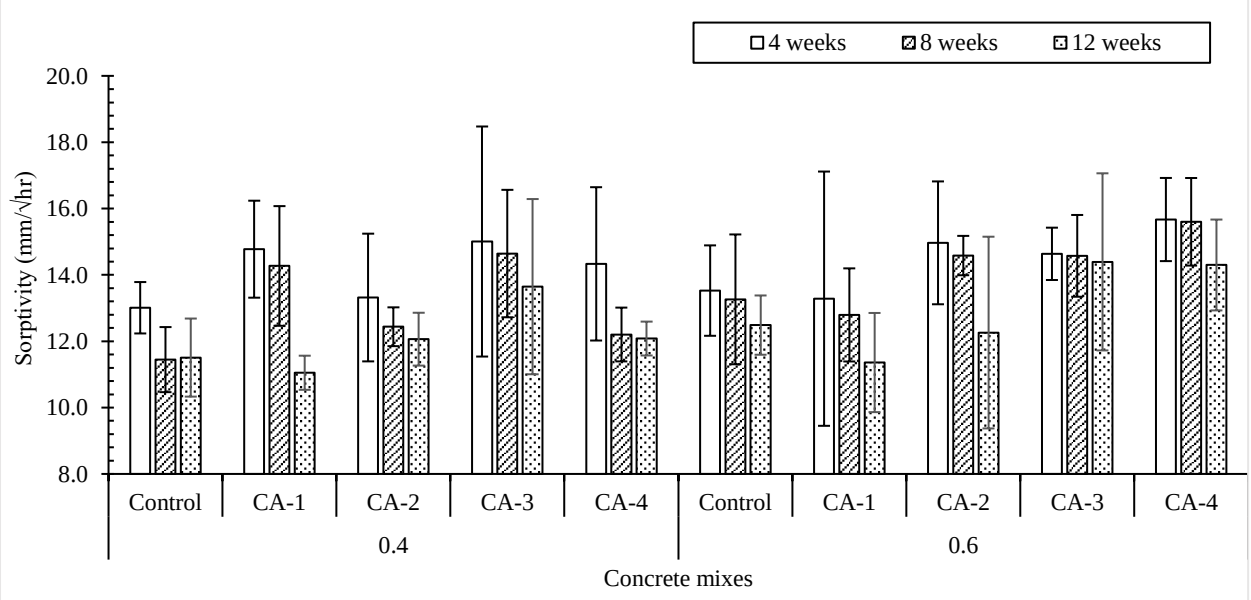

Figure 4-38: Sorptivity results of cracked concrete with different crystalline admixtures at two w/b ratios (crack width less than 0.3 mm)

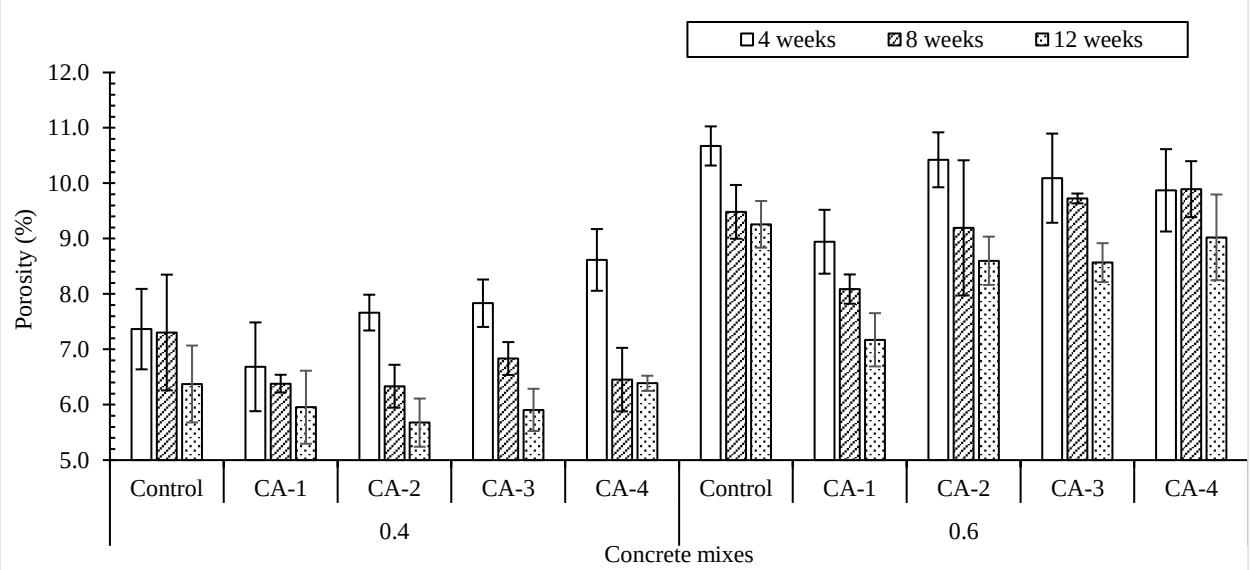

Figure 4-39: Water filled porosity results of cracked concrete with different crystalline admixtures at two w/b ratios (crack width less than 0.3 mm)

A water sorptivity test was conducted on cracked concrete crack width less than 0.3 mm. The results of sorptivity and water filled porosity are presented in Figure 4-38 and Figure 4-39. All concrete mixes had sorptivity values, which indicate “poor” quality. Similar to cracked concrete with crack widths more than 0.3 mm, the sorptivity values have a wide range of values due to cracks. A capillary force led to an uptake of liquid through the crack area resulting in higher sorptivity values. From the results, crystalline admixtures concrete did not significantly alter the sorptivity values. Incorporating the crystalline additives did not influence concrete properties as the additives had a similar chemical composition as ordinary cement.

From Figure 4-39, water filled porosity results show the influence of the w/b ratio on the water filled porosity of cracked concrete. A decrease in w/b led to lower water filled porosity as the void space between cement particles and the crack area is filled with hydration products. However, in a higher w/b ratio, the extent to which hydration products fill up the voids and the crack area is limited, resulting in higher water filled porosity after hydration.

4.4.5. Water permeability test results (cracked concrete)

Crack self-healing promote a decrease in concrete permeability, thus, reducing the ingress of fluids that potentially contain aggressive components. A water permeability test was conducted to quantify the healing performance. During testing, water flow increased non-linearly with time. The non-linearity was attributed to the non-continuity

concrete matrix on the induced cracks area. The water permeability test was conducted until the constant water flow was achieved, thus, allowing the permeability of the specimens to be determined according to D'Arcy's law.

Water permeability tests were conducted on cracked concrete at curing ages of 4, 8, and 12 weeks. The water permeability results of concrete with crack widths less and more than 0.3 are presented in Figure 4-40 and Figure 4-41. Detailed water permeability results are presented in Appendix G.

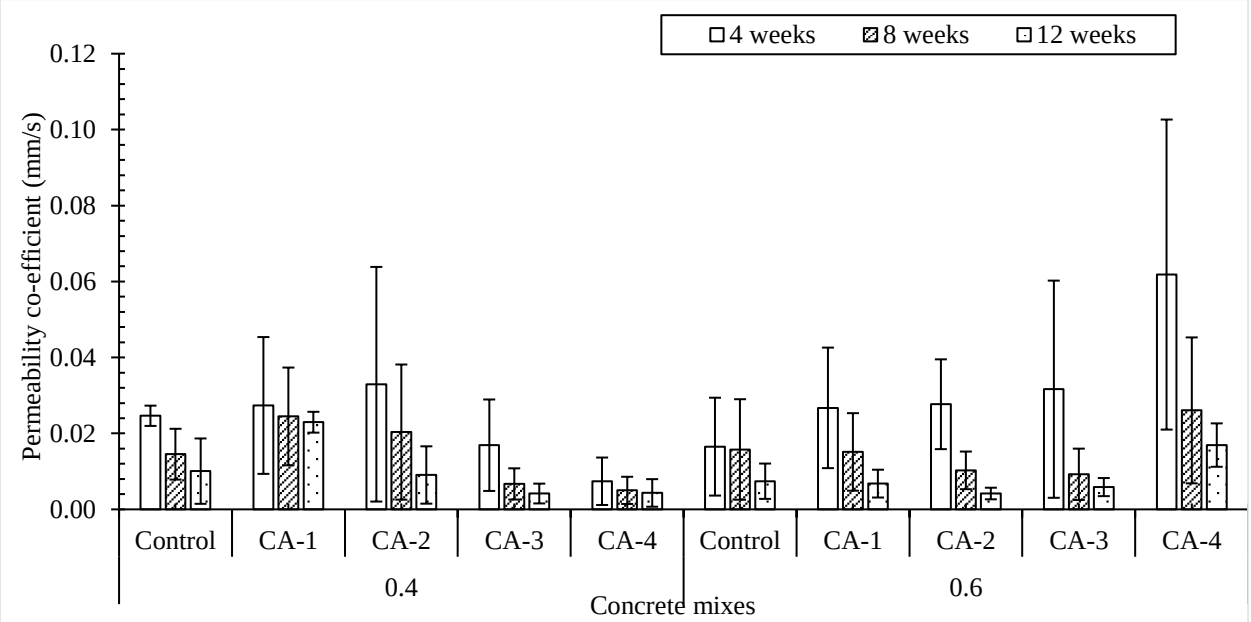

Figure 4-40: Water permeability results of cracked concrete with different crystalline admixtures at two w/b ratios (crack width more than 0.3 mm)

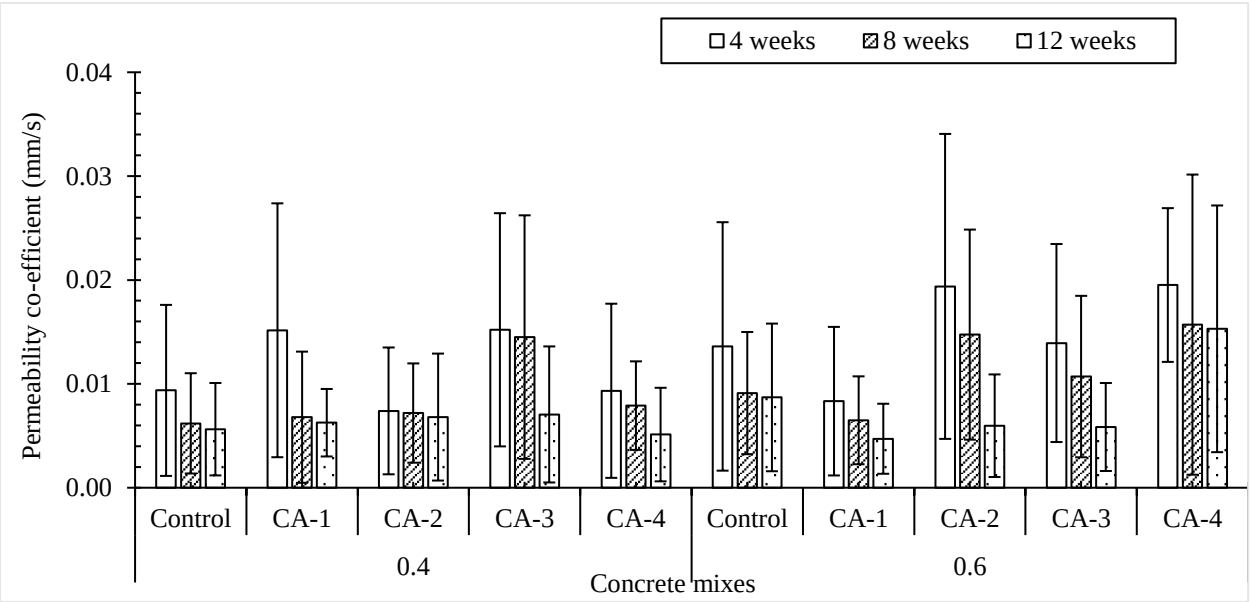

Figure 4-41: Water permeability results of cracked concrete with different crystalline admixtures at two w/b ratios (crack width less than 0.3 mm)

From Figure 4-40 and Figure 4-41, permeability (k) of concrete decreased as curing time increased for all concrete specimens with crack width more than and less than 0.3 mm. This was attributed to the continued hydration of cement. The permeability of the concrete mixes increased with the increase in crack width. Similar results were observed by Wang et al., (1997), where the surface crack width less than 50 microns under loading had little effect on concrete permeability. However, with the crack opening displacement increasing from 50 to 200 microns, concrete permeability increased rapidly.

The high variability of the permeability values was attributed to the crack geometry. Crack geometry is dependent on the concrete matrix of the specimen during crack induction. Since the specimens were small, the arrangement of aggregates within the specimen affects the crack geometry leading to different crack profiles. Thus, the comparison of permeability between concrete mixes proved to be insignificant due to the high variability in the test results. The results are skewed by the fact that the control mix starts with a lower permeability than most other mixes, thus, any improvement in the crystalline admixture does not result in a long-term permeability that is lower than that of the control mix. Thus, it was feasible to discuss the results on independent concrete mixes. Employing Equation 3-1, the percentage reduction in water permeability between four (4) weeks and 12 weeks for concrete specimens with crack width more than and less than 0.3 mm were calculated for analysis and are presented for discussion.

Table 4-3: Water permeabilities reduction as a function of curing time between 4 and 12 weeks (crack width more than 0.3 mm)

w/b	**0.4**					**0.6**				
Concrete mix	**Control**	**CA-1**	**CA-2**	**CA-3**	**CA-4**	**Control**	**CA-1**	**CA-2**	**CA-3**	**CA-4**
Permeability reduction (%)	59	16	73	75	42	55	75	85	81	73

Table 4-4: Water permeabilities reduction as a function of curing time between 4 and 12 weeks (crack width less than 0.3 mm)

w/b	**0.4**					**0.6**				
Concrete mix	**Control**	**CA-1**	**CA-2**	**CA-3**	**CA-4**	**Control**	**CA-1**	**CA-2**	**CA-3**	**CA-4**
Permeability reduction (%)	40	58	8	54	45	36	43	69	58	22

For all specimens, it was observed that the permeability (k) of concrete decreases over curing time. The tests were performed using the long-term (i.e., more than 28 days) aged concrete specimens. From Table 4-3 and Table 4-4, the results show an overall trend of concrete with crystalline admixture to have a larger reduction in permeability with time compared to concrete without admixture. This can be attributed to the precipitation of calcium carbonate crystals by the crystalline admixtures which suggests that these admixtures do have a positive effect in reducing permeability.

Similar results were observed by Yi, Hyun & Kim, (2011), where they concluded that the decrease in permeability was mainly due to precipitation of calcium carbonate crystals at the crack area. The decrease was attributed to autogenous healing as the tests were performed using long term aged specimens; thus, the influence of continued hydration was minimised.

4.5. Chapter Summary

This chapter presented the results, analysis and discussion of the laboratory investigations described in Chapter Three. The chapter is subdivided into four sections. The introduction of the chapter analysing the tests and results to be discussed is presented in section one.

Section two discussed the results of microscopy tests (XRF and SEM-EDS) in order to meet objective one of determining the self-healing mechanism of crystalline admixtures. In XRF test results, the chemical composition of crystalline admixtures and cement were found to be similar. Their similarity was also observed in SEM-EDS test results where the morphologies of the precipitates located in the crack area were mainly composed of calcium carbonate polymorphs. The presence of Sr^{2+} ions in the concrete matrix was attributed to the formation of the precipitates.

Section three presented and discussed the strengths results to meet objective two of determining the influence of crystalline admixtures on the mechanical properties of concrete. The incorporation of the crystalline admixtures in concrete generally increases the strength properties of concrete due to the more refined microstructure resulting from continuing cement hydration and cement being a significant component of some CA's. The presence of cement and reactive silica components has a slightly positive influence on concrete strength development. Furthermore, concrete with w/b ratio of 0.4 indicated lower improvement in the pore structure in comparison to concretes with w/b ratio of 0.6. Since, these crystalline admixtures are typically used

in "high quality" concretes with lower w/b ratios, their effectiveness in improving the durability properties are greatly minimised except in the case of soft water attack.

Section four presented and discussed the results of durability tests to meet the last objective of determining the influence of the crystalline admixtures on the durability properties of concrete. Tests conducted on uncracked concrete indicated that the addition of the crystalline admixtures increases some of the durability properties of concrete (i.e., OPI, WSI, and water filled porosity). This was attributed to the swelling of the matrix and precipitation of calcite crystals. Similar observations were observed in the WSI test results for uncracked concrete specimens.

WSI and water permeability tests were conducted on cracked concrete to quantify the effectiveness of the crystalline admixtures in promoting crack-healing. In WSI test results, the incorporation of crystalline admixtures was found to have little effect in improving the sorptivity values of cracked concrete due to similar chemical compositions between admixtures and ordinary cement. Furthermore, this result concurs with the findings Wang et al., (2018) deducing that the precipitation of $CaCO_3$ does not contribute much to the decrease in permeability, but rather the swelling of the concrete matrix. Percentage reduction of permeability were calculated for water permeability test results relating the individual permeability of CA-concrete and control concrete. Differences in crack profiles rendered comparison between different concrete permeability insignificant. Thus, the comparison was made between specific concrete mix and w/b ratio. Similar to WSI test results, the permeability (k) of concrete decreases with curing time. It was concluded that the decrease in permeability was mainly due to precipitation of calcium carbonate crystals at the crack area.

5. Conclusions and recommendations

5.1. Conclusions

This study aimed at investigating the influence of crystalline admixtures on the mechanical and durability properties of cracked and uncracked concrete. The study was motivated by the presence of crystalline admixtures products marketed in the South Africa market that claim to induce autonomous self-healing and improve the mechanical and durability properties of concrete. Literature has revealed that the influence on mechanical properties is not substantial during the first 28 days of curing. This study determined the influence of crystalline admixtures beyond 28 days curing. The crystalline admixtures were found to have little to no noticeable effect on compressive strength when used in high quality concretes. In practice the crystalline admixtures should be used in concretes with w/b ratio greater than 0.4.

The following specific conclusions can be drawn from the results that were analysed and discussed in Chapter 4.

5.1.1. The self-healing mechanism of the crystalline admixtures

The XRF results show that the oxides of major and trace elements present in the studied crystalline admixtures are similar. Furthermore, the chemical composition is similar to the oxides of ordinary Portland cement. Based on hydration of cement it was deduced that the hydration of the crystalline admixtures will behave similar to that of cement and cement is a significant component of CA's. SEM-EDS tests were then conducted to study the morphology of the hydrated compounds. Precipitates extracted from the crack area after healing were studied and found to be composed of polymorphs of calcium carbonate and CSH. Calcium carbonate precipitates were influenced by the presence of Sr^{2+} and Mg in the concrete matrix.

The calcium carbonate precipitation as the self-healing product in presence of crystalline admixture is correlates with the observations of Escoffres, Desmettre & Charron, (2018) and Roig-Flores et al., (2015). The similarity between hydration of crystalline admixtures and hydration based on their oxides compositions attributes to the similarity of precipitates at the crack area.

5.1.2. The influence on mechanical properties of concrete

The mechanical properties studied were compressive strength and tensile splitting strength. The compressive strength results indicated that the incorporation of crystalline admixtures generally improve the compressive strengths of concretes with higher water filled porosity (i.e., w/b ratio of 0.6) than the concretes with lower water filled porosity (i.e., w/b ratio of 0.4) compared to control concrete. In practice, these crystalline admixtures probably have little to no noticeable effect on compressive strength when used in high quality concretes.

The splitting strength results indicated that CA-1 concrete had a slightly higher splitting strength at 28 days for w/b ratios of 0.6 most likely due to the proportion of cement found in some CA. In addition, the development of splitting strengths from 28-day to 112-day was not observed for both w/b ratios of 0.4 and 0.6 which indicates no apparent improvement after the introduction of crystalline admixtures nor improved tensile capacity of the paste.

5.1.3. The influence on durability properties of concrete

Optical microscope analysis was carried out on healed specimens after 84 days of wet curing to observe the precipitated crystals along the cracks. The cracks were filled with white crystal products which did not completely restore the continuity of the matrix. The whitish products of calcium carbonates were located not only at the mouth of the crack but also inside the crack when the specimens were split open to collect the precipitates.

OPI, WSI, and water filled porosity tests were conducted on uncracked concrete to determine the influence of addition of crystalline admixtures on the durability properties of concrete. The OPI values expressed in co-efficient of permeabilities (k) indicated that the quantum of decreasing permeability was different for specimens with different crystalline admixtures. CA-4 concrete had the highest decrease in permeability of 51.02% for w/b of 0.4 and 43.77% for w/b of 0.6. The decrease in permeability was attributed to the swelling of the matrix and precipitation of calcite crystals as presented in SEM results of CA-4 concrete. Furthermore, the decrease in permeability was attributed to the increased dosage of CA-4 in the concrete mix. WSI results indicated that all the concrete mixes showed “good” quality with sorptivity values at curing ages 4, 8, and 12 weeks except concretes with w/b of 0.4 at 12 weeks with excellent quality.

A trend was observed where the sorptivity values decreased with an increase in curing age. This was attributed to the continuing hydration, which refines the microstructure of concrete, increasing the resistance to capillary absorption of liquid.

WSI, water filled porosity, and water permeability tests were conducted on cracked concrete to quantify the effectiveness of the crystalline admixtures in promoting crack-healing. In WSI test results, the incorporation of crystalline admixtures was found to have little effect in improving the sorptivity values of cracked concrete due to similar chemical compositions between admixtures and ordinary cement. Percentage reduction of permeability were calculated for water permeability test results relating the individual permeability of CA-concrete and control concrete. Differences in crack profiles rendered comparison between different concrete permeability insignificant. Thus, the comparison was made between specific concrete mixes. Similar to WSI test results, the water permeability (k) of concrete decreases over curing time. It was concluded that the decrease in water permeability was mainly due to the precipitation of calcium carbonate crystals at the crack area.

5.2. Recommendations

In this experimental programme, the quality of the data collected and analysed may be further refined to reduce variability in results obtained due to crack geometry and variability of test approach which will bring more insight into the influence of crystalline admixtures on concrete properties. In general, the following recommendations can be used in further research studies to add to the body of knowledge about the influence of crystalline admixtures in promoting the self-healing of concrete. The recommendations are presented to improve the outcome of this research topic and future related work.

a) An extended curing duration should be employed to continue monitoring the healing process to determine the duration of full self-healing if any.
b) An interrupted curing regime should be employed, where CA concrete may perform better.
c) Other microscopic techniques such as Thermogravimetric analysis (TGA) and X-Ray Diffraction Analysis (XRD) should be used on the crystalline admixtures to determine the reactivity, thermal/oxidative stabilities, and analysis of the structures of the crystalline admixtures. The tests will provide

further insight and understanding on the underlying self-healing mechanism of crystalline admixtures, if any.

d) The use of uniform controlled crack width to minimise the variability in the test results collected as a result of crack geometry. However, the uniform crack width specimens should be used in conjunction to free occurring cracks width for correlation of both test results and in-service performance.

e) The use of water permeability test under pressure to minimise the test duration. The test is especially useful to determine the water permeability of uncracked specimens. Thus, the comparison between uncracked and cracked concrete can be analysed.

f) The influence of the CA as a measure to reduce or slow soft water attack should be investigated.

References

ACI 301-10. 2010. Specifications for Structural Concrete. *American Concrete Institute*. 77.

ACI Committee 201. 2001. *Guide to Durable Concrete*.

Addis, Brian. & Goodman, John. 2009. Concrete mix design. In *Fulton's Concrete Technology*. 9th ed. G. Owens, Ed. Midrand: Cement & Concrete Institute. 219–228.

Ahn, T.-H. & Kishi, T. 2010. Crack Self-healing Behavior of Cementitious Composites Incorporating Various Mineral Admixtures. *Journal of Advanced Concrete Technology*. 8(2):171–186. DOI: 10.3151/jact.8.171.

Alexander, Mark. 2017. *Durability Index Testing Procedure Manual*. Cape Town.

Alexander, Mark. & Beushausen, Hans. 2009. Deformation and volume change of hardened concrete. In *Fulton's Concrete Technology*. 9th ed. G. Owens, Ed. Midrand: Cement & Concrete Institute. 111–154.

Alexander, M., Bentur, A. & Mindess, S. 2017a. *Durability of Concrete Design and Construction*. 1st ed. New York: CRC Press.

Alexander, M., Bentur, A. & Mindess, S. 2017b. *Durability of Concrete Design and Construction*. 1st ed. New York: CRC Press.

Alexander, Mark., Ballim, Yunus. & Beushausen, Hans. 2009. Durability of concrete. In *Fulton's Concrete Technology*. 9th ed. G. Owens, Ed. Midrand: Cement & Concrete Institute. 155–188.

ASTM C1723-16. 2016. Standard guide for examination of hardened concrete using scanning electron microscopy. *Annual Book of ASTM Standards*. 00(Reapproved 2004):1–95. DOI: 10.1520/C1723-16.can.

ASTM E1621-13. 2013. Standard guide for elemental analysis by wavelength dispersive X-Ray fluorescence spectrometry. *Annual Book of ASTM Standards*. i:1–9. DOI: 10.1520/E1621-13.2.

Azarsa, P., Gupta, R. & Biparva, A. 2019. Assessment of self-healing and durability parameters of concretes incorporating crystalline admixtures and Portland Limestone Cement. *Cement and Concrete Composites*. 99(February):17–31. DOI: 10.1016/j.cemconcomp.2019.02.017.

Ballim, Yunus. & Graham, Peter. 2009. Thermal properties of concrete and temperature development at early ages in large concrete elements. In *Fulton's*

Concrete Technology. 9th ed. G. Owens, Ed. Midrand: Cement & Concrete Institute. 273–286.

Bamforth, P.B. 2018. Control of cracking caused by restrained deformation in concrete. *Construction Industry Research and Information Association.* 250.

Batog, M. & Giergiczny, Z. 2017. Influence of mass concrete constituents on its properties. *Construction and Building Materials*. 146:221–230. DOI: 10.1016/J.CONBUILDMAT.2017.04.085.

Bran-Anleu, P., Caruso, F., Wangler, T., Pomjakushina, E. & Flatt, R.J. 2018. Standard and sample preparation for the micro XRF quantification of chlorides in hardened cement pastes. *Microchemical Journal*. 141(April):382–387. DOI: 10.1016/j.microc.2018.05.040.

BS EN 12390-8. 2009. Testing hardened concrete Part 8: Depth of penetration of water under pressure. *British Standard*.

Coppola, L., Coffetti, D. & Crotti, E. 2018. Innovative carboxylic acid waterproofing admixture for self-sealing watertight concretes. *Construction and Building Materials*. 171:817–824. DOI: 10.1016/j.conbuildmat.2018.03.201.

Cuenca, E., Tejedor, A. & Ferrara, L. 2018. A methodology to assess crack-sealing effectiveness of crystalline admixtures under repeated cracking-healing cycles. *Construction and Building Materials*. 179:619–632. DOI: 10.1016/j.conbuildmat.2018.05.261.

Elsalamawy, M., Mohamed, A.R. & Abosen, A.E. 2019. Performance of crystalline forming additive materials in concrete. *Construction and Building Materials*. 230:117056. DOI: 10.1016/j.conbuildmat.2019.117056.

Escoffres, P., Desmettre, C. & Charron, J.P. 2018. Effect of a crystalline admixture on the self-healing capability of high-performance fiber reinforced concretes in service conditions. *Construction and Building Materials*. 173:763–774. DOI: 10.1016/j.conbuildmat.2018.04.003.

Ferrara, L., Krelani, V. & Carsana, M. 2014. A “fracture testing” based approach to assess crack healing of concrete with and without crystalline admixtures. *Construction and Building Materials*. 68:535–551. DOI: 10.1016/j.conbuildmat.2014.07.008.

Ferrara, L., Van Mullem, T., Alonso, M.C., Antonaci, P., Borg, R.P., Cuenca, E., Jefferson, A., Ng, P.L., et al. 2018. Experimental characterization of the self-healing capacity of cement based materials and its effects on the material performance: A

state of the art report by COST Action SARCOS WG2. *Construction and Building Materials*. 167:115–142. DOI: 10.1016/j.conbuildmat.2018.01.143.

Ferrara, L., Asensio, E.C., Monte, F. Lo, Flores, M.R., Moreno, M.S., Snoeck, D., Mullem, T. Van & Belie, N. De. 2018. Experimental Characterization of the Self-Healing Capacity of Cement Based Materials: An Overview. *Proceedings*. 2(8):454. DOI: 10.3390/ICEM18-05322.

Gavin Alexander, M., Ballim, Yunus. & Mackechnie, J.R. 1999. *Guide to the use of durability indexes for achieving durability in concrete structures*.

Grieve, Graham. 2009. Cementitious materials. In *Fulton's Concrete Technology*. 9th ed. G. Owens, Ed. Midrand: Cement & Concrete Institute. 1–16.

Haoliang, H. & Ye, G. 2014. A review on self-healing in reinforced concrete structures in view of serving conditions. *In 3rd International Conference on Service Life Design for Infrastructure, Zhuhai, China*. 1–14.

Huang, H., Ye, G., Qian, C. & Schlangen, E. 2016. Self-healing in cementitious materials: Materials, methods and service conditions. *Materials and Design*. 92:499–511. DOI: 10.1016/j.matdes.2015.12.091.

Jiang, Z., Li, W., Yuan, Z. & Yang, Z. 2014. Self-healing of cracks in concrete with various crystalline mineral additives in underground environment. *Journal Wuhan University of Technology, Materials Science Edition*. 29(5):938–944. DOI: 10.1007/s11595-014-1024-2.

Joshi, S., Goyal, S., Mukherjee, A. & Reddy, M.S. 2017. Microbial healing of cracks in concrete: a review. *Journal of Industrial Microbiology and Biotechnology*. 44:1511–1525. DOI: 10.1007/s10295-017-1978-0.

Kellerman, John. & Crosswell, Steve. 2009. Properties of fresh concrete. In *Fulton's Concrete Technology*. 9th ed. G. Owens, Ed. Midrand: Cement & Concrete Institute. 83–95.

Klemczak, B., Batog, M., Pilch, M. & Żmij, A. 2017. Analysis of Cracking Risk in Early Age Mass Concrete with Different Aggregate Types. *Procedia Engineering*. 193:234–241.

Luo, M., Qian, C.X. & Li, R.Y. 2015. Factors affecting crack repairing capacity of bacteria-based self-healing concrete. *Construction and Building Materials*. 87:1–7. Available: http://dx.doi.org/10.1016/j.conbuildmat.2015.03.117.

Meharie, M.G., Kaluli, J.W. & Abiero-Gariy, Z. 2017. Factors affecting the self-healing efficiency of cracked concrete structures. *American Journal of Applied Scientific Research*. 3:86–92. DOI: 10.11648/j.ajasr.20170306.12.

Mindess, Sidney., Young, J.Francis. & Darwin, David. 2003. *Concrete*. 2nd ed. New Jersey: Prentice Hall. DOI: 10.3785/j.issn.1008-973X.2009.11.016.

Mircea, C.G.R. & Faur, A. 2012. Thoughts Upon Shrinkage Induced Cracking of Concrete . a Structural Designer Perspective. *CONCRACK3 - RILEM-JCI International Workshop on Crack Control of Mass Concrete and Related Issues Concerning Early-Age of Concrete Structures*. 157–166.

Moore, Amy., Bakera, Alice. & Alexander, Mark. 2021. A critical review of the Water Sorptivity Index (WSI) parameter for potential durability assessment: Can WSI be considered in isolation of porosity? *Journal of the South African institution of civil engineering*. (June). DOI: 10.17159/2309-8775/2021/v63n2a4.

Muhammad, N.Z., Shafaghat, A., Keyvanfar, A., Majid, M.Z.A., Ghoshal, S.K., Mohammadyan Yasouj, S.E., Ganiyu, A.A., Samadi Kouchaksaraei, M., et al. 2016. Tests and methods of evaluating the self-healing efficiency of concrete: A review. *Construction and Building Materials*. 112:1123–1132. DOI: 10.1016/j.conbuildmat.2016.03.017.

Palin, D., Wiktor, V. & Jonkers, H.M. 2015. Autogenous healing of marine exposed concrete: Characterization and quantification through visual crack closure. *Cement and Concrete Research*. 73:17–24. DOI: 10.1016/j.cemconres.2015.02.021.

Palin, D., Jonkers, H.M. & Wiktor, V. 2016. Autogenous healing of sea-water exposed mortar: Quantification through a simple and rapid permeability test. *Cement and Concrete Research*. 84:1–7. DOI: 10.1016/j.cemconres.2016.02.011.

Park, B. & Cheol, Y. 2019. Investigating a new method to assess the self-healing performance of hardened cement pastes containing supplementary cementitious materials and crystalline admixtures. *Integrative Medicine Research*. (x x):1–16. DOI: 10.1016/j.jmrt.2019.09.080.

Park, B. & Choi, Y.C. 2018. Quantitative evaluation of crack self-healing in cement-based materials by absorption test. *Construction and Building Materials*. 184:1–10. DOI: 10.1016/j.conbuildmat.2018.06.206.

Phelan, W.S., Violetta, B.K., Eller, R., Korhonen, C.J., Nkinamubanzi, P.-C., Roberts, L.R., Stokes, D.B., Strickland, B.R., et al. 2010. *Report on Chemical Admixtures for Concrete*. Michigan.

Qian, C., Chen, H., Ren, L. & Luo, M. 2015. Self-healing of early age cracks in cement-based materials by mineralization of carbonic anhydrase microorganism. *Frontiers in Microbiology*. 6(NOV). DOI: 10.3389/fmicb.2015.01225.

Qiu, J., Tan, H.S. & Yang, E.H. 2016. Coupled effects of crack width, slag content, and conditioning alkalinity on autogenous healing of engineered cementitious composites. *Cement and Concrete Composites*. 73:203–212. DOI: 10.1016/j.cemconcomp.2016.07.013.

Restuccia, L., Reggio, A., Andrea, G. & Tulliani, J. 2017. New self-healing techniques for cement-based materials. *Procedia Structural Integrity*. 3:253–260.

Roig-Flores, M., Moscato, S., Serna, P. & Ferrara, L. 2015. Self-healing capability of concrete with crystalline admixtures in different environments. *Construction and Building Materials*. 86:1–11. DOI: 10.1016/j.conbuildmat.2015.03.091.

Roig-Flores, M., Pirritano, F., Serna, P. & Ferrara, L. 2016. Effect of crystalline admixtures on the self-healing capability of early-age concrete studied by means of permeability and crack closing tests. *Construction and Building Materials*. 114:447–457. DOI: 10.1016/j.conbuildmat.2016.03.196.

Rooij, M. de (Ed), Tittelboom, K.V. (Ed), Belie, N.D. (Ed) & Schlangen, E. (Ed). 2013. *Self-healing phenomena in cement-based materials (A State of the Art Report of RILEM Technical Committee 221-SHC)*. Delft. DOI: 10.1007/978-94-007-6624-2.

Sangadji, S. 2017. Can Self-healing Mechanism Helps Concrete Structures Sustainable? *Procedia Engineering*. 171:238–249. DOI: 10.1016/j.proeng.2017.01.331.

SANS 201. 2008. Sieve analysis, fines content, and dust content of aggregates. *South African National Standard*. (2.2):1–14.

SANS 3001-CO3-1. 2015. Civil engineering test methods Part CO3-1: Concrete durability index testing — Preparation of test specimens. *South African National Standards*. (1):4.

SANS 3001-CO3-2. 2015. Civil engineering test methods Part CO3-2: Concrete durability index testing — Oxygen permeability test. *South African National Standards*. (1):16.

SANS 5861-1. 2006. Concrete tests Part 1: Mixing fresh concrete in laboratory. *South African National Standards*. (2.1):2.

SANS 5861-2. 2006. Concrete tests Part 2: Sampling of freshly mixed concrete. *South African National Standards*. (2.1):3.

SANS 5861-3. 2006. Concrete tests Part 3: Making and curing of test specimens. *South African National Standards*.

SANS 5863. 2006. Concrete tests — Compressive strength of hardened concrete. *South African National Standards*. (2.1):3.

SANS 5864. 2006. Concrete tests - Flexural strength of hardened concrete. *South African National Standards*. (2.1):5.

SANS 6253. 2006. Concrete tests - Tensile Splitting Strength of Concrete. *South African National Standard*. (1.1):4.

SANS 10100-1. 2000. *The structural use of concrete. Part 1: Design*. South African Bureau of Standards.

Sisomphon, K., Copuroglu, O. & Koenders, E.A.B. 2012. Self-healing of surface cracks in mortars with expansive additive and crystalline additive. *Cement and Concrete Composites*. 34:566–574.

Snoeck, D., Dewanckele, J., Cnudde, V. & De Belie, N. 2016. X-ray computed microtomography to study autogenous healing of cementitious materials promoted by superabsorbent polymers. *Cement and Concrete Composites*. 65:83–93. DOI: 10.1016/j.cemconcomp.2015.10.016.

Sohawon, H. 2018. Service life extension of reinforced concrete structures using hydrophobic impregnation. The University of Cape Town.

Stuckrath, C., Serpell, R., Valenzuela, L.M. & Lopez, M. 2014. Quantification of chemical and biological calcium carbonate precipitation: Performance of self-healing in reinforced mortar containing chemical admixtures. *Cement and Concrete Composites*. 50:10–15. DOI: 10.1016/j.cemconcomp.2014.02.005.

Suleiman, A.R. & Nehdi, M.L. 2018. Effect of environmental exposure on autogenous self-healing of cracked cement-based materials. *Cement and Concrete Research*. 111:197–206. DOI: 10.1016/j.cemconres.2018.05.009.

Van Tittelboom, K., De Belie, N., Van Loo, D. & Jacobs, P. 2011. Self-healing efficiency of cementitious materials containing tubular capsules filled with healing

agent. *Cement and Concrete Composites*. 33(4):497–505. DOI: 10.1016/j.cemconcomp.2011.01.004.

Van Tittelboom, K., Wang, J., Araújo, M., Snoeck, D., Gruyaert, E., Debbaut, B., Derluyn, H., Cnudde, V., et al. 2016. Comparison of different approaches for self-healing concrete in a large-scale lab test. *Construction and Building Materials*. 107:125–137.

Tong, Z. 2015. Cause and Influence of Mass Concrete Crack. *International Conference on Chemical, Material and Food Engineering*. 497–499.

Wang, K., Jansen, D.C., Shah, S.P. & Karr, A.F. 1997. Permeability study of cracked concrete. *Cement and Concrete Research*. 27(3):381–393.

Wang, X., Fang, C., Li, D., Han, N. & Xing, F. 2018. A self-healing cementitious composite with mineral admixtures and built-in carbonate. *Cement and Concrete Composites*. 92:216–229. DOI: 10.1016/j.cemconcomp.2018.05.013.

Wu, M., Johannesson, B. & Geiker, M. 2012. A review: Self-healing in cementitious materials and engineered cementitious composite as a self-healing material. *Construction and Building Materials*. 28(1):571–583. DOI: 10.1016/j.conbuildmat.2011.08.086.

Yang, Y., Yang, E.H. & Li, V.C. 2011. Autogenous healing of engineered cementitious composites at early age. *Cement and Concrete Research*. 41(2):176–183. DOI: 10.1016/j.cemconres.2010.11.002.

Yi, S.T., Hyun, T.Y. & Kim, J.K. 2011. The effects of hydraulic pressure and crack width on water permeability of penetration crack-induced concrete. *Construction and Building Materials*. 25(5):2576–2583. DOI: 10.1016/j.conbuildmat.2010.11.107.

Zhang, G., Wang, L., Wang, P. & Yu, S. 2018. Effects of fly ash and crystalline additive on mechanical properties of two-graded roller compacted concrete in a high RCC arch dam. *Construction and Building Materials*. 182:682–690. DOI: 10.1016/j.conbuildmat.2018.06.101.

Zhou, G., Yu, J.C., Wang, X. & Zhang, L. 2004. Sonochemical synthesis of aragonite-type calcium carbonate with different morphologies. *The Royal Society of Chemistry and the Centre National de la Recherche Scientifique*. 1027–1031.

Appendices

Appendix A: X-Ray Fluorescence (XRF) test results

Table A-1 shows detailed XRF test results. These data were used to compare the reactivity of cement and crystalline admixtures.

Table A-1: X-ray Fluorescence (XRF) test results

Oxide/Sample	**SiO_2**	**TiO_2**	**$Al2O_3$**	**Fe_2O_3**	**MnO**	**MgO**	**CaO**	**Na_2O**
	wt.%	**wt.%**	**wt.%**	**wt.%**	**wt.%**	**wt.%**	**wt.%**	**wt.%**
CA-1	35.74	0.36	4.39	2.15	0.05	2.47	46.80	0.60
CA-2	15.36	0.17	4.30	1.63	0.07	3.97	54.95	7.52
CA-3	6.47	0.11	1.33	0.81	0.02	0.52	46.91	1.96
CA-4	9.76	0.15	2.55	1.61	0.04	0.66	49.68	6.28
Oxide/Sample	**K_2O**	**P_2O_5**	**SO_3**	**Cr_2O_3**	**NiO**	**H_2O-**	**LOI**	**Total**
	wt.%	**wt.%**	**wt.%**	**wt.%**	**wt.%**	**wt.%**	**wt.%**	**wt.%**
CA-1	0.29	0.15	1.37	0.01	0.01	0.60	4.41	99.40
CA-2	0.78	0.21	2.36	b.d.	b.d.	1.04	7.43	99.80
CA-3	0.22	0.10	0.80	b.d.	b.d.	4.10	36.19	99.56
CA-4	0.38	0.02	1.28	b.d.	b.d.	1.26	25.49	99.15

(**Note:** b.d. = below detection)

Appendix B: SEM-EDS Test Results

Table B-1 to presents the detailed EDS test results. These results were used with SEM images to characterise the chemical composition of precipitates at the crack location.

Table B-1: Detailed EDS test results of control concrete

w/b ratio	Spectrum	Elemental Composition (%)						
		Ca	Si	Al	Fe	C	O	Sr
0.4	Spectrum 1	28.02	-	-	-	19.36	48.65	2.57
	Spectrum 2	27.43	-	-	-	18.23	49.11	b.d.
	Spectrum 3	25.12	-	-	-	18.01	54.06	2.56
	Spectrum 4	33.57	-	-	-	18.24	45.93	3.01
0.6	Spectrum 1	24.15	5.01	1.54	1.56	11.37	56.10	-
	Spectrum 2	20.01	2.84	2.43	1.46	12.23	58.14	-
	Spectrum 3	25.32	8.04	1.22	1.87	15.65	50.09	-

(**Note:** b.d. = below detection)

Table B-2: Detailed EDS test results of concrete with CA-1

w/b ratio	Spectrum	Elemental Composition (%)					
		Ca	Al	C	O	S	Sr
0.4	Spectrum 1	27.54	-	18.05	54.15	-	2.14
	Spectrum 2	29.12	-	18.00	52.65	-	2.54
	Spectrum 3	25.92	-	21.13	53.18	-	-
0.6	Spectrum 1	12.87	3.01	21.12	58.63	6.12	4.59

Table B-3: Detailed EDS test results of concrete with CA-2

w/b ratio	Spectrum	Elemental Composition (%)			
		Ca	C	O	Sr
0.4	Spectrum 1	24.12	18.11	56.83	-
	Spectrum 2	34.11	16.01	50.26	-
	Spectrum 3	27.71	18.02	57.12	-
	Spectrum 4	59.92	7.11	34.54	-
	Spectrum 5	34.51	15.92	48.76	-
0.6	Spectrum 1	33.86	15.16	49.23	4.10
	Spectrum 2	18.56	26.45	51.58	4.33

Table B-4: Detailed EDS test results of concrete with CA-3

w/b ratio	Spectrum	Elemental Composition (%)					
		Ca	Al	C	O	S	Sr
0.4	**Spectrum 1**	4.14	1.12	49.13	46.13	1.30	-
0.6	**Spectrum 1**	25.12	-	21.12	53.12	-	3.42

Table B-5: Detailed EDS test results of concrete with CA-4

w/b ratio	Spectrum	Elemental Composition (%)				
		Ca	Al	C	O	Sr
0.4	**Spectrum 1**	29.92	-	18.02	51.23	1.76
	Spectrum 2	19.95	-	30.11	49.94	1.02
0.6	**Spectrum 1**	32.12	1.07	18.16	50.25	-

Appendix C: Detailed compressive strength test results

Table C-1 to Table C-5 shows the compressive strength of concretes with different crystalline admixtures.

Table C-1: Detailed compressive strength results of control concrete

w/b	Age (days)	Cube	Height (mm)	Breadth (mm)	Length (mm)	Mass (kg)	Load (kN)	Compressive strength (MPa)	Validity
0.4	7	1	100.65	100.00	100.00	2.460	540	53.7	OK
		2	102.83	100.00	100.00	2.495	560	54.5	
		3	103.70	100.00	100.00	2.530	565	54.5	
		Average					**555**	**54.2**	
	28	1	101.72	100.00	100.48	2.475	606	59.6	OK
		2	102.22	100.00	100.56	2.495	594	58.1	
		3	102.83	100.00	101.13	2.470	604	58.7	
		Average					**601**	**58.8**	
	112	1	99.21	100.00	100.00	2.425	684	68.9	OK
		2	101.31	100.00	101.00	2.420	712	70.3	
		3	99.30	100.00	101.00	2.425	690	69.5	
		Average					**695**	**69.6**	
0.6	7	1	102.06	100.00	100.00	2.465	376	36.8	OK
		2	104.06	100.00	100.00	2.475	380	36.5	
		3	100.52	100.00	100.00	2.450	390	38.8	
		Average					**382**	**37.4**	
	28	1	101.56	100.00	100.48	2.460	428	42.1	OK
		2	101.14	100.00	100.56	2.435	382	37.8	
		3	100.71	100.00	101.13	2.450	404	40.1	
		Average					**405**	**40.0**	
	112	1	101.29	100.00	100.00	2.480	482	47.6	OK
		2	100.40	100.00	101.00	2.465	470	46.8	
		3	99.59	100.00	101.00	2.425	485	48.7	

w/b	Age (days)	Cube	Height (mm)	Breadth (mm)	Length (mm)	Mass (kg)	Load (kN)	Compressive strength (MPa)	Validity
		Average					**479**	**47.7**	

Table C-2: Detailed compressive strength of concrete with CA-1

w/b	Age (days)	Cube	Height (mm)	Breadth (mm)	Length (mm)	Mass (kg)	Load (kN)	Compressive strength (MPa)	Validity
0.4	7	1	98.82	100.00	100.00	2.465	516	52.2	OK
		2	100.52	100.00	100.00	2.475	546	54.3	
		3	100.04	100.00	100.00	2.450	530	53.0	
		Average					**531**	**53.2**	
	28	1	100.66	100.00	100.48	2.470	680	67.6	OK
		2	102.29	100.00	100.56	2.540	626	61.2	
		3	100.71	100.00	101.13	2.520	650	64.5	
		Average					**652**	**64.4**	
	112	1	100.28	100.00	100.00	2.500	720	71.8	OK
		2	102.57	100.00	101.00	2.510	702	68.4	
		3	100.63	100.00	101.00	2.485	714	71.0	
		Average					**712**	**70.4**	
0.6	7	1	99.68	100.00	100.00	2.390	389	39.0	OK
		2	100.41	100.00	100.00	2.410	384	38.2	
		3	100.56	100.00	100.00	2.350	386	38.4	
		Average					**386**	**38.6**	
	28	1	99.03	100.00	100.48	2.365	498	50.3	OK
		2	100.27	100.00	100.56	2.435	460	45.9	
		3	99.58	100.00	101.13	2.420	480	48.2	
		Average					**479**	**48.1**	
	112	1	100.64	100.00	100.00	2.420	454	45.1	OK
		2	100.31	100.00	101.00	2.420	500	49.8	
		3	99.89	100.00	101.00	2.430	502	50.3	

w/b	Age (days)	Cube	Height (mm)	Breadth (mm)	Length (mm)	Mass (kg)	Load (kN)	Compressive strength (MPa)	Validity
		Average					**485**	**48.4**	

Table C-3: Detailed compressive strength results of concrete with CA-2

w/b	Age (days)	Cube	Height (mm)	Breadth (mm)	Length (mm)	Mass (kg)	Load (kN)	Compressive strength (MPa)	Validity
0.4	7	1	103.22	100.00	100.00	2.465	546	52.9	OK
		2	102.56	100.00	100.00	2.475	532	51.9	
		3	101.69	100.00	100.00	2.450	540	53.1	
		Average					**539**	**52.6**	
	28	1	102.02	100.00	100.48	2.495	602	59.0	OK
		2	101.77	100.00	100.56	2.500	604	59.3	
		3	100.40	100.00	101.13	2.500	596	59.4	
		Average					**601**	**59.2**	
	112	1	100.74	100.00	100.00	2.470	672	66.7	OK
		2	100.91	100.00	101.00	2.470	656	65.0	
		3	101.42	100.00	101.00	2.475	684	67.4	
		Average					**671**	**66.4**	
0.6	7	1	100.90	100.00	100.00	2.460	376	37.3	OK
		2	100.87	100.00	100.00	2.420	374	37.1	
		3	100.51	100.00	100.00	2.465	375	37.3	
		Average					**375**	**37.2**	
	28	1	101.97	100.00	100.48	2.425	400	39.2	OK
		2	101.66	100.00	100.56	2.465	430	42.3	
		3	100.74	100.00	101.13	2.470	430	42.7	
		Average					**420**	**41.4**	
	112	1	101.55	100.00	100.00	2.475	478	47.1	OK
		2	100.49	100.00	101.00	2.445	472	47.0	
		3	100.57	100.00	101.00	2.480	470	46.7	

w/b	Age (days)	Cube	Height (mm)	Breadth (mm)	Length (mm)	Mass (kg)	Load (kN)	Compressive strength (MPa)	Validity
		Average					**473**	**46.9**	

Table C-4: Detailed compressive strength results of concrete with CA-3

w/b	Age (days)	Cube	Height (mm)	Breadth (mm)	Length (mm)	Mass (kg)	Load (kN)	Compressive strength (MPa)	Validity
0.4	7	1	103.39	100.00	100.00	2.515	554	53.6	OK
		2	100.91	100.00	100.00	2.445	600	59.5	
		3	103.39	100.00	100.00	2.500	570	55.1	
		Average					**575**	**56.1**	
	28	1	101.14	100.00	100.48	2.480	646	63.9	OK
		2	101.84	100.00	100.56	2.515	620	60.9	
		3	102.16	100.00	101.13	2.485	638	62.5	
		Average					**635**	**62.4**	
	112	1	100.32	100.00	100.00	2.465	744	74.2	OK
		2	98.65	100.00	101.00	2.415	682	69.1	
		3	99.08	100.00	101.00	2.430	700	70.6	
		Average					**709**	**71.3**	
0.6	7	1	102.78	100.00	100.00	2.475	406	39.6	OK
		2	100.79	100.00	100.00	2.430	410	40.9	
		3	100.59	100.00	100.00	2.445	402	40.3	
		Average					**406**	**40.3**	
	28	1	102.53	100.00	100.48	2.500	432	42.0	OK
		2	100.19	100.00	100.56	2.425	419	41.6	
		3	99.67	100.00	101.13	2.500	420	41.8	
		Average					**424**	**41.8**	
	112	1	100.99	100.00	100.00	2.450	528	52.3	OK
		2	101.70	100.00	101.00	2.460	526	51.7	
		3	102.53	100.00	101.00	2.455	528	51.5	

w/b	Age (days)	Cube	Height (mm)	Breadth (mm)	Length (mm)	Mass (kg)	Load (kN)	Compressive strength (MPa)	Validity
		Average					**527**	**51.8**	

Table C-5: Detailed compressive strength results of concrete with CA-4

w/b	Age (days)	Cube	Height (mm)	Breadth (mm)	Length (mm)	Mass (kg)	Load (kN)	Compressive strength (MPa)	Validity
0.4	7	1	99.60	100.00	100.00	2.430	536	53.8	OK
		2	98.89	100.00	100.00	2.460	535	54.1	
		3	98.99	100.00	100.00	2.450	535	54.0	
		Average					**535**	**54.0**	
	28	1	101.59	100.00	100.48	2.445	574	56.5	OK
		2	98.07	100.00	100.56	2.385	612	62.4	
		3	99.74	100.00	101.13	2.425	596	59.8	
		Average					**594**	**59.6**	
	112	1	100.99	100.00	100.00	2.480	696	68.9	OK
		2	102.81	100.00	101.00	2.500	644	62.6	
		3	100.92	100.00	101.00	2.450	650	64.4	
		Average					**663**	**65.3**	
0.6	7	1	99.13	100.00	100.00	2.375	380	38.3	OK
		2	99.20	100.00	100.00	2.405	366	36.9	
		3	99.59	100.00	100.00	2.338	374	37.6	
		Average					**373**	**37.6**	
	28	1	102.85	100.00	100.48	2.480	402	39.1	OK
		2	98.31	100.00	100.56	2.355	402	40.9	
		3	104.08	100.00	101.13	2.465	428	41.1	
		Average					**411**	**40.4**	
	112	1	98.75	100.00	100.00	2.325	470	47.6	OK
		2	97.36	100.00	101.00	2.355	484	49.7	
		3	98.31	100.00	101.00	2.355	480	48.8	

w/b	Age (days)	Cube	Height (mm)	Breadth (mm)	Length (mm)	Mass (kg)	Load (kN)	Compressive strength (MPa)	Validity
		Average					478	48.7	

Appendix D: Detailed splitting strength test results

Table D-1 to Table D-5 shows the tensile splitting strength of concretes with different crystalline admixtures.

Table D-1: Detailed splitting strength results of control concrete

w/b	Age (days)	Cube	Height (mm)	Breadth (mm)	Length (mm)	Mass (kg)	Load (kN)	Compressive strength (MPa)	Validity
0.4	7	1	101.41	100.00	100.00	2.455	58	3.6	OK
		2	101.46	100.00	100.00	2.510	56.0	3.5	
		3	101.20	100.00	100.00	2.450	57	3.6	
		Average					**57**	**3.6**	
	28	1	102.24	100.00	100.00	2.455	88	5.5	OK
		2	103.33	100.00	100.00	2.510	82.0	5.1	
		3	102.11	100.00	100.00	2.450	84	5.2	
		Average					**85**	**5.3**	
	112	1	100.87	100.00	100.00	2.460	89	5.6	OK
		2	101.43	100.00	100.00	2.465	93	5.8	
		3	101.29	100.00	100.00	2.500	90	5.7	
		Average					**91**	**5.7**	
0.6	7	1	101.41	100.00	100.00	2.445	48	3.0	OK
		2	101.46	100.00	100.00	2.440	46	2.9	
		3	101.20	100.00	100.00	2.440	49	3.1	
		Average					**48**	**3.0**	
	28	1	102.30	100.00	100.00	2.445	66	4.1	OK
		2	101.71	100.00	100.00	2.440	68	4.3	
		3	101.72	100.00	100.00	2.440	68	4.3	
		Average					**67**	**4.2**	
	112	1	101.63	100.00	100.00	2.480	66	4.1	OK
		2	101.16	100.00	100.00	2.465	74	4.7	
		3	101.32	100.00	100.00	2.485	72	4.5	

w/b	Age (days)	Cube	Height (mm)	Breadth (mm)	Length (mm)	Mass (kg)	Load (kN)	Compressive strength (MPa)	Validity
		Average					**71**	**4.4**	

Table D-2: Detailed splitting strength results of concrete with CA-1

w/b	Age (days)	Cube	Height (mm)	Breadth (mm)	Length (mm)	Mass (kg)	Load (kN)	Compressive strength (MPa)	Validity
0.4	7	1	102.04	100.00	100.00	2.500	52	3.2	OK
		2	99.58	100.00	100.00	2.515	52	3.3	
		3	102.06	100.00	100.00	2.495	50	3.1	
		Average					**51**	**3.2**	
	28	1	101.44	100.00	100.00	2.460	80	5.0	OK
		2	102.02	100.00	100.00	2.420	86.0	5.4	
		3	102.45	100.00	100.00	2.430	82	5.1	
		Average					**83**	**5.2**	
	112	1	102.88	100.00	100.00	2.530	84	5.2	OK
		2	102.88	100.00	100.00	2.525	86.0	5.3	
		3	101.98	100.00	100.00	2.430	90	5.6	
		Average					**87**	**5.4**	
0.6	7	1	101.02	100.00	100.00	2.490	37	2.3	OK
		2	100.20	100.00	100.00	2.440	38	2.4	
		3	100.79	100.00	100.00	2.430	38	2.4	
		Average					**38**	**2.4**	
	28	1	100.34	100.00	100.00	2.415	72	4.6	OK
		2	100.16	100.00	100.00	2.385	70.0	4.4	
		3	100.14	100.00	100.00	2.400	68	4.3	
		Average					**70**	**4.4**	
	112	1	100.45	100.00	100.00	2.420	74	4.7	OK
		2	102.62	100.00	100.00	2.495	70.0	4.3	
		3	100.39	100.00	100.00	2.450	72	4.6	

w/b	Age (days)	Cube	Height (mm)	Breadth (mm)	Length (mm)	Mass (kg)	Load (kN)	Compressive strength (MPa)	Validity
		Average					**72**	**4.5**	

Table D-3: Detailed splitting strength results of concrete with CA-2

w/b	Age (days)	Cube	Height (mm)	Breadth (mm)	Length (mm)	Mass (kg)	Load (kN)	Compressive strength (MPa)	Validity
0.4	7	**1**	102.23	100.00	100.00	2.485	50	3.2	OK
		2	99.97	100.00	100.00	2.440	58	3.6	
		3	99.97	100.00	100.00	2.350	54	3.4	
		Average					**54**	**3.4**	
	28	**1**	100.98	100.00	100.00	2.480	66	4.1	OK
		2	101.18	100.00	100.00	2.470	62	3.9	
		3	100.08	100.00	100.00	2.450	64	4.1	
		Average					**64**	**4.0**	
	112	**1**	102.55	100.00	100.00	2.530	82	5.1	OK
		2	100.91	100.00	100.00	2.470	90	5.7	
		3	101.42	100.00	100.00	2.530	88	5.5	
		Average					**87**	**5.4**	
0.6	7	**1**	102.82	100.00	100.00	2.495	48	3.0	OK
		2	102.36	100.00	100.00	2.310	42	2.7	
		3	99.46	100.00	100.00	2.425	48	3.0	
		Average					**46**	**2.9**	
	28	**1**	103.08	100.00	100.00	2.525	58	3.6	OK
		2	100.56	100.00	100.00	2.430	52	3.3	
		3	101.97	100.00	100.00	2.500	58	3.6	
		Average					**56**	**3.5**	
	112	**1**	102.18	100.00	100.00	2.455	69	4.3	OK
		2	101.33	100.00	100.00	2.455	65	4.1	
		3	101.97	100.00	100.00	2.460	65	4.1	

w/b	Age (days)	Cube	Height (mm)	Breadth (mm)	Length (mm)	Mass (kg)	Load (kN)	Compressive strength (MPa)	Validity
		Average					**66**	**4.1**	

Table D-4: Detailed splitting strength results of concrete with CA-3

w/b	Age (days)	Cube	Height (mm)	Breadth (mm)	Length (mm)	Mass (kg)	Load (kN)	Compressive strength (MPa)	Validity
0.4	7	1	102.66	100.00	100.00	2.500	74	4.6	OK
		2	99.16	100.00	100.00	2.395	71	4.6	
		3	101.88	100.00	100.00	2.450	71	4.4	
		Average					**72**	**4.5**	
	28	1	101.14	100.00	100.00	2.490	72	4.5	OK
		2	100.35	100.00	100.00	2.460	76	4.8	
		3	100.21	100.00	100.00	2.455	78	5.0	
		Average					**75**	**4.8**	
	112	1	98.86	100.00	100.00	2.570	85	5.5	OK
		2	102.45	100.00	100.00	2.540	77	4.8	
		3	98.86	100.00	100.00	2.565	82	5.3	
		Average					**81**	**5.2**	
0.6	7	1	98.73	100.00	100.00	2.310	50	3.2	OK
		2	101.27	100.00	100.00	2.435	55	3.5	
		3	99.67	100.00	100.00	2.440	54	3.4	
		Average					**53**	**3.4**	
	28	1	102.48	100.00	100.00	2.485	67	4.2	OK
		2	101.58	100.00	100.00	2.470	65	4.1	
		3	99.67	100.00	100.00	2.485	64	4.1	
		Average					**65**	**4.1**	
	112	1	100.12	100.00	100.00	2.605	64	4.1	OK
		2	101.30	100.00	100.00	2.615	67	4.2	
		3	100.78	100.00	100.00	2.440	67	4.2	

w/b	Age (days)	Cube	Height (mm)	Breadth (mm)	Length (mm)	Mass (kg)	Load (kN)	Compressive strength (MPa)	Validity
		Average					**66**	**4.2**	

Table D-5: Detailed splitting strength results of concrete with CA-4

w/b	Age (days)	Cube	Height (mm)	Breadth (mm)	Length (mm)	Mass (kg)	Load (kN)	Compressive strength (MPa)	Validity
0.4	7	1	101.50	100.00	100.00	2.460	72	4.5	OK
		2	98.64	100.00	100.00	2.390	72	4.6	
		3	100.92	100.00	100.00	2.450	70	4.4	
		Average					**71**	**4.5**	
	28	1	98.63	100.00	100.00	2.390	74	4.8	OK
		2	102.68	100.00	100.00	2.500	81	5.0	
		3	102.01	100.00	100.00	2.445	71	4.4	
		Average					**75**	**4.7**	
	112	1	102.38	100.00	100.00	2.530	83	5.2	OK
		2	101.04	100.00	100.00	2.475	91	5.7	
		3	102.01	100.00	100.00	2.445	85	5.3	
		Average					**86**	**5.4**	
0.6	7	1	100.70	100.00	100.00	2.430	56	3.5	OK
		2	98.79	100.00	100.00	2.380	6	3.9	
		3	99.50	100.00	100.00	2.440	58	3.7	
		Average					**58**	**3.7**	
	28	1	97.89	100.00	100.00	2.360	69	4.5	OK
		2	101.13	100.00	100.00	2.445	65	4.1	
		3	101.85	100.00	100.00	2.480	63	3.9	
		Average					**66**	**4.2**	
	112	1	101.21	100.00	100.00	2.445	70	4.4	OK
		2	102.78	100.00	100.00	2.485	68	4.2	
		3	101.85	100.00	100.00	2.480	67	4.2	

w/b	Age (days)	Cube	Height (mm)	Breadth (mm)	Length (mm)	Mass (kg)	Load (kN)	Compressive strength (MPa)	Validity
		Average					68	4.3	

Appendix E: Oxygen permeability index results (OPIs)

Table E-1: Detailed oxygen permeability results for uncracked concrete

Age	Specimen	0.4					0.6				
		Control	**CA-1**	**CA-2**	**CA-3**	**CA-4**	**Control**	**CA-1**	**CA-2**	**CA-3**	**CA-4**
4	1	10.43	10.49	10.37	10.33	10.59	10.25	10.48	10.38	9.92	10.41
	2	10.54	10.34	10.37	10.21	10.61	10.01	10.37	10.40	10.08	10.58
	3	10.37	10.48	10.35	10.20	10.65	10.48	10.29	10.33	10.05	10.53
	4	10.46	10.48	10.34	10.09	10.69	10.49	10.12	10.29	10.04	10.53
	Average OPI	**10.45**	**10.45**	**10.36**	**10.21**	**10.64**	**10.31**	**10.32**	**10.35**	**10.02**	**10.51**
	Std deviation (σ)	**0.07**	**0.07**	**0.01**	**0.10**	**0.04**	**0.23**	**0.15**	**0.05**	**0.07**	**0.07**
8	1	10.41	10.61	10.59	10.42	10.70	10.33	10.50	10.52	10.05	10.54
	2	10.35	10.55	10.40	10.29	10.60	10.25	10.43	10.45	10.18	10.56
	3	10.61	10.49	10.41	10.39	10.76	10.39	10.48	10.50	10.28	10.60
	4	10.42	10.38	10.58	10.37	10.74	10.50	10.48	10.39	10.29	10.53
	Average OPI	**10.45**	**10.51**	**10.49**	**10.37**	**10.70**	**10.37**	**10.47**	**10.47**	**10.20**	**10.55**
	Std deviation (σ)	**0.12**	**0.10**	**0.10**	**0.06**	**0.07**	**0.11**	**0.03**	**0.06**	**0.11**	**0.03**
12	1	10.43	10.74	10.81	10.38	10.80	10.42	10.51	10.61	10.18	10.66
	2	10.35	10.73	10.53	10.35	10.59	10.25	10.51	10.57	10.29	10.53
	3	10.61	10.69	10.51	10.47	10.86	10.30	10.48	10.67	10.52	10.66
	4	10.43	10.78	10.58	10.57	10.78	10.52	10.50	10.56	10.54	10.61
	Average OPI	**10.45**	**10.72**	**10.61**	**10.44**	**10.76**	**10.37**	**10.50**	**10.60**	**10.38**	**10.62**
	Permeability (k) x 10^{-11}	**3.55**	**1.91**	**2.45**	**3.63**	**1.74**	**4.27**	**3.16**	**2.51**	**4.17**	**2.40**
	Percentage decrease (%)	**0.00**	**46.30**	**30.82**	**-2.30**	**51.02**	**0.00**	**25.87**	**41.12**	**2.28**	**43.77**
	Std deviation (σ)	**0.11**	**0.03**	**0.14**	**0.10**	**0.12**	**0.12**	**0.02**	**0.05**	**0.17**	**0.08**

Table E-2: Detailed relative OPI results for uncracked concrete

Age	Concrete Mix					Water/binder ratio
	Control	CA-1	CA-2	CA-3	CA-4	
4	100	100	99	98	102	0.4
8	100	101	100	99	102	
12	100	103	101	100	103	
4	100	100	100	97	102	0.6
8	100	101	101	98	102	
12	100	101	102	100	102	

Appendix F: Water Sorptivity index test results (WSI)

Table F-1: Detailed water sorptivity results for uncracked concrete

Age	Specimen	0.4					0.6				
		Control	CA-1	CA-2	CA-3	CA-4	Control	CA-1	CA-2	CA-3	CA-4
		Sorptivity (mm/√hr)									
4	1	6.08	7.05	6.92	6.76	6.24	7.85	9.23	7.92	7.92	9.48
	2	6.55	6.59	6.87	6.98	6.11	8.25	8.29	7.85	7.96	7.96
	3	7.05	7.21	6.23	7.56	6.01	8.88	8.74	9.11	7.13	6.55
	4	7.40	6.96	6.87	6.14	6.00	7.71	8.46	8.93	6.73	7.85
	Average	**6.77**	**6.95**	**6.67**	**6.86**	**6.09**	**8.17**	**8.68**	**8.45**	**7.44**	**7.96**
	Standard deviation (σ)	**0.58**	**0.27**	**0.39**	**0.59**	**0.11**	**0.52**	**0.41**	**0.66**	**0.61**	**1.20**
8	1	6.50	7.11	7.55	5.66	5.95	7.99	7.97	7.31	7.37	8.27
	2	6.73	6.37	6.95	5.36	5.94	7.67	7.91	8.05	7.21	7.92
	3	6.45	5.58	6.02	7.10	5.95	8.41	8.74	8.09	6.83	6.92
	4	6.54	6.93	5.87	6.56	5.40	7.00	8.46	7.89	6.87	7.85
	Average	**6.55**	**6.50**	**6.60**	**6.17**	**5.81**	**7.77**	**8.27**	**7.84**	**7.07**	**7.74**
	Standard deviation (σ)	**0.12**	**0.69**	**0.79**	**0.80**	**0.27**	**0.59**	**0.40**	**0.36**	**0.27**	**0.58**
12	1	6.93	6.73	7.50	6.45	5.67	8.13	6.71	6.70	6.82	7.05
	2	6.91	5.97	7.04	6.36	5.76	7.10	7.53	8.25	6.47	7.88
	3	5.85	6.91	5.82	5.24	5.89	7.93	7.84	7.08	6.53	7.28
	4	5.67	5.81	5.87	5.42	4.80	6.28	6.40	6.85	7.00	7.45
	Average	**6.34**	**6.35**	**6.56**	**5.87**	**5.53**	**7.36**	**7.12**	**7.22**	**6.71**	**7.40**

Age	Specimen	0.4					0.6				
		Control	CA-1	CA-2	CA-3	CA-4	Control	CA-1	CA-2	CA-3	CA-4
		Sorptivity (mm/√hr)									
	Standard deviation (σ)	**0.67**	**0.54**	**0.84**	**0.62**	**0.49**	**0.85**	**0.57**	**0.71**	**0.25**	**0.43**

Table F-2: Detailed water filled porosity results for uncracked concrete

Age	Specimen	0.4					0.6				
		Control	CA-1	CA-2	CA-3	CA-4	Control	CA-1	CA-2	CA-3	CA-4
		Water Filled Porosity (%)									
4	1	7.39	8.11	7.16	7.82	8.72	10.05	8.30	10.25	10.39	11.00
	2	7.42	7.67	7.50	9.15	8.42	10.57	9.68	9.93	9.72	9.96
	3	7.60	8.06	8.63	7.69	8.06	9.34	9.89	9.64	9.41	10.75
	4	8.29	8.18	9.33	7.81	8.46	10.23	9.51	9.90	10.31	9.91
	Average	**7.67**	**8.01**	**8.16**	**8.12**	**8.42**	**10.05**	**9.34**	**9.93**	**9.96**	**10.40**
	Standard deviation (σ)	**0.42**	**0.23**	**1.00**	**0.69**	**0.27**	**0.52**	**0.19**	**0.25**	**0.47**	**0.55**
8	1	7.42	7.64	7.67	7.59	7.91	10.03	7.63	9.86	10.06	10.35
	2	7.78	7.56	7.90	7.99	7.73	10.30	9.99	10.21	9.38	9.66
	3	7.34	8.06	8.57	7.36	7.63	9.87	9.89	10.03	9.17	10.07
	4	7.80	8.00		8.00	7.57	9.74	9.51	9.76	9.59	9.91
	Average	**7.58**	**7.82**	**8.05**	**7.74**	**7.71**	**9.98**	**9.26**	**9.96**	**9.55**	**10.00**
	Standard deviation (σ)	**0.24**	**0.25**	**0.47**	**0.31**	**0.15**	**0.24**	**0.26**	**0.20**	**0.38**	**0.29**
12	1	7.45	7.17	6.65	7.36	7.09	10.00	8.97	9.47	9.74	9.69
	2	8.13	7.10	7.10	6.82	7.03	10.02	9.37	10.50	9.04	9.36
	3	7.07	7.3	8.68	7.04	7.19	10.40	9.67	10.42	8.94	9.40

Age	Specimen	0.4					0.6				
		Control	CA-1	CA-2	CA-3	CA-4	Control	CA-1	CA-2	CA-3	CA-4
		Water Filled Porosity (%)									
	4	7.31	6.98	9.33	8.19	6.68	9.25	8.68	9.62	8.86	9.11
	Average	**7.49**	**7.14**	**7.94**	**7.35**	**7.00**	**9.92**	**9.17**	**10.00**	**9.14**	**9.48**
	Standard deviation (σ)	**0.45**	**0.13**	**1.27**	**0.60**	**0.22**	**0.48**	**0.44**	**0.54**	**0.40**	**0.18**

Table F-3: Detailed water sorptivity results for cracked concrete with crack width more than 0.3 mm

Age	Specimen	0.4					0.6				
		Control	CA-1	CA-2	CA-3	CA-4	Control	CA-1	CA-2	CA-3	CA-4
		Sorptivity (mm/√hr)									
4	1	11.96	11.63	12.13	13.65	13.57	11.55	12.11	18.14	14.70	15.19
	2	16.14	14.21	18.55	14.51	12.43	11.32	14.70	14.93	13.64	15.79
	3	11.76	10.40	12.65	13.70	18.13	11.55	13.36	19.27	13.61	15.32
	4	16.14	11.12	15.53	13.71	13.61	11.43	12.70	16.97	13.34	15.15
	Average	**14.00**	**11.05**	**13.44**	**13.89**	**13.21**	**11.43**	**12.72**	**18.13**	**13.82**	**15.36**
	Standard deviation (σ)	**2.47**	**0.62**	**1.83**	**0.41**	**0.67**	**0.13**	**0.62**	**1.15**	**0.16**	**0.29**
8	1	10.96	14.82	12.28	15.97	12.69	10.55	10.88	15.27	12.97	13.54
	2	14.14	15.67	12.56	15.04	13.21	10.31	11.90	15.30	13.29	19.03
	3	11.26	13.13	18.56	11.81	13.29	9.55	11.20	14.72	13.09	12.58
	4	9.34	13.41	14.22	13.07	12.60	11.32	11.53	13.34	12.93	15.01
	Average	**11.42**	**13.79**	**14.40**	**13.97**	**12.95**	**10.43**	**11.43**	**14.66**	**13.07**	**15.04**
	Standard deviation (σ)	**2.00**	**0.91**	**2.90**	**1.88**	**0.35**	**0.73**	**0.73**	**0.92**	**0.17**	**2.84**
12	1	12.00	10.56	11.69	14.56	14.17	4.24	10.58	14.72	12.46	17.49
	2	15.50	5.23	13.58	12.71	12.48	11.20	16.23	14.48	15.52	13.74
	3	13.43	12.57	12.68	12.40	14.99	13.41	9.45	13.35	14.80	15.47

Age	Specimen	0.4					0.6				
		Control	CA-1	CA-2	CA-3	CA-4	Control	CA-1	CA-2	CA-3	CA-4
		Sorptivity (mm/√hr)									
	4	14.18	14.61	12.64	15.19	12.40	5.36	6.06	14.21	13.94	18.13
	Average	**13.78**	**10.74**	**12.65**	**13.72**	**13.51**	**8.55**	**10.58**	**14.19**	**14.18**	**16.21**
	Standard deviation (σ)	**1.46**	**4.03**	**0.77**	**1.37**	**1.28**	**4.45**	**4.23**	**0.60**	**1.32**	**2.00**

Table F-4: Detailed water filled porosity results for cracked concrete with crack width more than 0.3 mm

Age	Specimen	0.4					0.6				
		Control	CA-1	CA-2	CA-3	CA-4	Control	CA-1	CA-2	CA-3	CA-4
		Water Filled Porosity (%)									
4	1	7.65	7.63	7.96	7.59	8.16	10.50	8.96	10.55	9.21	10.29
	2	8.55	7.22	7.28	7.93	8.52	11.09	10.29	10.15	11.14	10.20
	3	7.65	7.69	7.29	7.76	7.76	10.55	10.21	8.68	11.12	10.73
	4	8.55	6.14	7.03	7.92	8.26	11.45	10.26	10.05	10.53	10.57
	Average	**8.10**	**7.17**	**7.39**	**7.80**	**8.17**	**10.90**	**9.93**	**9.86**	**10.93**	**10.45**
	Standard deviation (σ)	**0.52**	**0.72**	**0.40**	**0.16**	**0.32**	**0.46**	**0.65**	**0.81**	**0.35**	**0.25**
8	1	7.35	7.13	6.87	6.89	6.83	10.50	9.41	9.76	8.89	9.01
	2	8.61	5.99	7.44	7.12	6.55	8.56	7.75	9.99	9.87	10.10
	3	7.15	7.01	7.38	6.91	7.03	9.34	7.21	9.19	9.45	10.05
	4	8.05	7.04	7.40	6.98	6.93	10.34	8.00	8.89	9.57	9.83
	Average	**7.79**	**6.79**	**7.27**	**6.97**	**6.84**	**9.68**	**8.09**	**9.46**	**9.44**	**9.74**
	Standard deviation (σ)	**0.67**	**0.54**	**0.27**	**0.11**	**0.21**	**0.91**	**0.94**	**0.51**	**0.41**	**0.51**
12	1	7.31	4.94	5.97	6.00	6.55	9.19	8.30	9.36	9.16	9.41

Age	Specimen	0.4					0.6				
		Control	CA-1	CA-2	CA-3	CA-4	Control	CA-1	CA-2	CA-3	CA-4
		Water Filled Porosity (%)									
	2	8.37	6.15	5.85	5.36	7.04	10.79	8.51	9.56	8.20	9.00
	3	7.37	3.45	6.96	6.29	6.89	10.82	8.23	8.37	9.13	8.85
	4	8.31	5.23	6.24	6.03	6.40	9.17	8.15	9.12	8.79	8.78
	Average	**7.84**	**4.94**	**6.26**	**5.92**	**6.72**	**9.99**	**8.30**	**9.10**	**8.82**	**9.01**
	Standard deviation (σ)	**0.58**	**1.12**	**0.50**	**0.40**	**0.30**	**0.94**	**0.15**	**0.52**	**0.45**	**0.28**

Table F-5: Detailed water sorptivity results for cracked concrete with crack width less than 0.3 mm

Age	Specimen	0.4					0.6				
		Control	CA-1	CA-2	CA-3	CA-4	Control	CA-1	CA-2	CA-3	CA-4
		Sorptivity (mm/√hr)									
4	1	10.74	11.32	15.94	13.12	17.52	12.69	16.49	11.34	15.51	15.23
	2	10.89	10.88	12.16	13.81	12.03	13.34	14.92	16.19	13.68	17.50
	3	10.54	10.42	13.54	17.45	13.63	12.69	13.98	9.30	14.97	14.44
	4	9.29	11.59	11.63	14.19	14.15	11.23	7.75	12.22	14.38	15.24
	Average	**10.37**	**11.05**	**13.32**	**14.64**	**14.33**	**12.49**	**13.28**	**12.26**	**14.64**	**15.60**
	Standard deviation (σ)	**0.73**	**0.51**	**1.92**	**1.92**	**2.31**	**0.89**	**3.83**	**2.89**	**0.79**	**1.32**
8	1	10.74	14.88	13.16	17.46	12.54	12.69	14.72	17.68	17.97	16.05
	2	8.34	15.69	11.74	11.35	12.34	13.34	11.40	13.86	11.62	12.78
	3	10.74	13.14	12.52	12.92	11.37	10.32	12.29	14.61	14.55	13.86
	4	10.89	14.07	12.33	12.86	12.07	11.39	12.76	13.72	13.43	14.51
	Average	**10.18**	**14.44**	**12.44**	**13.65**	**12.08**	**11.94**	**12.79**	**14.97**	**14.39**	**14.30**

Age	Specimen	0.4					0.6				
		Control	CA-1	CA-2	CA-3	CA-4	Control	CA-1	CA-2	CA-3	CA-4
		Sorptivity (mm/√hr)									
	Standard deviation (σ)	**1.23**	**1.09**	**0.59**	**2.64**	**0.51**	**1.35**	**1.40**	**1.85**	**2.67**	**1.37**
12	1	10.68	16.05	11.56	19.80	12.54	12.96	11.67	14.02	14.46	14.31
	2	12.34	13.40	13.14	14.15	13.06	11.48	12.67	14.53	16.32	15.10
	3	11.54	15.69	12.18	14.56	11.15	14.87	9.73	15.20	14.04	17.22
	4	11.46	13.97	11.37	11.52	12.23	12.45	11.37	14.56	13.48	16.04
	Average	**11.51**	**14.78**	**12.06**	**15.01**	**12.25**	**12.94**	**11.36**	**14.58**	**14.58**	**15.67**
	Standard deviation (σ)	**0.68**	**1.29**	**0.80**	**3.47**	**0.81**	**1.43**	**1.22**	**0.48**	**1.23**	**1.25**

Table F-6: Detailed water filled porosity results for cracked concrete with crack width less than 0.3 mm

Age	Specimen	0.4					0.6				
		Control	CA-1	CA-2	CA-3	CA-4	Control	CA-1	CA-2	CA-3	CA-4
		Water Filled Porosity (%)									
4	1	7.88	6.47	8.07	8.28	8.23	10.24	8.74	10.30	9.81	9.24
	2	6.85	7.82	7.28	7.73	9.38	11.05	9.53	10.99	11.14	9.35
	3	7.88	6.52	7.62	7.29	8.17	10.56	9.27	9.81	9.22	10.84
	4	6.85	5.93	7.69	8.03	8.68	10.85	8.24	10.59	10.19	10.06
	Average	**7.37**	**6.69**	**7.66**	**7.83**	**8.61**	**10.67**	**8.94**	**10.42**	**10.09**	**9.87**
	Standard deviation (σ)	**0.59**	**0.80**	**0.32**	**0.43**	**0.56**	**0.35**	**0.58**	**0.50**	**0.81**	**0.74**
8	1	6.57	6.51	6.46	6.93	5.62	9.34	7.88	7.47	9.71	9.47
	2	6.85	6.20	6.70	6.43	6.87	10.67	8.12	9.21	9.72	10.63
	3	7.34	6.43	5.79	7.14	6.80	9.45	8.45	9.96	9.84	9.72

Age	Specimen	0.4					0.6				
		Control	CA-1	CA-2	CA-3	CA-4	Control	CA-1	CA-2	CA-3	CA-4
		Water Filled Porosity (%)									
	4	5.64	6.60	6.38	6.83	6.52	9.46	7.90	10.14	9.63	9.76
	Average	**6.60**	**6.43**	**6.33**	**6.83**	**6.45**	**9.73**	**8.09**	**9.19**	**9.73**	**9.89**
	Standard deviation (σ)	**0.71**	**0.17**	**0.39**	**0.30**	**0.57**	**0.63**	**0.26**	**1.22**	**0.09**	**0.51**
12	1	7.06	5.19	6.10	5.59	6.40	9.56	7.16	8.20	8.74	8.19
	2	8.45	6.35	5.32	6.41	6.52	10.44	6.66	8.53	8.18	8.63
	3	7.25	6.32	6.00	5.63	6.25	9.85	7.25	9.06	8.97	9.94
	4	8.27	5.89	5.28	6.01	6.39	8.37	7.61	8.59	8.38	9.34
	Average	**7.76**	**5.94**	**5.68**	**5.91**	**6.39**	**9.56**	**7.17**	**8.60**	**8.57**	**9.03**
	Standard deviation (σ)	**0.70**	**0.54**	**0.44**	**0.38**	**0.11**	**0.87**	**0.39**	**0.35**	**0.35**	**0.77**

Appendix G: Water Permeability test results (WPT)

Table G-1: Detailed water permeability test results for cracked concrete with crack width less than 0.3 mm

Age	Specimen	0.4					0.6				
		Control	CA-1	CA-2	CA-3	CA-4	Control	CA-1	CA-2	CA-3	CA-4
		Permeability (mm/s)									
4	1	0.01885	0.02770	0.00286	0.00597	0.00029	0.01532	0.00103	0.01311	0.00398	0.02672
	2	0.00398	0.01450	0.01434	0.01195	0.01684	0.00088	0.00865	0.00889	0.01482	0.01991
	3	0.00528	0.00328	0.00499	0.02770	0.01087	0.02461	0.01532	0.03616	0.02299	0.01193
	Average	**0.00937**	**0.01516**	**0.00740**	**0.01521**	**0.00933**	**0.01360**	**0.00833**	**0.01938**	**0.01393**	**0.01952**
	Standard deviation (σ)	**0.00823**	**0.01222**	**0.00610**	**0.01123**	**0.00838**	**0.01196**	**0.00715**	**0.01468**	**0.00953**	**0.00740**
8	1	0.00597	0.01402	0.00328	0.01267	0.00346	0.01466	0.00261	0.01618	0.00311	0.01466
	2	0.01114	0.00398	0.01252	0.00381	0.00831	0.00294	0.01100	0.00398	0.01865	0.00180
	3	0.00149	0.00236	0.00577	0.02704	0.01195	0.00973	0.00587	0.02405	0.01035	0.03064
	Average	**0.00620**	**0.00679**	**0.00719**	**0.01450**	**0.00791**	**0.00911**	**0.00649**	**0.01474**	**0.01070**	**0.01570**
	Standard deviation (σ)	**0.00483**	**0.00632**	**0.00478**	**0.01172**	**0.00426**	**0.00588**	**0.00423**	**0.01011**	**0.00777**	**0.01445**
12	1	0.00425	0.00328	0.00036	0.01434	0.00490	0.00617	0.00720	0.00212	0.00960	0.00278
	2	0.01061	0.00973	0.01252	0.00518	0.00073	0.01672	0.00088	0.01154	0.00126	0.02640
	3	0.00204	0.00577	0.00753	0.00164	0.00973	0.00320	0.00607	0.00425	0.00668	0.01672
	Average	**0.00564**	**0.00626**	**0.00680**	**0.00706**	**0.00512**	**0.00870**	**0.00472**	**0.00597**	**0.00585**	**0.01530**
	Std dvtn (σ)	**0.00445**	**0.00325**	**0.00611**	**0.00655**	**0.00450**	**0.00711**	**0.00337**	**0.00494**	**0.00424**	**0.01188**

Age	Specimen	0.4					0.6				
		Control	CA-1	CA-2	CA-3	CA-4	Control	CA-1	CA-2	CA-3	CA-4
		Permeability (mm/s)									
% Reduction		39.81	58.71	8.11	53.58	45.12	36.03	43.34	69.20	58.00	21.62

Table G-2: Detailed water permeability test results for cracked concrete with crack width more than 0.3 mm

Age	Specimen	0.4					0.6				
		Control	CA-1	CA-2	CA-3	CA-4	Control	CA-1	CA-2	CA-3	CA-4
		Permeability (mm/s)									
4	1	0.02351	0.04800	0.06660	0.03030	0.00998	0.02080	0.04261	0.01418	0.02997	0.01515
	2	0.02273	0.01482	0.00587	0.00699	0.01195	0.00204	0.02672	0.03272	0.00393	0.07949
	3	0.02770	0.01926	0.02640	0.01341	0.00029	0.02672	0.01087	0.03616	0.06104	0.09086
	Average	**0.02465**	**0.02736**	**0.03296**	**0.01690**	**0.00741**	**0.01652**	**0.02673**	**0.02769**	**0.03165**	**0.06183**
	Standard deviation (σ)	**0.00267**	**0.01801**	**0.03089**	**0.01204**	**0.00624**	**0.01288**	**0.01587**	**0.01182**	**0.02859**	**0.04082**
8	**1**	0.02223	0.03728	0.00073	0.00490	0.00912	0.03064	0.00589	0.00499	0.00797	0.03062
	2	0.01127	0.01154	0.03544	0.01140	0.00328	0.01140	0.01341	0.01482	0.01654	0.00499
	3	0.01010	0.02461	0.02490	0.00381	0.00261	0.00528	0.02609	0.01100	0.00320	0.04261
	Average	**0.01453**	**0.02448**	**0.02036**	**0.00670**	**0.00501**	**0.01578**	**0.01513**	**0.01027**	**0.00924**	**0.02607**
	Standard deviation (σ)	**0.00669**	**0.01287**	**0.01779**	**0.00411**	**0.00358**	**0.01323**	**0.01021**	**0.00495**	**0.00676**	**0.01921**
12	1	0.00164	0.02103	0.00354	0.00126	0.00014	0.01267	0.01087	0.00425	0.00831	0.01326
	2	0.00973	0.02174	0.00597	0.00499	0.00617	0.00577	0.00567	0.00567	0.00577	0.01402
	3	0.01885	0.02609	0.01766	0.00627	0.00668	0.00381	0.00381	0.00261	0.00354	0.02351
	Average	**0.01007**	**0.02295**	**0.00906**	**0.00417**	**0.00433**	**0.00741**	**0.00678**	**0.00418**	**0.00587**	**0.01693**

Age	Specimen	0.4					0.6				
		Control	CA-1	CA-2	CA-3	CA-4	Control	CA-1	CA-2	CA-3	CA-4
		Permeability (mm/s)									
	Standard deviation (σ)	0.00861	0.00274	0.00755	0.00260	0.00363	0.00465	0.00366	0.00153	0.00238	0.00571
% Reduction		59.15	16.12	72.51	75.33	41.57	55.15	74.64	84.90	81.45	72.62

Appendix H: Sieve analysis test results

Table H-1: Sieve analysis results (19 mm greywacke stone)

Sieve opening (mm)	Mass of Sieve (g)	Mass of sieve and aggregate (g)	Mass retained (g)	Mass retained (%)	Cumulative Retained (%)	Cumulative % passing (%)
37.5	1615.00	1615.00	0.00	0.0	0.0	100.00
26.5	1630.00	1630.00	0.00	0.0	0.0	100.00
19	1505.00	2550.00	1045.00	26.1	26.1	73.9
13.2	1360.00	3740.00	2380.00	59.5	85.6	14.4
9.5	1415.00	1940.00	525.00	13.1	98.8	1.3
6.7	1475.00	1520.00	45.00	1.1	99.9	0.1
0.075	1415.00	1420.00	5.00	0.1	100.0	0.0
Pan	1180.00	1180.00	0.00	0.00	100.0	-

Table H-2: Sieve analysis results (Crusher sand)

Sieve opening (mm)	Mass of Sieve (g)	Mass of sieve and aggregate (g)	Mass retained (g)	Mass retained (%)	Cumulative Retained (%)	Cumulative % passing (%)
4.75	657.89	704.39	46.5	9.3	9.3	90.7
2.36	412.94	595.44	182.5	36.5	45.8	54.2
1.18	350.22	454.72	104.5	20.9	66.7	33.3
0.6	519.94	578.94	59	11.8	78.5	21.5
0.3	280.93	320.93	40	8	86.5	13.5
0.15	473.26	501.76	28.5	5.7	92.2	7.8

Sieve opening (mm)	Mass of Sieve (g)	Mass of sieve and aggregate (g)	Mass retained (g)	Mass retained (%)	Cumulative Retained (%)	Cumulative % passing (%)
0.075	463.19	493.19	30	6	98.2	1.8
Pan	446.19	455.19	9	1.8	100	0

Table H-3: Sieve analysis results (Dune sand)

Sieve opening (mm)	Mass of Sieve (g)	Mass of sieve and aggregate (g)	Mass retained (g)	Mass retained (%)	Cumulative Retained (%)	Cumulative % passing (%)
4.75	657.89	657.89	0	0	0	100
2.36	412.94	412.94	0	0	0	100
1.18	350.22	363.72	13.5	2.7	2.7	97.3
0.6	519.94	727.44	207.5	41.5	44.2	55.8
0.3	280.93	405.43	124.5	24.9	69.1	30.9
0.15	473.26	598.76	125.5	25.1	94.8	5.2
0.075	463.19	484.69	21.5	4.3	99.1	0.9
Pan	446.19	450.69	4.5	0.9	100	0

Appendix I: Physical and chemical properties of crystalline admixtures

Table I-1: Physical and chemical properties of the crystalline admixtures according to manufacturer's guide

Crystalline admixture	Physical properties					Chemical properties			
	Appearance	**Colour**	**Relative density (R.D)**	**Solubility in water**	**Dosage (% of binder weight)**	**Chemical composition (%)**	**Alkali content (% Na_2O)**	**Chloride content (%)**	**pH**
CA-1	Aggregated powder	Grey	> 1.3 at 20°C	Partially soluble	0.8 – 1.0	>50% cement (OPC)	< 0.35	-	> 12
CA-2	Powder	Grey	-	-	0.8 – 1.0	65 - 80% (Cement, Portland, chemicals) 10 - 30% CTS-15-1 [Trade Secret] 5 - 10% CTS-15-2 [Trade Secret] 1.5 - 6% Calcium magnesium	-	-	10.0 – 13.0

Crystalline admixture	Physical properties					Chemical properties			
	Appearance	**Colour**	**Relative density (R.D)**	**Solubility in water**	**Dosage (% of binder weight)**	**Chemical composition (%)**	**Alkali content (% Na_2O)**	**Chloride content (%)**	**pH**
						hydroxide ($CaMg(OH)_4$) 1.5 – 6% Calcium magnesium hydroxide oxide ($CaMg(OH)_2O$) 1.0 – 2% Calcium hydroxide			
CA-3	Powder	Greyish	0.75	Soluble	1.0	Mixture of cements, amino alcohols, and fillers	≤ 3	< 0.1	12

Crystalline admixture	Physical properties					Chemical properties			
	Appearance	**Colour**	**Relative density (R.D)**	**Solubility in water**	**Dosage (% of binder weight)**	**Chemical composition (%)**	**Alkali content (% Na_2O)**	**Chloride content (%)**	**pH**
CA-4	Powder	Light grey	-	-	2.0/1.0	35 - 60% (PC) 5 - 20% Alkaline earth compounds (Calcium dihydroxide) 30 - 40% (Silica sand) (< 0.005% (w/w) 10 µm respirable silica	-	< 0.1	12.0-12.4